UNIVERSITÀ DEGLI STUDI DI ROMA "TOR VERGATA"

FACOLTA' DI INGEGNERIA

DOTTORATO DI RICERCA IN
INGEGNERIA DEI MICROSISTEMI

CICLO DEL CORSO DI DOTTORATO
XXI

Plantoid: Plant inspired robot for subsoil exploration and environmental monitoring

Alessio Mondini

A.A. 2008/2009

Docente Guida/Tutor: Dott. Barbara Mazzolai
Dott. Virgilio Mattoli
Prof. Cecilia Laschi
Prof. Paolo Dario

Coordinatore: Prof. Aldo Tucciarone

Abstract

Biorobotics is a novel approach in the realization of robot that merges different disciplines as Robotic and Natural Science. The concept of biorobotics has been identified for many years as inspiration from the animal world. In this thesis this paradigm has been extended for the first time to the plant world. Plants are an amazing organism with unexpected capabilities. They are dynamic and highly sensitive organisms, actively and competitively foraging for limited resources both above and below ground, and they are also organisms which accurately compute their circumstances, use sophisticated cost–benefit analysis, and take defined actions to mitigate and control diverse environmental insults.

The objective of this thesis is to contribute to the realization of a robot inspired to plants, a plantoid. The plantoid robot includes root and shoot systems and should be able to explore and monitoring the environment both in the air and underground. These plant-inspired robots will be used for specific applications, such as in situ monitoring analysis and chemical detections, water searching in agriculture, anchoring capabilities and for scientific understanding of the plant capabilities/behaviours themselves by building a physical models.

The scientific work performed in this thesis addressed different aspects of this innovative robotic platform development: first of all, the study of the plants' characteristics and the enabling technologies in order to design and to develop the overall plantoid system. The proposed system can be easily sub-divided in two major sections, the aerial part and the subsoil part.

About the subsoil part, the activity focused on the realization of a miniaturized mechatronic system that imitates the behaviour of the plant radical apex. Plants show a peculiar directional growth in response to external stimulations, such as light (phototropism), gravity (gravitropism), touch (thigmotropism) or water/humidity gradient (hydrotropism). Tropisms frequently interact between and among each other, and the final grown form of the plant is influenced by such interactions. In order to imitate the powerful performances of the plant root system, a novel actuator has been proposed. This actuator is based on the osmotic principle (osmotic actuator) and, differently by the state-of-the-art actuators based on the osmotic principle, it has been designed in order to have a reversible reaction. This actuator permits to perform the elongation and the typical steering capabilities of the root apex, generating high forces with low power consumption (in the time scale of the plant). Theoretical studies on this actuator show interesting performances in terms of actuation pressure (more than 20 atm) with power in the order of some mW and with actuation in the hours scale time. The robotic root apex was designed to be equipped with sensors (gravity and moisture) to imitate the plants sensing characteristics, and with the novel osmotic actuator to drive the growth in the correct direction. An embedded microcontroller implements the basic root behaviour on the basis of the information coming from the sensors.

About the aerial part the activity in this thesis was focused on the realization of a sort of environmental monitoring module in order to imitate the high sensing capabilities of the plants. This part has been designed and realized in a more traditional way, without attempt to imitate completely the plant behaviour but taking inspiration from the fundamental characteristics (energy scavenging, wide sensing capabilities and communication). In order to integrate a wide amount of sensors an innovative interface board that guarantees the conditioning of the sensor, with plug-and-play capabilities and low power consumption, was developed.

Several aspects of the plantoid system are not faced yet and they will be part of the future works. In particular, the growing mechanism of the roots (some possible solutions are proposed and explained in this thesis) and the integration of chemical sensors in the root apex.

Foreword

The work performed in this thesis has been produced during the period of my PhD as student in Microsystems Engineering at the CRIM lab of Scuola Superiore Sant'Anna of Pisa from 2005 to 2009. During these years I was part of Prof. Paolo Dario team and in particular of the Dr. Barbara Mazzolai group, that is focused on technologies and robotic systems for environmental monitoring. In these years I had the chance to collaborate with several people both internal to the CRIM Laboratory than from other international groups.

Two special persons for beginning the acknowledgments: Barbara Mazzolai and Virgilio Mattoli. They have accepted me at the beginning of this adventure; I have shared with them the greater amount of these last years. They are not only tutors but masters, partners and above all friends.

I am thankful to Prof. Paolo Dario and Prof. Cecilia Laschi for supporting and tutoring me during the PhD studies.

I am thankful to Paolo Corradi that has collaborated with me during these years and in particular he has helped me in this final important phase as an added tutor.

Then a special thanks to:

- Gabriele Ferri the odour expert (even if less than his doggie), the demo man, the first price avoidance, he has been a reference in these years;
- Silvia Taccola for her collaboration and "practical" help;
- Carlo Filippeschi the "Mayor of Luciana" for sponsoring me and for all the fruitful conversations;
- Stefano Zampolli and Simona Raffa that have supplied me most of the knowledge necessary to pass the first difficult phases of the PhD;
- The Porf. Stefano Mancuso group for the collaboration in this amazing project.

Finally, I wish to express my thanks to my family and Mary that are all for me and that have supported me along these years.

Luciana, May 2009
Alessio Mondini

Table of Contents

1 Objectives and Motivations

This thesis aims at contributing to the realization of a plant inspired robot: a plantoid. Plants represent an excellent source of inspiration for developing a new generation of robotics systems, with monitoring, control and communication capabilities typical of the Plant World.

From a technological point of view, plants present interesting characteristics, such as:

- capacity of directional growth and exploration/monitoring capability in response to external stimulations;
- osmotic actuation principle, used for plant cells elongation;
- sensibility to wide amount of different physical and chemical stimuli both in the aerial and in the underground part;
- efficient use of energy resources with optimization of source-sink relationship.

These characteristics can be source of inspiration for the realization of several technological systems as:

- innovative robotic probes, with thrusting capabilities for reducing the energy consumption during the soil penetration;
- new classes of actuators with very low power consumption (small current requirement), high modulation actuation capability (high accuracy, resolution), slow actuation, high force/pressure actuation;
- novel sensor fusion algorithms for multi sensors signal processing, which permits to drive the root growth properly and moreover can be used for the scientific understanding of the plant behaviour;
- new strategies for energy use optimization;
- new communications techniques and strategies based on distributed intelligence.

There are several application fields where the use of a plant-inspired robot is justified. They could be useful for specific applications, such as:

- in situ monitoring analysis and chemical detections, therefore in all the applications where a long term analysis of an area is necessary, both above and underground; this can be important in polluted area, or also in spatial applications, where it is important to know, not only the air quality condition, but also the underground physical/chemical content;
- water searching in agriculture, exploiting the roots exploration capabilities and the tropistic behaviour of the plants;
- anchoring capabilities, that can be useful in particular in environment with low gravity (as asteroids) or with strong wind;

- for scientific understanding of the plant capabilities/behaviours themselves by building physical models, because many aspects of the plants world are still unknown;
- for high-impact perspectives in developing new communication strategies and control algorithms inspired by plants.

2   Introduction

The realization of a plantoid robot puts together several disciplines. The main three are biorobotics, microsystem technology and plant biology (together with chemistry, electronics, etc.). This chapter reports a brief introduction to these main aspects.

2.1   Biorobotics

2.1.1   Robotics evolution

The modern robotics in the last times has pushed towards the satisfactions of needs that human beings have felt for years: to have machines that can help the people in tiring and dangerous activities.

In the '70s the robotics was associated essentially to industrial robotics; in fact the "robot" word was intended as *"an automatically controlled, reprogrammable, multipurpose manipulator programmable in three or more axes which may be either fixed in place or mobile for use in industrial automation applications"* (*Robotics Industry Association*). So, robotics was developed mainly in the industrial automation field, where still now has a strong development line.

The great results obtained in the industrial field have encouraged the development of "service robots":

- robots for applications in hazardous environments, like space, submarine environments, or in dangerous tasks like disposal of unexploded devices or robots for rescue application;
- robots for biomedical applications, where robots for surgery, rehabilitation and elderly and disable people care are designed and developed;
- robots for environmental monitoring applications.

The technological progress and the coming of the microelectronics have brought to the realization of more complex robot that integrates structures with actuators, sensors, control and processing electronics, power system, communication infrastructure and user interface. So the definition of robot has changed in the last years. Today a robot is seen as "a mechatronic machine that can generate and control movements and forces". The robot has a body that is subjected to all the physical laws that rule the environment where the robot moves. Thanks to the integrated electronics, it has a certain amount of intelligence that can use to accomplish some tasks in an autonomous way [1].

A robot defined in this way can be easily compared with a biological system: both are furnished of a locomotion system, sensors, actuators, need of a control system, and they interact with the environment. The biological systems are the demonstration that many of the goals of the robotic researchers are possible and can become an inspiration source for components and behaviours of the next generation robots [2].

The synergy between robotics and biological systems has resulted in the generation of a new discipline known as Biorobotics.

2.1.2 Definition of Biorobotics

Biorobotics is a novel technological-scientific field that merges robotics and bioengineering. In particular, it is the science that is involved in the design and realization of robotic systems that take inspiration from the biological world or that have a biomedical application [3] (Fig. 1).
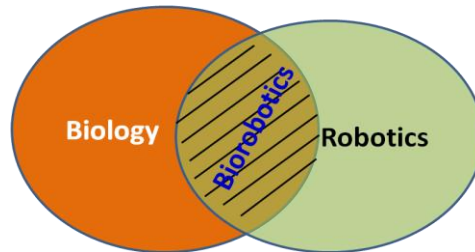
Fig. 1. Biorobotics can be defined as the intersection between biology and robotics.

Biorobotics can be seen from two different perspectives:

- "biomimetic robotics", as a science that is used to generate new knowledge through discoveries in the scientific field, contributing in this way to the scientific progress;
- "bioinspired robotics", as an engineering application to create new technology.

In both two cases, the robot is not only an advanced machine tool, but a real biomechatronic system that is designed and realized on the basis of a deep knowledge and an engineering modelling of the biological system that is inspired to.
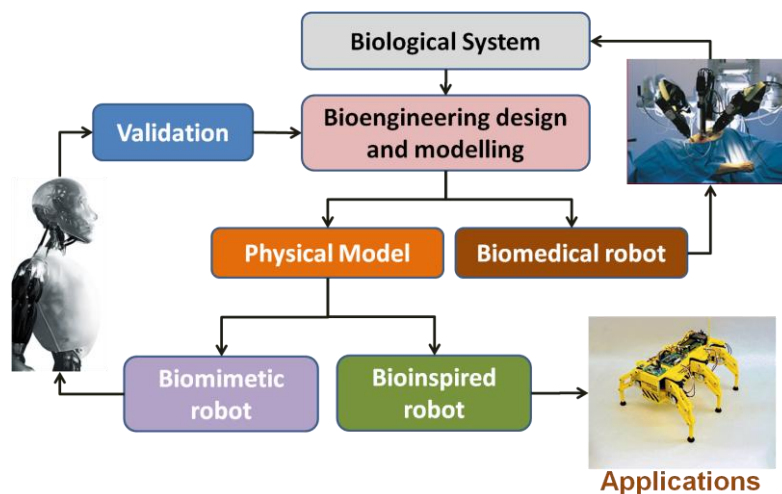
Fig. 2. Different perspectives of Biorobotics: the model of the biological system can be useful to develop a biomedical robot that can be used to accomplish actions on the biological system, or to develop a very realistic physical model of the studied biological system (biomimetic robot) that can be used as a scientific tool to study and validate the same model of the biological system, or to realize a bioinspired robot for scientific/commercial applications.

The main focus of Biorobotics is to analyze biological systems from a "biomechatronic" point of view, trying to understand the scientific and engineering principles underlying their extraordinary performance. Biomechatronics is a recent paradigm of machine design, which considers a mechatronic system together with its interactions with the external world and with the human operator.

Biorobotics has two main objectives:

- from a scientific point of view, to generate new knowledge on how biological systems work and interact with the environment and with human beings. This new knowledge can be acquired by modelling living creatures as well as by building biomimetic robots. The development of bioinspired machines provides novel insight for the biological systems that are inspired to, ranging from invertebrates to humans;

- from an engineering point of view, to develop innovative theory and technology for designing and building high performance robots. These robots, which may or may not be bioinspired, will incorporate scientific knowledge on biological systems in order to be more effective and acceptable than traditional robots.

2.1.3 Biomimetic Robotics

The advancements of robotics and microsystems technologies have led to a great interest in the biomimetic robotics and in the scientific (biology) fields. In fact, biomimetic robotics can represent today a powerful tool for experimental investigation of the sophisticated mechanisms and amazing sensory-motor performance that many living organisms show.

Building a biomimetic robot allows to thoroughly understanding the biomechanics, control, perception, and behaviour of the reference animal. At the same time, biomimetism can be a key approach to design and develop novel robotic systems, possessing sensory-motor performance more similar to those of the living organisms of the real-world. Mimicking animals, or even plants, requires deep investigation of new materials, mechanisms, sensors, actuators, and control and can lead to breakthrough advances of robotic technologies.

Biomimetic robotics is a science born to investigate phenomena of the biological world that are not yet fully understood. Traditionally the process for the study of a specific phenomenon is the formulation of an hypothesis, the realization of a computational model and the simulation of the phenomenon by the developed computational model for the validation. The simulation must model not only the biological system and the studied phenomenon, but also the external world and the related interaction with them. When a model is studied there is always an approximation and so an error. For this reason, the biological system is often directly used in the experiments, avoiding the modelling of the world and the interactions with that, because the biological system can interact directly with the real world.

On these bases, the use of robotic model instead of the biological system can be powerful in several cases. This robotic model should have suitable biomorphic characteristics in order to be successfully used to perform the planned experiments. Comparing the performances and the behaviour of the robot with the original biological system, it is possible to validate the initial hypothesis [3] (Fig. 3).
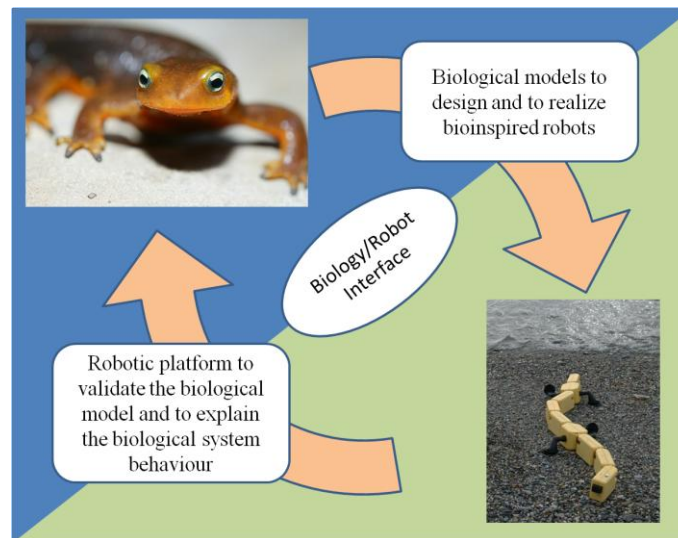
Fig. 3. The bidirectional relation between robotics and biological systems following the biomimetic approach.

This approach is defined cybernetic and it aims at the unification of the study on living organisms and machines. In particular, the machines become models used to test scientific hypothesis in order to produce scientific results.

The cybernetic approach is based on the following elements:

- The technological model (a machine) allows the realization of experiments in more controlled conditions respect to the original biological system;
- The technological model permits to obtain results that cannot be easily anticipated with the formal model;
- The technological model does not need to be biomimetic in all the aspects but just in the functions and behaviours under study.

This approach is functional to three paths:

1. Verify or deny an hypothesis, evaluating if the robotic system and the biological system has the same behaviour or not in the same conditions;
2. Be able to chose between two different options by choosing the robotic behaviour that better replicates the real behaviour;
3. Generating new hypothesis on the functional structure of the biological system.

The cybernetic approach is very ancient, for many centuries the human beings have tried to imitate themselves, but until the end of the 20th century there were technological limitations that blocked the development. The most evident representation of this evolution path is that named *"humanoid robotics",* which for example contributes to the understanding of neuroscientific mechanisms that control the sensomotorial coordination and the human behaviour (neuro-robotics). An important example of study in this field is the activity on the humanoid performed by Waseda University of Tokyo where the humanoid are developed replicating with great detail the anatomy, the morphology and the neurophysiology of the human. It can also used to study the human themselves. This is the case of the

Wabian 2, a humanoid robot capable of advanced bipedal walking that is used to simulate the walking of the elderly people with the aim to develop new assistance accessories [4] (Fig. 4).
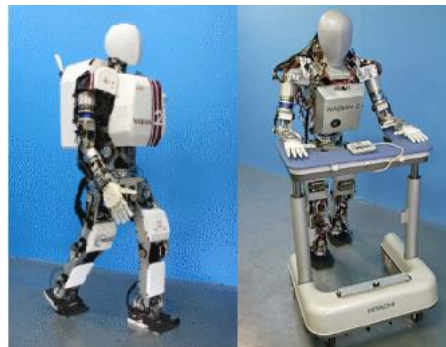
Fig. 4. Wabian as human simulator and instrument to design and evaluate the devices for deambulation.

Another important and very wide branch of the Biorobotic is the "*animaloid robotics*". The enormous amount and variety of leaving organisms that populate earth represent a great source of inspiration for the robotics (e.g. for the study of the locomotion mechanisms). In fact, the leaving organisms swim, fly, run, jump and move quickly in the worst environments, thanks to advanced mechanisms that the scientists and the roboticists aims to understand in order to realize robots with amazing performances. For example the small arthropods are capable to move at high speed over unstructured environment maintaining stability. This is an important characteristic in order to obtain high performances in the terrestrial locomotion. Studies performed on cockroaches have suggested the principles to design the family of the Sprawl robots, quick and stables hexapod robots, capable to run [5] (Fig. 5).
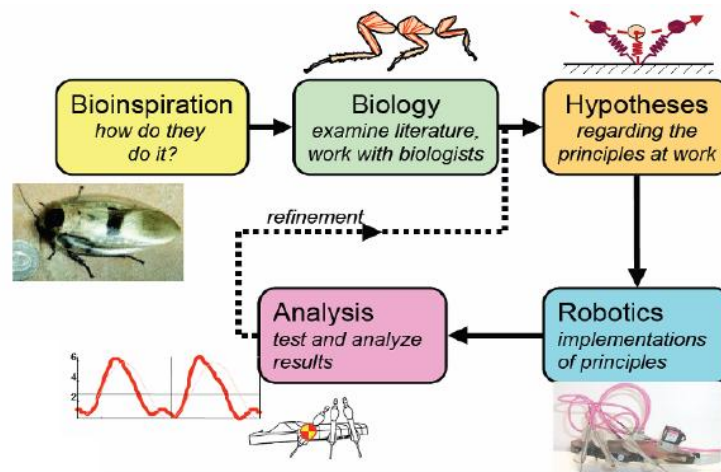
Fig. 5. Analytical study of the cockroach locomotion mechanism for the realization of hexapod robots (Sprawl robots) characterized by high performances in the terrestrial locomotion.

In biology, the study of relatively simple animals permits to acquire knowledge that can be useful for the understanding the behaviour of also more complex animals. For example, the nervous system of the lamprey, even if simple, has similar characteristics respect to the vertebrates nervous system. The study on the lamprey nervous system has permitted to discover the mechanisms for the generation of the

locomotion rhythmic movements of many vertebrates, included those of human [6]. This mechanism has been called "Central Pattern Generator (CPG)". Added to the computational modelling of the CPG and to the model validation through simulations, today Biorobotics permits the robot realization, on the base of the anatomical and morphological characteristics of lamprey, in order to validate the CPG model.

2.1.4 Bioinspired Robotics

Biorobotics can be also used to invent new technological solutions; this permits to talk about biorobotic engineering. An important example in this contest is the surgery, where Biorobotics allowed the realization of integrated surgical systems. Biorobotics consists in this case in the use of a bio-mechatronic approach in order to develop robotic technologies that do not intend to imitate the biological world but that search completely novel solutions starting from the observation of a biological model.

Biorobotics comprises also the area related to the development of limb prosthesis, where one of the most important challenges is the connection of the prosthesis with the brain [7]. To do that, a deep brain and nervous system knowledge are needed.

Another important case of biorobotic technology is the MIT-Manus robot. This robot is used for the rehabilitative therapy of the upper-limb. At the present, it is the most advanced rehabilitation robot for its cinematic characteristics and with the greater potential for clinic application. This great result has been reached because the MIT-Manus robot was designed by a roboticist (Neville Hogan) and a neuro-scientist (Emilio Bizzi) starting from the neuro-scientific knowledge on the control of the upper-limbs.

In the bioinspired robotics there are cases of study that take inspiration from the locomotion and adhesion system of some animals, like worms, for the realization of robots that have the capabilities to move within the human body, for endoscopy. The starting point is the engineering understanding of the undulatory movement made by those animals that permits the robot design [8] (Fig. 6).
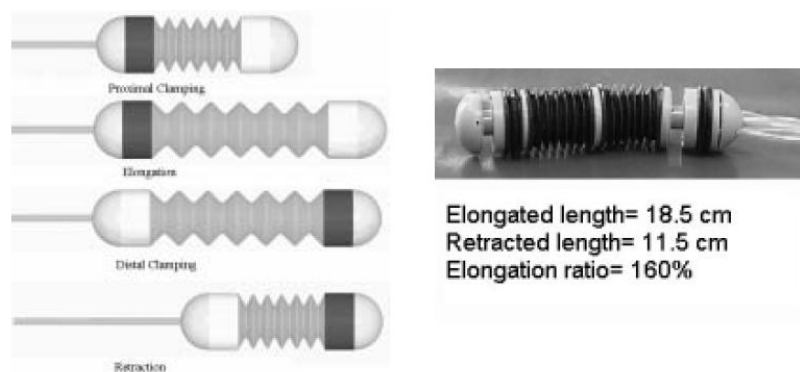

Fig. 6. Realization of an endoscopic probe inspired to the locomotion and adhesion mechanism of the worms.

2.2   Microsystems

Each system composed of several microfabricated components can be considered a microsystem. In the last years, this kind of systems has penetrated the market realizing a wide amount of microdevices for specific applications. Microtechnologies include device technologies such as those used for Micro-Electro-Mechanical-Systems (MEMS), microsystems engineering, micro-machining technologies, micro-sensors and actuators and micro-fluidics. The miniaturization allows a reduction of the required resources both during the production (amount of material) and during the functioning (amount of power consumed). Moreover the scaling potentially guarantees even better performances.

The concept of miniaturization and integration of devices and systems brings mainly to the following advantages [3]:

- Amount of required resources (energy and materials) are drastically reduced;
- MEMS can substitute many discrete components and devices;
- The components can be produced with "batch" processes; that brings to a reduction of the costs and higher reliability during operation;
- Performances for cost and mass unit are higher, that means it is possible to decrease the cost of the whole system, or at given overall costs, increasing performances;
- Faster devices with increased selectivity, sensitivity and wider dynamic range.

One of the research fields that have taken more advantage by this trend is Robotics, but there are also other applications that do not refer to a specific research field but that take advantages from different areas. An example is the so called "Internet of Things". The Internet of Things is a technological revolution that represents the future of computing and communications, and its development depends on dynamic technical innovation in a number of important fields, from wireless sensors to nanotechnology *[ITU Internet Reports 2005:The Internet of Things]*. The importance of micro-technology is in the following areas: communication and systems for automatic identification (RFID); realization of network of sensors; realization of distributed intelligence by providing the devices spread in the environment of embedded intelligence; sensor and actuator technologies. Finally, advancements in miniaturization and nanotechnology mean that smaller and smaller things will have the ability to interact and connect. A combination of all of these developments will create an Internet of Things that connects the world's objects in both a sensory and an intelligent manner.

A microsystem can be considered composed by actuators and sensors that interact with the environment and a control system that manages them. Microsensors detect changes in the parameters to be controlled; the controller then operates microactuators based on information from the sensors, to bring the parameter to be controlled within the desired limits.

2.2.1 Microsensors

Micromachining and MEMS are technologies that have improved the market of sensors for the great performance, low size and cost that have the sensors realized. The most important voice in the MEMS market is microsensors. One of the most important fields that have made profit from the development of the microfabrication is the micromachined inertial sensors: silicon micromachined accelerometers and gyroscopes. These sensors are one of the most important types of silicon-based sensors. Microaccelerometers and pressure sensors have the largest sales volume, and for gyroscopes the expecting for the next years are similar. The large volume demand for accelerometers is due to their automotive applications (air bags, vehicle stability systems and electronic suspension). However, accelerometers are used also in biomedical applications for activity monitoring, in sport equipment, in videogame console and in robot positioning. High-sensitivity accelerometers are crucial components in robot navigation and guidance systems. The impact of low-cost, small, high-performance, micromachined accelerometers in these applications is not just limited to reducing overall size, cost, and weight. It opens up new market opportunities such as personal navigators for consumer applications, or it enhances the overall accuracy and performance of the systems by making formation of large arrays of devices feasible [9]. Micromachined gyroscopes for measuring rate or angle of rotation can be used either as a low-cost miniature companion with micromachined accelerometers to provide heading information for inertial navigation in robotic application (both terrestrial and marine) or in other areas, including automotive applications for ride stabilization or some consumer electronic applications, such as video-camera stabilization.

These sensors are essentially based on silicon technologies. An accelerometer generally consists of a proof mass suspended by compliant beams anchored to a fixed frame. External acceleration displaces the support frame relative to the proof mass, which in turn changes the internal stress in the suspension spring. Both this relative displacement and the suspension-beam stress can be used as a measure of the external acceleration.

Other kinds of sensors that have taken advantage by the miniaturization are gas sensors. An example of this kind of sensors is the MOX (metal oxide) sensor. These sensors are characterized by a hotplate that through a flowing current can rises up the temperature up to 300-400 °C in a limited area. In this way, an active material lied down on this hotplate reacts with selected gas and changes its electrical characteristics (in particular the resistance). Many commercial gas sensors are based on this technology. Metal oxide gas sensors change in their electrical resistance in the presence of reducing or oxidising species. In particular, tin and tungsten oxide based sensors behave as n-type semiconductors and their resistance decreases in the presence of oxidising species such as ethylene, ethanol or ammonia. In recent years, several Universities and Research Institutes have developed micromachined hotplates for a variety of applications where a high operating temperature must be achieved. Several technologies are used, aiming at realising small heated structures featuring a low thermal mass and a good thermal

isolation from the surrounding objects. In most cases, Silicon technology is used, and the isolation is mostly achieved by thin dielectric membranes (Si_3N_4 and/or SiO_2) [10] or by porous Silicon structures [11]. The hotplates are designed to be robust and stable for temperatures as high as 600°C [12].
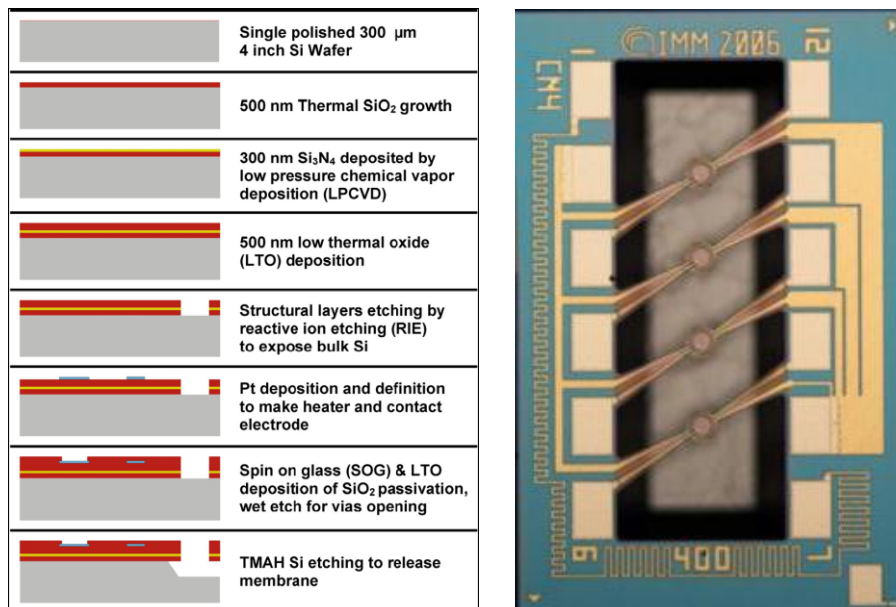
Fig. 7. Ultra Low Power (ULP) hotplate fabrication process flow and picture (CNR IMM, Bologna).

The resulting MOX sensor presents a power consumption of few mW and a footprint of only 1.5mm×1.0mm for a four sensors array chip. This permits to enable some emerging applications like portable devices, wireless sensor networks or semi-passive RFID tags [13], [14], [15].

Another example of technology for gas sensors fabrication is the thin film technique. A thin film of different metal in presence of some gas typologies can react with that. This results in a change of resistance. This behaviour can be used to realize thin film sensors. An example of this sensor typology is the mercury sensor realized at the CRIM Lab of Scuola Superiore Sant'Anna di Pisa [16], [17], [18].

The gaseous mercury sensor realized is based on the resistivity changes of thin gold films. The sensor consists of four identical thin gold film resistors mounted in a Wheatstone bridge configuration. In order to minimise the influence of temperature variation, two resistors work as sensitive elements while the others work as reference. The absorption of mercury on the gold film produces a change in the resistivity of the film itself. The resistance increase, due to a partial mercury overlay on gold, is produced by the change in the surface scattering of the electrons. The deposition of thin gold films is performed by sputtering deposition. The thickness of the gold film is 200 nm.
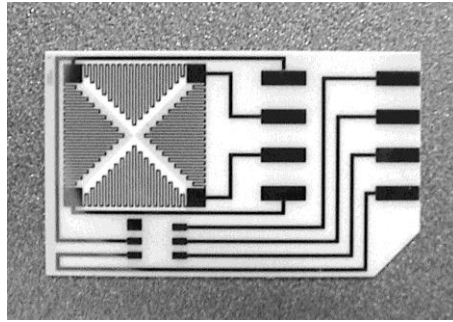
Fig. 8. Mercury sensor developed at the CRIM Lab.

The sensors can be integrated both in static sampling station than in mobile devices. An example of mobile device for personal monitoring is the dosimeter developed at the CRIM Lab of the Scuola Superiore Sant'Anna to monitoring the exposition of a worker [19]. Another possible application is the integration of these sensors in mobile platform for mapping and source finding in polluted areas [20], [21].

2.2.2 Microactuators

The development of microactuators is less mature than that of microsensors because of the initial lack of appropriate applications and the difficulty to miniaturize the actuators of the macroscopic world. Although the earliest microactuators were driven by electrostatic forces, devices now exist that are driven by thermal, thermal phase-change, shape-memory alloy, magnetic and piezoelectric forces to name a few. Each method has its own advantages, disadvantages and appropriate set of applications [22]. The choice of the actuator has a fundamental role in many applications as in the robot. The shape, the size, the weight, the strength, the time of response of the actuation system are in fact important parameters that reflects on the potential performances and capabilities of the robot and usually they fix the greater limits [23].

Nowadays the actuators represent the real bottleneck in most of the robotic applications, especially in the biomimetic robotics, where the objective is to develop robots with locomotion and manipulation capabilities similar to those of the leaving organisms.

The use of conventional actuators in robotics presents the advantage of a known, tested and reliable technology; the used actuators are an evolution of the motor employed in the industrial automation. The more used traditional actuation systems are:

- pneumatic actuators, that convert the energy supplied by a compressor in mechanic energy through pistons and air turbine;
- hydraulic actuators, that convert the hydraulic energy in mechanic energy through suitable pumps;
- electric actuators, that convert electric energy in mechanic energy.

The conventional actuators present the following characteristics:

- big acceleration;
- high positioning precision;
- high power/weight ratio;
- wide speed range.

The traditional actuators present a series of drawbacks, if used in biomimetic applications:

- high weight;
- size of the overall system (actuator, batteries, compressors, ..);
- miniaturization problems;
- stiffness of the structure.

For these reasons for many years alternative solutions to the traditional actuators have been studied [24]. These researches have looked to the Nature and to the actuation solutions found by it in order to provide the biology organisms of movement capabilities: the muscles. The muscles present a wide number of characteristics that researchers try to replicate in order to realize an equivalent artificial device in terms of functionalities. The development of artificial muscles that replicate the performances of the biological muscles can support the development of robots with manipulation and locomotion capabilities impossible to replicate by the conventional mechanisms [25].

This approach in the last years has contributed to the technological progress with the introduction of new materials with amazing characteristics. These materials are known generically as *smart materials*, e.g. SMA (*Shape Memory Alloys)* and the EAP (*electroactive polymers*) [26], [27], [28], [29].

Another example of actuation mechanism extremely interesting is that realized by the Nature for the vegetal kingdom, which will be described in detail in the next paragraph. In particular in this thesis it will be approached the possibility to realize an innovative class of bioinspired actuators that take inspiration from the locomotion/growth mechanism of the plant roots for underground extension. Moreover, there are many other characteristics and amazing properties of the plants that make these organisms original and interesting from the biorobotic point of view. The study for the realization of a plant root bioinspired actuator is a part of a wide research area that aims at expanding the biorobotic concept to the vegetal kingdom for the realization of plantoids.

In the next paragraph a wide description of the main characteristics and functionalities of the plants has been supplied with particular reference to the roots characteristics.

2.3 Plants: a new source of bioinspiration and biomimicking

Bioinspiration and biomimicking are often associated to inspiration from animals and human beings. In this thesis, the concept of bioinspiration and biomimicking has been extended to the plant world.

Plants are organisms characterized by an aerial part and a root system. In order to compensate their sessile nature, they have developed growth responses to deal with the copious and rapid changes in their

environment. These responses are known as tropisms and they are marked by a directional growth response that is the result of differential cellular growth and development in response to external stimulations such as light (phototropism), gravity (gravitropism), touch (thigmotropism) or water/humidity gradient (hydrotropism) [30], [31]. The combination of these mechanisms allows plants to overtake hostile or inaccessible environments and colonize the soil, leading to the generation of ramified root systems that assure their stability and survival. For that purpose, root systems often far exceed in mass and length the aboveground portions of the plant, being provided with few to many main roots and thousands of ramifications. Moreover, in spite of their slenderness and delicate structure, the spiralling forward thrust of the root tips and the pressure of their expanding cells are sufficient to split solid rock. The process by which plant tissue expands in tight places involves water uptake through osmosis and imbibitions, and an overall increase in size by cell division. Currently, there is a general agreement that higher plants are not only able to receive diverse signals from the environment but that they also possess mechanisms for rapid signal transmission [32]. In fact, each root tip is able to get information from the environment by their embedded sensors; the information is then transduced and processed in the whole root system and used to direct the growth towards regions of the soil with the best minerals and water availability, slowing down and stopping to grow, thus saving energy, whereas a too compact soil or a hostile environment do not allow life. Moreover, on the surface of the epidermis of the distal portion of the root, tiny cellular projections called root hairs extend into the soil to absorb water and minerals. Root hairs are a competitive tool to increase the surface area of the roots, increasing the capacity to absorb nutrients and water. Therefore plants demonstrate to successfully reach their needs even without a conventional locomotion system. Although plants cannot physically move, active root growth allows exploration of soil niches for nutrition. This implies that root apices are not only sites of nutrient uptake but also sites of forward movement.

2.3.1 Structure of the whole plant

The concept of plant is very wide; there are more than 350000 species and it is difficult to characterize uniformly all the typologies. In this thesis the analyzed species are the Plants that are composed of:

- roots, that aims at anchoring the plant to the soil and at water and nutrients up-taking;
- trunk and stems, that are the structure of the plant, they sustain the whole plant and contain the vessels for lymph transportation;
- leaves, that carry out the photosynthesis supplying nutrients to the plant.

The tissue systems are continuous throughout the plant, and the functions of the different organs are interconnected. Understanding plant structure and function requires the study of each organ and the tissue systems in a coordinated way.

Aerial part of a plant is intimately correlated with the surrounding environment. Because of its sessile nature, a plant must organize rapid and specific responses to any changes in vital environmental

parameters, such as light, changing the direction of growth and the exposure of the photosynthetic machinery towards optimal locations (i.e. escaping from high or weak irradiance). Basically, shoots respond positively to two main physical parameters: light and gravity. Regarding the response to light, heliotropic leaf movements are active responses to the movement of the sun. It has been well documented that heliotropic leaf movements are induced by blue wavelengths but not others. In many plant species, plant parts that become shaded move away by tropic growth, a phenomenon termed phototropism [33]. Plants are capable to distinguish between the light reflected from, or transmitted through, neighbouring vegetation. In particular reflected light is a red to far-red (R : FR) ratio lower than that of light that has not passed a plant canopy. Photomorphic responses to low R : FR ratios are used by plants for shade avoidance and it is useful to elevate leaves towards unfiltered daylight [34].

The above part of the plant is essentially devoted to the energy collection. Photosynthesis is fundamental to plant metabolism, and the acquisition of radiant energy and CO_2 is critical for plant growth. Radiation that is photosynthetically active (PAR) represents only a part of the visible light. In particular, only the wavelength between 400 and 700nm are adsorbed by the plants for their metabolism, instead other wavelengths affect the plant behaviour. The energy collection is not the only functionality of the above part. In fact, it has sensible to a wide amount of different stimuli (Fig. 9).
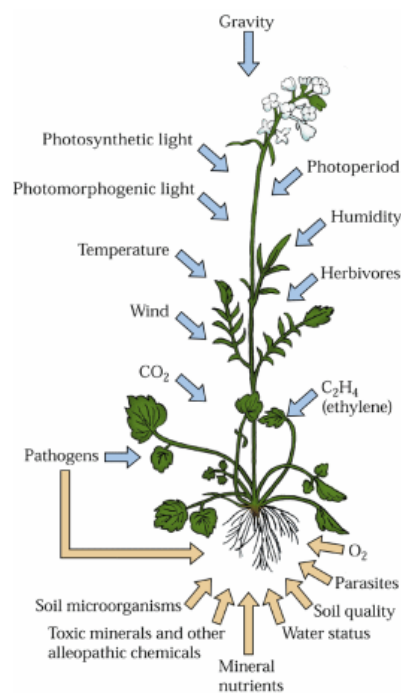

Fig. 9. The wide amount of stimuli that plants sense.

The most important (as already specified) are light and gravity, but there are also other interesting stimuli, as the sensibility to the CO_2. Plants respond to changes in CO_2 concentration of their immediate environment by adjusting the size of stomatal pores to the CO_2 demand of photosynthesis and to plant

water status. Other stimuli are wind, temperature, humidity that are useful to the plant to understand the environment conditions and optimize the energy allocation in order to permit the plant survival.

2.3.2 Root system and its architecture

Plant root systems perform many essential adaptive functions including water and nutrient uptake, anchorage to the soil and the establishment of biotic interactions at the rhizosphere. Evidently, roots monitor a wide spectrum of physical and chemical parameters, and then integrate the signals obtained in order to perform appropriate and often complex growth responses to cope with the immediate environmental circumstances. The more acute sensitivity of roots to various types of signals already mentioned, when compared to shoots, is related to the root apex.

Changes in the architecture of the root system, therefore, can profoundly affect the capacity of plants to take up nutrients and water. Three major processes affect the overall architecture of the root system. First, cell division at the primary root meristem (i.e. of initial cells) enables indeterminate growth by adding new cells to the root. Second, lateral root formation increases the exploratory capacity of the root system; and third, root-hair formation increases the total surface of primary and lateral roots. Alterations to any of these three processes can have profound effects on root-system architecture and on the capacity of plants to grow in soils in which water and nutrient resources are limiting.

As a preliminary example of plants' ability to form an extensive, wide and deep root system, in the desert the roots of mesquite (genus *Prosopis*) may extend down more than 50m to reach groundwater. Annual crop plants developed a root system that can usually grow until 2.0m in depth and extend laterally to distances up to 1.0m. As a general behaviour, the annual production of roots may easily surpass that of shoots, so the aboveground portions of a plant can be correctly defined as the tip of an iceberg.

The apical region of a plant root is called root apex and morphologically includes three regions: meristem, transition zone, and elongation region (Fig. 10).
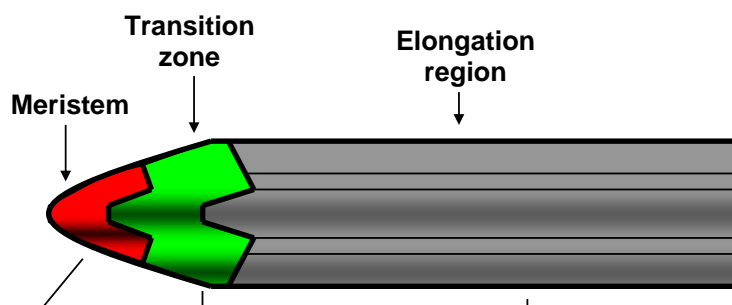
**Fig. 10.** On the basis of cytological observations, growing root apex is composed of three distinct zones: an apical Meristem or Division Zone (with fast dividing cells), an Elongation Zone (composed by elongated-shape, mature and almost fully vacuolated cells, with the nucleus close to the cell wall) and a Transition Zone, a unique zone intercalated between the two more obvious regions. ([32]).

The meristem is mainly delegated to cell division, which happens in both the direction of the root base in order to form new-born cells with the aim to differentiate into the tissues of the functional root and to form the root cap in the direction of the root apex.

Cell division at the real root apex proper is relatively slow; for this reason this region is known as the quiescent center. After a few cycles of slow cell divisions, root cells displaced from the apex by about 0.1 mm begin to divide more rapidly. Cell division again tapers off at about 0.4 mm from the apex, and the cells expand equally in all directions. After the transition zone, the root apex shows the elongation region, which begins 0.7 to 1.5 mm from the apex. In this zone, the elongation of the cells goes on a very rapid manner.

Root hairs, with their large surface area for absorption of water and solutes, first appear outside the proper root apex, in another region called the maturation zone. Here that the ascendant conducting pathway of the plants (xylem) develops the capacity to translocate substantial quantities of water and solutes to the shoot [33]. The formation of root hairs increases the volume of soil in contact with, and therefore exploitable by, the root.

2.3.3 The transition zone: a 'command centre' for the environment exploration

A new vision of the root system comes out from the morphological observation that root apices are composed of three distinct zones, the interplay of which allows their effective exploration of soil [32] in searching both nutrients and water. In standard conditions, root cell elongation is much more rapid than the shoot cells one: as a consequence, any cell division in the region of rapid elongation is not allowed. On the contrary, cell cycling and cell elongation occur concomitantly in shoot apices. The clear separation of division and elongation regions in root apices permits to identify a very unique zone, the so-called transition zone, included between the two other (and well-known) regions [36], [37], which is a peculiar region for environmental sensing. In fact, this region is able to detect more than 10 chemical and physical parameters from the surrounding environment.

Experimental evidences show that root apices are the main sites for the first perception of low-temperature [38] and drought [39], and are able to immediately transmit the information to the aboveground part. Root apices serve also for plant-to-plant communication, as they can emit and receive volatiles, whose production is induced by the herbivore attack of above-ground organs [40], [41]. Particular interest is directed to the polar auxin transport, which is accomplished along very complex pathways in root apices. The transition zone is a sort of processor or command centre which, processes sensory information from the surrounding environment, stores memories and takes decisions about future exploratory and adaptive root behaviour. The command centre needs a huge amount of ion-channel activity. All these processes also require an enormous ATP consumption: consequently, it is logical that the transition zone cells should also have the highest oxygen requirements of the whole root apex, more than the division zone. The peak of oxygen uptake coincides with the peak of synaptic auxin

transport [42] but is also extremely sensitive to gravistimulation. Repositioning a growing root apex from vertical to horizontal position induces extremely rapid changes (in the order of a few seconds) in oxygen uptake at the upper side of such a gravistimulated root.

2.3.4 The root cap and the soil penetration

Plant roots may exert pressures of up to 1MPa in order to penetrate hard soils [43]. Consequently, virtually all plants which grow in soil have evolved root caps which protect the root meristem from physical damage or abrasion by soil particles.

Root cap consists of mucilage-secreting cells (one to two layers beneath the lateral and peripheral tissue surface); the cap cells are continually being produced by the meristem and, after a period of hours or days, sloughed off from the outer surface of the root cap where may remain alive for a period of days after being detached from the root cap [44]. Despite the full knowledge of the mechanism that leads to the so called mucigel production, very poor certainties are given about its precise function. It has been suggested that lubricates and protects the root apex, promotes the transfer of nutrients to the root, and affects the interaction between roots and soil micro organisms. The root cap is also central to the perception of gravity, the signal that directs the growth of roots downward: this process is termed the gravitropic response.

The root cap must, therefore, play an important role not only in protecting the root meristem from damage, but also in determining the mechanical interaction between the root and the soil, namely the mode of soil deformation and the root–soil friction [45].

The mechanical resistance of the soil to root growth can be separated into two components: the pressure required deforming a cavity (in the soil) that is large enough for the root; and the pressure required to overcome the frictional resistance between the soil particles and the moving surface of the root. The resistance of the soil to deformation results in a pressure on the surface of the root which, in turn, is the cause of the frictional resistance between the root surface and the soil. The frictional stress, τ, between soil and the surface of a root is given by the equation   (**1**) [46]:

$$\tau = \sigma_N \tan\delta + c_a \qquad (1)$$

where σ_N is the stress normal to the surface of the root, δ is the angle of friction between the two surfaces, and c_a is the tangential component of adhesion between the surfaces. The direction of the frictional resistance is opposite to that of the velocity of the moving surface of the root. The total resistance to the elongation of a root is, therefore, the sum of the components of the cavity expansion pressure (= N), and in the axial direction. It is well proved that both mucilage exudation and root cap sloughing seem to participate in eliminating practically all frictional resistance to root growth [47]. A root cap cell will only move relative to the root if the friction between the cap cell and the surface of the root is smaller than the friction between the cap cell and the surrounding soil. Thus, in order for a cap cell to move relative to the root, the coefficient of friction between the cap cell and root surface

(including any adhesive forces) must be smaller than between the cap cell and the soil. Hence, by definition, a sloughed cap cell decreases the frictional resistance to soil penetration [46].

Removal of the root cap has recently been shown to halve the elongation rate of maize roots grown in compacted sandy loam soil (penetrometer resistance 1.0MPa), whereas root elongation rate was unaffected in loose soil (penetrometer resistance 0.06MPa) [48]. The reason for the slowing of root elongation was the associated increase in the root penetration resistance, equal to the force exerted per unit cross-sectional area of root tip, from 0.31MPa to 0.52MPa. This again demonstrates that the intact root cap and its associated border cells and mucilage facilitate root penetration by decreasing the coefficient of friction between the root surface and soil particles [46]. The relative contributions of border-cell sloughing and mucilage to decreasing root penetration resistance have been estimated as 58% and 42%, respectively, for maize roots grown in loamy sand soil [49].

2.3.5   Root growth

Models for root growth have not only been developed for the topological description of the complicated networks of root systems, but also for the growth of individual roots as their modular basis. For example, the growth of the root apex has been modeled using growth tensors and natural coordinate systems [51], [52]. Other authors have concentrated on the distribution of growth (velocity and rate) and also on cell length [53], [54], [55]. The distribution of growth is essential to understand the adaptation due to nutrients availability. Until now the approach to model such distributions has been based on conservation and kinetic equations, such as those used by Silk [56]. Mechanistic understanding of root growth needs to take into account the architecture of the root growth zone. The response of growing roots to their environment is a function of their cellular compounds [53]. As a given region of the plant axis moves away from the apex, its growth velocity increases (the rate of elongation accelerates) until a constant limiting velocity is reached equal to the overall organ extension rate. The reason for this increase in growth velocity is that with time, progressively more tissue is located between the moving particle and the apex, and progressively more cells are expanding, so the particle is displaced more and more rapidly. In a rapidly growing maize root, a tissue element takes about 8 hours to move from 2mm (the end of the meristematic zone) to 12mm (the end of the elongation zone).

Beyond the growth zone, elements do not separate; neighbouring elements have the same velocity (expressed as the change in distance from the tip per unit of time), and the rate at which particles are displaced from the tip is the same as the rate at which the tip moves through the soil. The root tip of maize is pushed through the soil at 3mm·h^{-1}. This is also the rate at which the no growing region recedes from the apex, and it is equal to the final slope of the growth trajectory.

The velocity increases with position in the growth zone. A constant value is obtained at the base of the growth zone. In the rapidly growing maize root, the growth velocity is 1mm·h^{-1} at 4mm, and it reaches its final value of nearly 3mm·h^{-1} at 12mm.

In physical terms, cell growth can be defined as an irreversible increase in cell volume and surface area [57]. Plant protoplasts are characterized by an univocal structure and organization, as they are surrounded and encased by a rigid, but expandable, cell wall due to elastic characteristics. The cell wall is infiltrated with water containing only a very low osmotically active amount of solutes. This situation enables the formation of a large difference in osmotic pressure ($\Delta\pi$) between the apoplastic and the symplastic space (0.6-1.0 MPa), compensated by a hydrostatic pressure, named turgor (P), of equal value when the cell is in a fully turgid state. The cell can be described as a simple osmometer that can enlarge by water uptake powered by a difference in water potential ($\Delta\Psi$) between protoplastic and simplastic space.

$$\Delta\Psi = \Pi - \Delta\pi \qquad (2)$$

According to eq. (2), water uptake driven by $\Delta\Psi$ can be achieved in two ways [57]: increase of π in the protoplast. In this type, cell enlargement is reversible (i.e. stomata guard cells) decrease in P. For producing growth, irreversible increase in cell volume is needed, and this mechanism is the most suitable. The only way to achieve this is by lowering the counter pressure exerted by the cell wall on the protoplast, and this happens only if the cell wall is a tensile stress state due to the turgor, and this stress is released by changes in the mechanical properties of the wall material (stress relaxation by wall loosening). Continuing wall loosening permits to liberate a driving force for water uptake, and it will restore the turgor to its previous level. This mechano-hydraulic process produces irreversible cell enlargement, namely growth. As growing cells generally maintain a constant $\Delta\pi$ by the osmoregulation process, they can reach a steady-state growth for hours or days.

Root growth can be described by a two-level characterisation: individual root elongation, and a network expansion through branching. Recently, [58] proposed a novel approach to model growth distribution, finding that the root apex can be modelled by a string of dividing and growing (elongating) cells controlled by hormones. In fact, active auxin transport is essential for the control of cell division, elongation and differentiation [59], while cell extensibility, turgor and water conductivity influence the growth rate profiles of roots. In 1965, Lockhart [60] formulated the following empirical equation for the description of cell growth rate in length:

$$g = \frac{dl}{dt} = l\phi(\Psi_p - Y) \qquad (3)$$

where g is the growth rate (μm min^{-1}), l is the cell length (μm), Φ is the wall extensibility (MPa$^{-1}\cdot$min^{-1}), Ψ_p is the turgor pressure (MPa) and Y is the yield threshold (MPa).

As growth occurs by uptake of water transported through the cell wall and cell membrane, the cell can also be described as a simple osmometer:

$$\frac{dV}{dt} = -A_s L(\Pi + P) \qquad (4)$$

where V is the volume of the cell (μm^3), As is the area of the cell surface (μm^2), L is the conductivity coefficient ($\mu m \cdot min^{-1} \cdot MPa^{-1}$) and Π is the osmotic potential (MPa).

2.3.6 Hormones and growth. The role of auxin

The growth and development of root cells and tissues rely on the establishment of cellular and sub-cellular asymmetries. The formation of the real cell shape and the positioning of molecules in the intracellular space commonly involve a persistent directional orientation along an axis, named cell polarity. Polar transport of auxin is directly linked as a signal to the regulation of both growth and polarity in the plants. As the plant body is shaped in response to numerous environmental stimuli (i.e. light and gravity; [61], [62]), these factors are able to influence the transport of auxin in a way that this hormone is delivered to tissues induced to grow via the establishment of auxin gradients, transport and response. Auxin is transported across the whole plant body via effective cell-cell transport mechanisms involving both the symplast and the apoplast. Cellular auxin influx and efflux, and the mechanisms that mediate the delivery and removal of potential polar auxin transport components from the plasma membrane, remain still open and discussed. For example, it is not clear why auxin bypasses the cytoplasmatic channels of the plasmodesmata crossing through the apoplast, as their diameter could easily accommodate several auxin molecules. Active auxin transport mediates cellular auxin concentration and is therefore a crucial component in the coordination of plant development. However, the specific relationship between auxin signalling and auxin transport is still quite unknown.

2.3.7 Tropism in plants

Plants, along their evolution, have had to face and solve a variety of problems to survive: developing support structures, creating a system of transport of water and nutrients through the whole organism, protecting the delicate reproductive organs, assuring the reproduction in the most convenient period of the year, improving the mechanisms of adaptation to the variable climatic conditions etc. All these needs has led to large modifications in metabolism and has brought to the acquisition of sensorial structures to set up a precise biological clock necessary to guarantee the constant monitoring of the surrounding situation to acclimatize them.

Plants can sense gravity, temperature, light quality and direction, etc., and if necessary they can act consequently. Plants feed themselves, breathe, and fight the infections. They live in continuous competition both with environmental agents and with other plants for the conquest of light, space and nourishing substances, and all those necessary elements to their survival. Due to their sessile nature, plants are forced to make the most of their immediate surroundings, which means adapting to an ever-changing environment. So they have been adapted to perceive and react to adverse situations with varies useful movements to the survival. Darwin noted that plants had a tendency to sense their environment so as to orient themselves for optimal growth and development, and he dedicated part of his studies to vegetal biology publishing with his son Francis a fascinating book "The Power of Movement in Plant"

[64] in which he encloses many interesting observations on plant life with special interest in movement. Darwin studied the two great categories of "movements in the plants": "tropisms" (directional movements in answer to external directional stimuli) and "nastic movements" (movements in answer to external stimuli, but independent to their direction). Plants are constantly being bombarded with changes in their environment. Temperature fluctuations, not enough light or water content in the soil, are just a few of the factors to which plants must be able to respond. Moreover, plants must respond to physical forces of nature such as gravity or touch stimulation. Plant tropisms are operationally defined as differential growth responses that reorient plant organs in response to direction of physical stimuli. An example of tropism regards the perception of gravity, also called "Gravitropism". "Phototropism" is the directional response in answer to a luminous source. Tropisms can be negative, such as a stem bending away from a gravity stimulation [65], or they can be positive, as in a stem bending toward a light stimulation [66] while example of nastic movements are the closing leaves, modified as fly-trap, of *Dionea muscipola*, the fast closing of the composed leaves of *Mimosa pudica* to a tactile stimulus, or the closing leaves of many leguminous during night (nictinastic movements). Darwin studied also another type of movement, oscillating and rhythmic, called "circumnutation": plants, during their growth, perform circular movements around a central axis [67]. Nearly all the plants present this growing movement, however it turns out to be more obvious in some species rather than in others, such as climbing plants.

Therefore tropisms are that group of reaction mechanisms that the plant acts in relation to directional stimuli. The most known and studied are:

- Phototropism – the answer to light
- Gravitropism – the answer to gravity
- Electrotropism – the answer to an electric field
- Hydrotropism – the answer to a gradient of water in soil
- Touchtropism - the answer to the presence of obstacles

Phototropism

Plants need light to grow. They will do everything they can to get as much of it as possible. One of the ways plants maximize their amount of light is phototropism or "moving toward light". Since most plants cannot really move their whole body, they move part of it. When light is all around, the plant grows straight, but if light is coming from only one side (for instance, from a window) plants will start to grow toward the source of the light. Stems exhibit positive phototropism (growth towards the stimulation), while roots exhibit negative phototropism (growth away from the stimulation). The way the plant does this is by making one side of the stem grow faster than the other side. This causes the bending. The part away from the light (the darker part) grows faster, and this has the effect of getting the rest of the plant closer to the light. The responsible of this asymmetric bending is a plant hormone, auxin. Auxin is produced at the tip of the plant and goes down promoting the elongation of cells. When

one side is darker than the other, more auxin goes to the darker side and it grows faster, bending the stem toward the light.

Gravitropism

Plants answer to a series of stimuli during their development, and gravity represents the main one. In the earth gravitational field the vegetative shoots grow upwards in order to maximize the absorption of light for the photosynthesis, while the roots grow towards the bottom for better supplying water and nutrients. This directional increase of plant organs in answer to the gravity force, takes the name of "Gravitropism". The mechanism of perception of the gravity is localized in the root tip, and in particular in the root cap, where gravity is perceived by amyloplasts that lay down at the bottom and give to the cell the information of the gravity vector. This theory, commonly famous like "starch/statolith hypothesis ", due to the sedimentation of the amyloplasts in the cells of the cap, is proposed to be the first step in the gravitropic response ([68], [69]). When laser ablation was used to remove the central root columella cells in Arabidopsis, a large inhibitory effect was seen with respect to root curvature in response to gravity stimulation [70]. Genetic studies using mutants that have few or no endodermal cells, lack amyloplasts, or have a problem in sedimentation of amyloplasts have proven to be useful tools in establishing the necessary role of the organelle in a plant's ability to respond to a change in gravity stimulation. More recently, however, other theories funded on scientific evidences have been formulated and the gravitropic response mechanisms are still controversial.

An important question in sensor physiology is the determination of the threshold dose of a stimulus in order to provoke the reaction of the plant organ. For the gravireaction of plant roots, it has been noticed that gravitational stimuli which last 1 s (perception time) can be actively perceived by plant roots [71], but one single stimulus is not sufficient to determine any organ response. So, a minimum time of continuous stimulus must occur (presentation time). Experimental data [71] shows that the presentation time is probably less than 10 s in roots in ground experiment. However, Mancuso et al. (unpublished data) found that during parabolic flights, the minimum presentation time for the evoking of a physiological response (in that case, a change in oxygen influx pattern) in maize roots was less than 2 sec after the beginning of microgravity conditions.
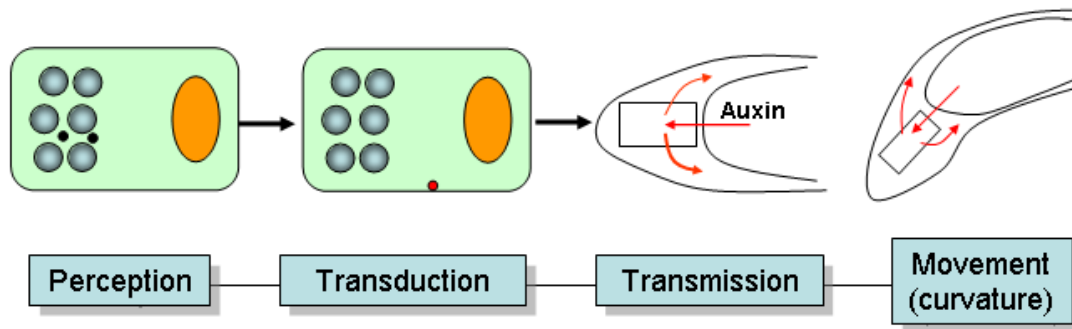
Fig. 11. The different phases of root gravitropism. When a root is subjected to a change of orientation in the gravitational field, the stimulus is perceived in less than 1 s. However, this 1 s stimulus is not sufficient to induce a gravitropic response – it must be repeated about ten times (or the stimulation must last 10 s) to initiate an asymmetrical signal within the statocytes (transduction phase). This leads to a downward lateral movement of auxin (transmission phase) that is the cause of the differential growth occurring after a latent time of 10 min. The four phases are represented in sequence but perception, transduction and transmission can persist for the whole period of the gravitropic reaction. The black circles represent activation of mechanosensors by amyloplasts. The red circle represents the start of the relocation of auxin efflux carriers. The green spheres represent the amyloplasts and the purple sphere represents the nucleus.

Electrotropism

Like all living tissues, the cells of plant roots produce an electric field due to the activities of ion transporters. This ion movement creates a flow of current through the tissue and the formation of electrical potential differences across the membrane. These electric fields can polarize cells and tissues and can affect growth of the root. For instance, electric fields may generate a lateral asymmetry of ions and hormones in the elongating zone. Application of electric fields can modify the direction of growth of certain plant cells or organs. This phenomenon, known as electrotropism, has been reported in fungi [72] and algae [73] as well as in roots [74], [75], and shoots [75]of higher plants. The preferred direction of growth relative to the applied electric field varies with the type of cell or organ tested and, in some cases, is species dependent. Some studies demonstrate the effect of electric field on the primary root of maize (Zea mays L.). Using different intensity of voltage, it has been observed a root curvature towards cathode.

Hydrotropism

Roots display hydrotropism in response to moisture gradients, which is thought to be important for controlling their growth orientation, obtaining water, and establishing their stand in the terrestrial environment. However, the molecular mechanism underlying hydrotropism remains unknown. Although some studies have identified the existence of hydrotropism (the directed growth of roots in a moisture gradient), it has proven difficult to differentiate between this response and gravitropism because the latter always interferes with the former here on Earth [76]. However, by using an agravitropic mutant (i.e. pea mutant ageotropum) or clinorotation to randomize the angle of gravitropic stimulation so that plants no longer exhibit gravity-directed growth, positive hydrotropism in roots has been demonstrated

[77], [78]. This rediscovery of a genuine hydrotropism in roots enabled us to elucidate some physiological aspects of hydrotropism and its universality in a wide range of plant species [76], but the underlying mechanisms that regulate hydrotropism remain unknown. Although the ecological role of hydrotropism in nature still needs to be clarified, the root response is thought to be important for finding water. Considering that limited water availability and/or precipitation affects agriculture and ecosystems throughout the world, understanding the molecular mechanisms mediating hydrotropism in roots could lead to methods for improving crop yield and biomass production. Compared with gravitropism, hydrotropism has not been popular in genetic studies because of the difficulty of establishing a large-scale screening system that provides an appropriate stimulus–response interaction. Therefore, the implementation of a screening procedure for the isolation of mutants with aberrant responses to water potential gradients is remarkable [31]. Putative mutants are selected based on their inability to develop a positive hydrotropic curvature and their failure to sustain continuous growth in the severe water-deficit conditions of the medium – this is important for distinguishing hydrotropic mutants from drought mutants. In our screen, we found only two negative hydrotropic mutant alleles (including one that germinates poorly). This is perhaps a consequence of either the screening medium (for instance, the threshold water potential for hydrostimulus perception was not developed in the plate) or of the low number of loci involved in the signaling mechanism of water sensing.

Touchtropism

Plant roots must sense and respond to a variety of environmental stimuli as they grow through the soil. Obstacles such as rocks will impede the general downwardly directed. The cells of the root cap are the first to encounter obstacles and new environments as the root grows through the soil, making them strong candidates for the site where sensors for touch are located. Touch modulates the gravity reaction in order to overpass such kind of obstacles. About the Arabidopsis has been demonstrated [84] that roots exhibited a differential growth response upon contacting the obstacle that directed the main axis of elongation parallel to the barrier. This growth habit was maintained until the obstacle was circumvented, at which point normal gravitropic growth was resumed.

3 Plantoid biomechatronic design

3.1 System functionalities and application scenarios

The plantoid has been conceived to mimic the plant behaviour in some aspects. In particular, the biomimicking is focused on the plant capabilities to penetrate the soil, to monitor the environmental chemical/physical parameters both above and underground and to move itself on the base of the received stimuli. These characteristics make the plantoid the ideal instrument to monitor itself, i.e. other plants, for example in agriculture applications. Nowadays the monitoring in the agriculture field is performed by using fixed stations installed by the control institutions for meteorological or hydrological applications. Some more advanced farms have also a personal station placed in a specific point of the field that assures the monitoring in a more accurate way. Anyway, these solutions do not take into account the microenvironment. In the same field there is the possibility to found similar plants subjected to different stresses. This is due to the specific composition of the soil, the slope of the field, the shading, the proximity with other cultures, the exposure to the wind, etc. For this reason in the last years the Wireless Sensor Network has been introduced in the agriculture field [85]. This technology permits to distribute the sensors in all the field, then the information are transmitted by wireless node to a gateway that sends all the information to a high level infrastructure, where the data are elaborated and the proper actions are carried out.

The plantoid may be a further evolution of this application. At the moment the system must be opportunely applied to the plants in order to install a WSN in a field. For example, in a vineyard some interesting sensors are the soil moisture sensors that are put at fixed depth, the sensors for measuring the differential temperature of the leaf, and the dendrometer (used to measure the stem diameter variation). These sensors must be applied with care to the plants, must be protected during the pruning and the harvesting, and must be reallocated in some cases with the plant growing. A plantoid or many plantoids that can be easily applied to the field and that measure all these quantities on themselves without interacting directly with the real plant can guarantee shorter installation time, less problems of interaction during the farmer activities and more accuracy in particular in the underground monitoring. To achieve this goal the overall plant behaviour must be properly modelled and implemented in the plantoid.

This technology can be useful also in other applications, for example for monitoring polluted area. In this case, chemical/physical sensors can be integrated in the plantoid for specific pollution application.

3.1.1 Space exploration scenario

Plant-inspired space probes could hopefully represent a new generation of planetary robotic explorers. A plantoid, or eventually many plantoids, disseminated like seeds in large lands, extending their roots in the ground, can autonomously analyse the composition of air and soil and detect the presence of a variety of chemical-physical parameters. The plantoid robot could contribute to the discussion on the space mission concepts of planetary subsurface analysis with a novel biomimetic approach. The main novelty in this approach is in the digging systems for sub-soil planetary exploration, stressing the concept of minimal power consumption and trying to conceive devices whose penetration in the soil is possibly far less traumatic than that accomplished by the current drilling system (this last feature is also particularly important thinking to dig in search of life traces, which can be considerably damaged, if not destroyed, by the harsh friction and consequently heat generated by the drilling tip).

This approach has been proposed to the European Space Agency (ESA) in the Ariadna Call. This feasibility study has been approved and financed by ESA showing great interest in the possibility to explore the environment by means of roots and moreover to anchor the robotic probe to the soil [79].

The first stages of the proposed scenarios could be qualitatively similar to those adopted by present planetary probes. The main difference could rely in skipping the final landing phase, i.e. the airbag-based landing, and make the plantoid withstand a free-fall by few meters in order to partially penetrate into the soil (as a plant "seed"), also assuring a first anchorage [80]. A soft land can be also evaluated, but this requires that roots start to dig into the soil from the outside, eventually requiring a counterbalance action by the probe in order to avoid a lift of the probe itself, especially in low-gravity celestial body (as Mars and Moon can be considered).

Three primary space mission targets have been envisaged so far, in partial accordance with main current ESA programs and ongoing projects: Mars, Moon and Asteroids.

Fig. 12. Possible targets for the plantoid: Mars, Moon and asteroids.

Harsh environments are expected in an increasing scale going from Mars, to the Moon and finally to the asteroids. Mars exploration can be considered as the most mild application for such a robot, thanks to its less strict constraints (if compared to the Moon or asteroids). On Mars the temperature averages between -87°C and -5°C (http://solarsystem.jpl.nasa.gov/planets/profile.cfm?Object=Mars), and a mean surface level atmospheric pressure of 0.6 kPa can be found (less than 0.01 terrestrial atmosphere).

Sub-surface characteristics are of crucial importance for the success of the penetrating principle of the roots. This is likely to be limited to a loose and fine sand and soil, while it is intuitively not able to

perforate hard bedrock. Indeed, the plantoid should be able to move away from similar obstacles, looking for different paths. Main terrain characteristics for these scenarios have been collected and described in the following. However, it seems not possible to foresee what the plantoid roots would exactly face under the surface.

On Mars, for example, while the first roughly 0.5-1 m under the surface, for instance, might be mainly composed of fine sand and loose soil, going deeper the subsurface could progressively host more hard rock layers with stones whose characteristics could correspond to those of our mafurite, carbonatite, diopside and diabase ([81], [82], [83]). The first soil layer that the plantoid would have to face (for the proposed targets) can be basically considered powder. Powders are probably the least predictable of all materials in relation to flowability, a fundamental characteristic in order to be able for the root to penetrate in the soil, because many factors affecting the rheological properties are present. The main factors that could affect flow properties in planetary exploration are: particle size, shape, cohesivity, particle interaction, attrition characteristic, hardness, stiffness, strength, and compaction condition.

A powder is a blend of particles: entrained gases or vacuum space among particles drastically affect the flow properties of the powder bulk. From a preliminary viewpoint, it seems more likely that the plantoid roots could penetrate into a terrain formed by relatively larger grains, rather than fine microscopic sandy grains, which after an initial compression, and without any back expulsion strategy typically applied by drillers, would compact in a harder surface. On the contrary, relatively large and stiff grains would possibly spatially redistribute under the pushing action of the root without compacting. Too large grains, finally, could be too heavy (even in reduced gravity as on Mars and Moon) and offer too high friction due to a larger surfaces, to not allow any penetration of the root of the plantoid.

The growing mechanisms of the root will likely to be relatively slow; therefore, the subsurface penetration will last a considerable amount of time. Considering that current missions have now successfully operated on the surface for over two years, it is reasonable to consider a mission scenario with a robotic probe whose working principle is designed to operate on plant-like time scale. The plantoid will be capable to start data transmission back to Earth right after landing, but the soil investigation will be carried out slowly, exactly as plants do, with a minimal consumption of power. This feature could allow designing relatively small solar panels and storage batteries.
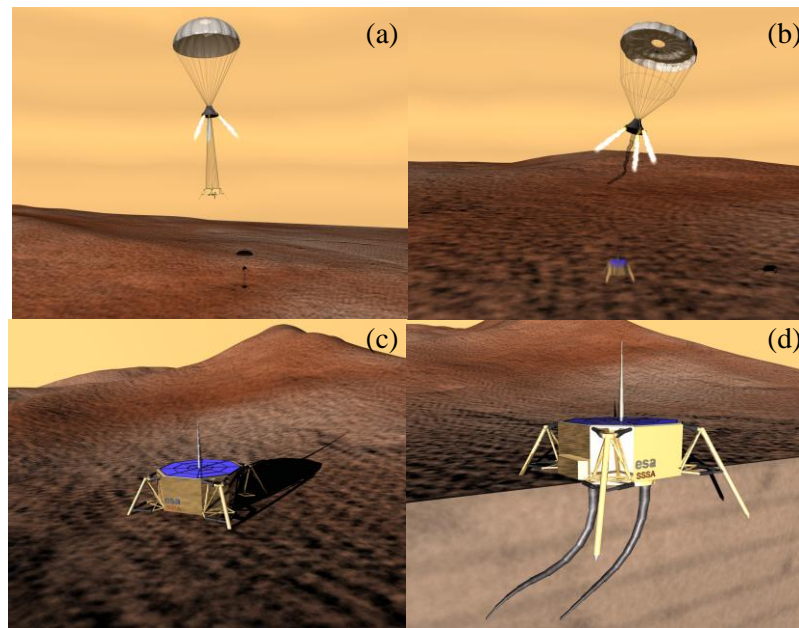
Fig. 13. Final sequence of the plantoid landing: (a) final descent, rocket ignition; (b) bridle cut; (c) anchoring into the soil and system initiation; (d) extension and orientation of the robot's roots.

Fig. 13 shows a schematic representation of the following robot's actions performed in the very final phases of the landing after the descent procedure (that could be very similar to those performed by the Mars rover mission):

- Rocket ignition to further decrease the speed;
- Bridle cut when close to the surface (few meters if it is possible a fine control) and free fall;
- Solar cell opening and activation of internal control modules ;
- Extension and orientation of the robot's roots.

3.2   Plantoid Architecture

As a mechatronic system, the robot has been designed in a modular way. The plantoid can be divided in two major sections: a first part, which corresponds to the trunk and leaves, which is the upper section of the robot, located out of the soil; a second part, which represents the roots, able to move in the soil. The aerial part and the root apices are connected by the elongation sections. The elongation section must guarantee the strength to penetrate the soil, the elongation to permit the growth, the bending to follow the apex during the exploration and in the same time the electrical connection of the apices with the main system. In this thesis some possible solutions for the realization has been proposed and discussed.

Fig. 14 shows the high level structure of the plantoid, with the aerial part connected to several root apices by the relative elongation sections.
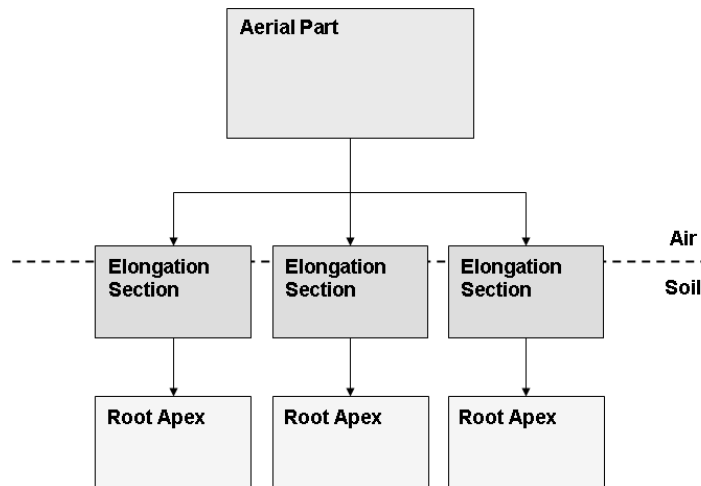
Fig. 14. Plantoid structure.

In particular, the upper part of the plantoid aims at:

- acquiring data from the chemical and physical sensors;
- acquiring energy from the sun by means of photovoltaic cells;
- storing the energy in a backup battery for, e.g, to work also during the night;
- managing the plant at high level;
- transmitting the data concerning the air and soil analysis to a remote station;
- eventually storing the "fuel" (water or other) of the osmotic process for root growth.

The underground part of the plantoid aims at:

- acquiring data from the integrated physical (and in the future chemical) sensors;
- exploring the soil following the external stimuli;
- anchoring the whole plantoid to the ground.

Fig. 15 shows a block diagram of the components constituting the plantoid.
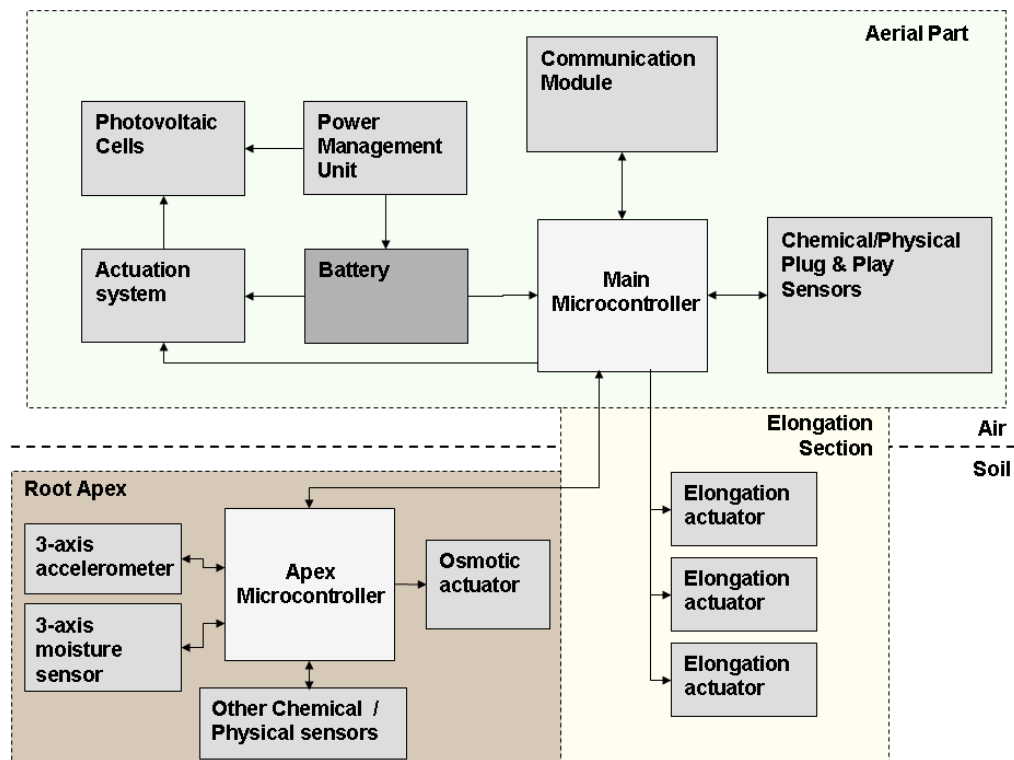
Fig. 15. Plantoid block diagram.

The energy is collected by solar panels; the surface of these panels can be quite small because the power required by the osmotic actuators is very limited. In particular, for the root apex a conservative value of current consumption (osmotic actuator plus microcontroller and sensors) is less than 10 mA that corresponds to a power consumption of 500mW for 10 root apices with a supply voltage of 5V. On Earth with a commercial solar panel and an average radiation of 1000 W/m^2 we can obtain about 100 W/m^2 of power (the efficiency of a solar panel varies from 6% to 30% for the most performing one).

About the aerial part, the most power demanding components are the communication system and the sensors for gas analysis. About the transmission block, the data to be sent are limited:

- the plant movement is very slow and, consequently, the soil analyzed is limited and the data to be acquired are few;
- the amount of data coming from the gas sensors depends from the application, but for a fixed station can be maintained under few samples for hour;

Thus the small amount of data can be transmitted in very narrow slot of time assuring low overall consumption.

Finally the only components that need a high power are the gas sensors. The consumption depends by the technology used for the fabrication of the sensors but the greater amount of gas sensors present on the market are based on MOX technology. The MOX sensors are based on a hot plate that heats an active material in order to permit the sensing of the target gas. The hot plate normally must reach a temperature in the order of 350-400°C that means high power consumption. For the commercial MOX sensors the typical power consumption is in the order of 50mW - 1W. Moreover, in order to have a good

accuracy, the sensors should be maintained always switched on (even if some research activities are performed in the field of the discontinued power supply [84]). A possible solution to reduce the sensors power consumption is to use ultra miniaturized hotplates that need to heat a very limited area and so they need less power [12].

The energy collected by the solar panels is stored in a battery in order to have energy during the absence of solar radiation and moreover to permit the supplying of current during the more demanding tasks. A Power Management Unit (PMU) is devoted to the management of the solar energy collected and battery recharging. Moreover in the "trunk" of the robot, there are located also the actuators for commanding the pull out of the solar panels and eventually (depending on the solution adopted for the elongation section) the tank of "fuel" (e.g. water) for the osmotic process.

These components are managed by a microcontroller, which performs several functions:

- it controls the high level tasks of the plantoid;
- it collects the data coming from the roots and it uses them to indicate to the roots the portion of soil that must be analyzed;
- it collects the data coming from the aerial sensors;
- it manages the transmission module;
- it commands the actuators for the solar panels;
- it manages the elongation section indicating to the roots when to grow.

The lower part of the plantoid is located into the soil and it is composed by the robotic roots. The plantoid roots will be able to grow following different stimuli, such as gravity direction, in order to explore the environment in terms of presence of a variety of chemical-physical parameters.

Each root is formed by an apex that comprises sensors and the control part electrically connected to the main microcontroller in the plant body, and by an elongation section that connects mechanically the apex and the trunk of the plantoid. Each apex embeds a microcontroller module for the emulation of the roots behaviour through the local implementation of networks adopting the real apexes behaviour as models. By imitating the plants strategy, the robot will move slowly, exploring efficiently the environment and showing high actuation forces and low power consumption. The plantoid apex will grow and move into the ground through a new electrochemical actuator, based on the variation of the osmotic pressure in a liquid, controlled by small electrical signal application (electro-osmotic actuators). These actuators allow a root movement on the plant time scale, applying relative high forces with low power consumption. The plantoid will be able to expand and actuate its roots, implementing de facto a biomimetic growing mechanism.

All the roots of the plants are then connected to the central body to realize a network that drives the growing of the roots in preferential directions, driven by the information acquired by the sensors on the apices.

As already described, the roots and in particular the root apices reply to the changes in the environment through mechanisms that are known as tropisms. In detail, the apex has sensors for the gravity (statolith), for the soil moisture and for chemicals, which produce respectively gravitropism, hydrotropism and chemotropism.

In order to imitate the plant behaviour, the following components are considered:

- an accelerometer to replicate the capability of the root to follow the gravity;
- a soil moisture sensor to follow the possible gradient of humidity in the soil;
- a microcontroller to realize the distributed control of the plant (every apex is an independent unit);
- a number of actuators (osmotic) for the steering and the penetration of the root into the soil;
- other sensors to perform chemical/physical analysis of the soil.
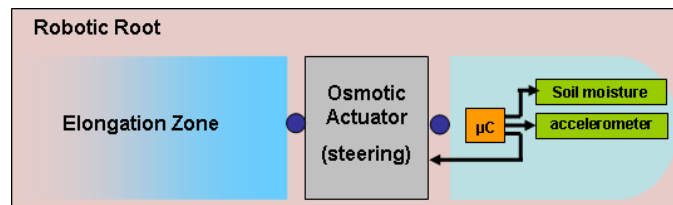
Fig. 16. A simplified schematic representation of a plantoid root apex

3.2.1 Root mechanical design

In this thesis a new actuator has been proposed to permit the movement of the robotic root with the performances typical of the biological root. This actuator is based on the osmotic principle (see section 4.2) and permits the generation of high pressure controlled by electrochemical processes. Several solutions can be exploited in order to achieve the steering of the apex by osmotic actuation. The main issue in the general design of the apex, as well as of the root, is related to the size of the structure (e.g., the cross-sectional area of the cylindrical body of the apex). Considering uniform sandy terrain, the steering and penetration capability of the apex is obviously affected by its size, because larger it is and more actuation force is required for the movement. As a consequence, being able to maintain the same actuation force, it can be concluded that thinner is the structure easier the movement of the apex into the soil. However, the force generated by the osmotic actuation principle directly relies on the size of an expandable area (S) internal to the structure of the apex, whose value is limited by the size of the structure itself, because the force generated equals the product of the expandable section area S and the generated pressure P. As a conclusion, there should be a sort of compromise between the apex size, e.g. its cross-sectional area, and the actuation force generated, which will be likely to depend on the particular soil probed. Computer simulations cannot give very meaningful results regarding soil penetration (the model is too complex to be well simulated). Hence, a final optimized design of the structure could come from testing the penetration into different soils by means of several "dummy" cone-shaped apexes, with different cross-sectional areas, for instance, and using different controlled

pushing forces (corresponding to the possible actuation forces generated by the conceived mechanism, which is finally dependent on the apex cross-sectional area). On the base of these results and other considerations about the steering capabilities and actuation time, an optimal apex diameter could be fixed (see section 4.5).

As preliminary target soil for testing the plantoid, a sandy terrain like, that is possible to find on beaches or deserts, could be used. These can be roughly considered as composed by powders. A powder is a blend of particles and it is probably the least predictable of all materials in relation to flowability, a fundamental characteristic in order to be able for the apex to steer and penetrate into the soil, because many factors affecting the rheological properties are present. These factors are both intrinsic to the powder or particles (e.g., particle size, size distribution, shape, surface texture, cohesivity, particle interaction, etc.) and external, due to the environment (e.g., vibration, temperature, tying substances, entrained gases, compact conditions, etc.).

From a preliminary viewpoint, it seems more likely that the plantoid apexes and roots could penetrate into a terrain formed by relatively larger grains, rather than fine microscopic sandy grains, which after an initial compression, and without any back expulsion strategy typically applied by drillers, would compact in a harder surface. It is known from industrial tests that the difference in energy needed to establish flow in a compacted powder may be 100 times that needed when the powder is aerated and possibly fluidised. For some powders, this ratio can be more than 1000 and in the most extreme case, 5000. Slight compaction, a small vibration, or the smallest amount of gas presence can significantly affect flowability. On the contrary, relatively large and stiff grains would possibly spatially redistribute under the pushing action of the root without compacting. Too large grains, however, could be too heavy to move and offer too large friction due to larger surfaces, to not allow any steering nor penetration of the root of the plantoid.

Complementary penetrating strategies to simple pushing can consequently be considered, as blowing gases from the apex tip (directly extracted from the outer environment and insufflated down to the apex), vibration of the apex, or even slow torsional movement of the apex itself (that seems to be the strategy adopted by the biological plant roots during the penetration) in order to allow grain re-distribution during penetration and thus better flowability. All these strategies are all likely to ease the penetration process, at least where powder-like terrain is present.

The root should be composed of two basic topologies of mechanical modules:

1. The apex module capable of steering actuation, in order to fix the direction of the soil penetration.
2. The root module working as an axial piston in order to push forward the apex for the soil penetration.

In the following, two concept designs are reported for the two mentioned modules.

Several solutions can be exploited for achieving the steering of the root by the osmotic actuator (see section 4.2). The easiest way is to use directly the osmotic cells with two pistons to move the apex in a plane (Fig. 17).
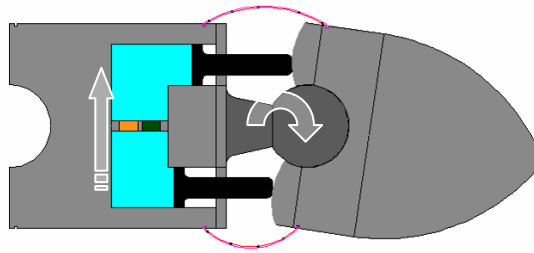

Fig. 17. A basic concept of the osmotic actuator for the steering of the plant root in a bi-dimensional case; the transparent straight arrow represents the osmotic water flow. The red curved lines schematically represents a surrounding membrane placed between the osmotic chamber and the apex tip, aimed at preventing the soil going in between the piston mechanism, thus blocking the actuation.

Considering square chambers with dimensions $d \times d$, the force that the chamber can generate on the piston is $F = d^2 * P$ with P pressure in the chamber. In this way with a $d = 10$mm, for instance, and a pressure generated in chamber $P = 6$ atm we can obtain a $F = 60$N on the root apex.

One important issue in the mechanical design of the root apex is the friction coefficient between the root and the soil. Various studies report that the friction coefficient of a metallic structure that penetrates into the soil is much greater than the friction of a root of the same dimension. This is due to a sort of natural lubrication of the root, which during the growth sloughs cells from the cap decreasing this component of friction. Taking inspiration from the secretion of mucilage that plants produce to easy the penetration of the roots in the terrain, this study suggests the use self-lubricant systems, keeping in mind that contaminant chemicals cannot be released in the soil in order to prevent any ambiguous detection. A possible strategy makes use of a Teflon based apex. This would help the root growth, because the actuation force is focused to contrast the friction with the soil at the root apex, while drastically decreasing the so-called sleeve friction forces that can become even more significant than the forces generated by the cone resistance, depending on the length of the moving root into the soil.

About the elongation section, in order to gain actuation power and at the same time having an easier penetration of the root apex, it is possible to think to use larger modules at the beginning of the root and smaller modules towards the apex. The extension of the modules could be simultaneous, being the force applied by the strongest root module the resulting force, while the total course would correspond to the sum of the course of each extended module (admitting each module can extend itself in the soil). On the other hand it would be more convenient to actuate the root modules close to the apex at the beginning of the penetration (where less force is required to dig) and keep the largest and strongest modules for the actuation of the final steps. However, as a negative consequence, the last actuated modules will have to push all the extended root, which means stronger friction will occur. However, no matter the size of the structure, there will be always a depth limit for the actuation mechanism, since the steering momentum

requested in order to move the surrounding soil will become too large while the apex is penetrating deeper into the soil.

For the realization of root elongation section it is possible to use a stack of modules based on osmotic actuation that are initially closed and then by mean of the osmotic process elongate itself. The limit of this solution is that the elongation does not overtake the 100% of the initial length. The root module can be envisioned as a "cylinder-piston" system. The piston itself can include the osmotic actuator as in Fig. 18 (in this way the disadvantage is that part of the pushing surface of the piston is lost). The piston is rigidly connected to a piston rod that goes out of the cylinder and axially pushes over the following root module by means of an intermediate module that works as a spherical joint.
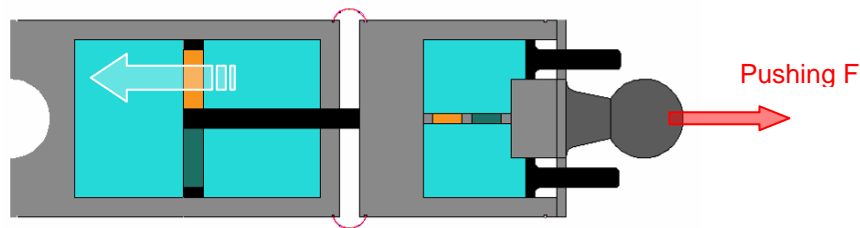
Fig. 18. A basic concept of the osmotic actuator for the root modules; the transparent white arrow represents the osmotic water flow, while the red arrow indicates for the pushing force direction.
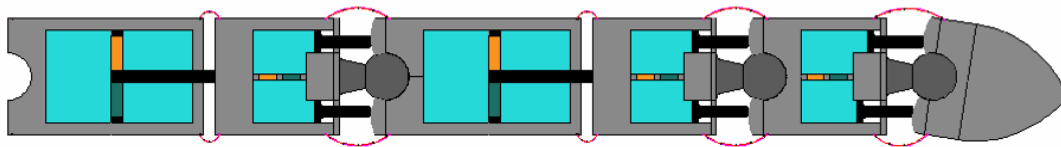
Fig. 19. A basic concept of the final part of the root with the apex and two root modules: the system has an intrinsic modular architecture.

The force generated by the osmotic actuation principle itself directly relies on the cross-section area of the root, because the force generated equals the product of the piston section area and the generated pressure. With a diameter of few centimetres (e.g. around 5-6 cm) of the cylinder, a root module could exert forces on the order of 1000 N with typical pressures of 5 atm in the actuators. While from a mechanical viewpoint it is possible to decrease the diameter of the root down to a couple of centimetres (and maybe even further), in order to have comparable and useful forces it is necessary to increase much more the internal pressure. Nevertheless, high pressures, of course, need stronger and thus larger mechanical parts. As a conclusion there should be a sort of compromise or optimization between the root cross-section area and the actuation force generated, which will depend on the particular soil probed.

4 Design and realization of a Robotic root Apex

4.1 Concept

Plants show a peculiar directional growth in response to external stimuli such as light (phototropism), gravity (gravitropism), touch (thigmotropism) or water/humidity gradient (hydrotropism) ([30], [31]). Tropisms frequently interact between and among each other, and the final growth form of the plant is influenced by such interactions. Although they cannot actively move, the combination of these mechanisms allows plants to overtake hostile or inaccessible environments and colonize the soil. The root system, the plant organ for water and nutrients scavenging and anchorage, under most natural conditions growths down through gravitropism until encountering an obstacle such as a rock, or a hard-pan layer of soil. At this point the root must re-orient its growth to move across or around the obstacle. The root structure is formed from an apical meristem. This divides to produce more root axes and a root cap. The cells of the root cap are the first to encounter obstacles and new environments, and they are covered with a thick layer of mucilage, which is secreted by the root tip and which helps to lubricate the root as it pushes through the soil. The cells of the root cap allow the root to sense the direction of gravity, as well as touch and light, and thus dictate the direction of the root growth.

Cells that form the root go through a phase of elongation, and it is this process that drives the root through the soil.

The entire behaviour is achieved by an osmotic actuation system that is steered by a distributed set of simple controllers located in each apex and by an overall increase in size by cell division. As a consequence, root apices are not only sites of nutrient uptake but also sites of forward movement. During growth, plant roots may exert pressures of up to 1 MPa in order to penetrate hard soils [43].

The study of plant behaviour and features can offer advanced and innovative solutions in robotics, both for designing and building new robots for specific applications, such as in situ monitoring analysis and specific chemical detection, water searching in agriculture, anchoring capabilities, and for developing robotic platforms for scientific understanding of the plant capabilities themselves.

A plant-like robotic system able to slowly penetrate inside the ground while sensing and looking for the planned target, could offer new and powerful features for subsurface exploration.

Starting from the knowledge on the plant roots behaviour, a robotic apex has been designed, based on a new plant-inspired actuation principle (so called electro-osmotic actuation) ([87], [88]).

A first prototype of a robotic apex is presented, including gravity and humidity sensors and the capabilities to steer following these stimuli.

The robotic root apex structure was designed as a cylindrical body containing the following main parts (Fig. 20):

- an osmotic actuator module for the steering of the root apex;

- a tip that includes the control and sensing module (gravity and moisture sensors);
- an elongation region.
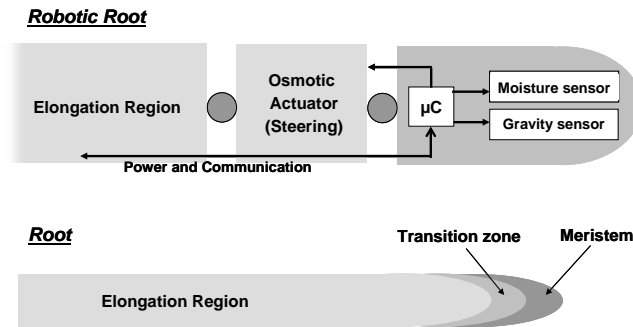
Fig. 20. Comparison between biological root and robotic root.

4.2 Osmotic Actuator

4.2.1 Bio-inspiration from plant root actuation

The movement/growing process in plant's roots is essentially actuated by two mechanisms: roots grow by a mechanism of cell division in the apical meristem just behind the tip, and by a cell elongation in a zone just behind the apex [50].
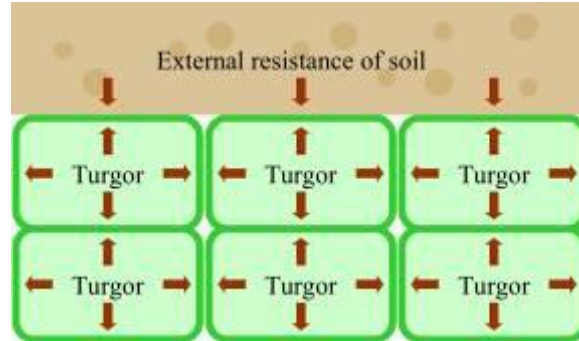
Fig. 21. Schematic diagram showing pressures acting in the epidermis of a root growing in soil

Water influx into cells generates turgor pressure (P), which provides the driving force for elongation and hence root growth (Fig. 21). The osmotic potential within cells in the elongation zone of a root generates the water potential gradient for water uptake into the cell [89]. Turgor pressure (P) is generated as the influx of water, which presses the protoplast against the confining pressure of the 'rigid' cell wall. Turgor pressure (P) is then given by

$P = \pi_o - \pi_i$ (5)

where π_i is the osmotic potential inside the cell, and π_o is the osmotic potential outside the cell. This equation assumes that water influx into the cell is not limiting to growth, there is no transpiration tension in the wall, and solutes have a reflection coefficient near unity. The water relations of expanding cells

have been reviewed in detail [89]. A typical value for the vacuolar osmotic potential (equal to π_i) inside a cell in the growing zone of an unimpeded root grown in hydroponics is around -0.7 MPa (about 7 Atm).

Classically, following experiments on cell walls isolated from giant algal cells [91], cell elongation has been regarded as plastic flow of the wall material under stress [60].

Where existing soil channels are smaller than the root diameter, roots must exert a growth pressure in order to displace soil particles, overcome friction and elongate through the soil. The growth pressure (σ) is equal in magnitude to the soil pressure that opposes root growth. In a root tip elongating through soil, cell turgor pressure (P) generates the growth pressure (σ), which results from the difference between P and the wall pressure (W) so that [92].

$$\sigma = P - W \qquad (6)$$

In unimpeded roots, σ is by definition zero and P is balanced by W. When roots are completely impeded and cannot elongate, σ attains a maximum value (σ_{max}). Roots exert growth pressures in both radial and axial directions, but we will only deal with axial growth pressures here. When water transport into growing cells is not limiting, root elongation rate can be considered in terms of a simplified Lockhart equation [60], as modified by Greacen and Oh [92] to take account of the soil impedance:

$$R = m[W - W_C] = m[P - W_C - \sigma] \qquad (7)$$

where R is the elongation rate, m is a cell wall extensibility coefficient, W is the wall pressure, W_C is the cell wall yield threshold, P is the turgor pressure and σ is the soil impedance (or growth pressure).

As showed the mechanism of root cells expansion is driven by the osmotic pressure. This osmotic expansion mechanism could be successfully used to design a new class of electrochemical actuators able to fit the necessary requirements (low power, slow actuation, high force/pressure).

4.2.2 The electro-osmotic actuator concept

As shown in the section 2.3, the movement/growth strategies adopted by the plant roots consist in exploiting the osmotic pressure generated into the cells (turgor pressure) as a driving force for the elongation and growth. The produced force is used to overtake the soil resistance and in this way to penetrate the soil. The idea of a new electro-osmotic actuators inspired by plants is based on the control of the osmotic pressure in a suitable "cell" containing liquid or gel matrix, by applying a small electrical current, and using the resulting osmotic pressure to induce an actuation (electro-osmotic actuation).

This kind of actuator will have the following features:

- Very low power consumption (small current requirement);
- Actuators response with high modulation capability (high accuracy, resolution);
- Slow actuation;
- High force/pressure actuation.

Osmosis is the diffusion of water through a semi-permeable membrane, from a solution of low solute concentration to a solution with high solute concentration. It is a physical process in which a solvent moves, without input of energy, across a semi-permeable membrane (permeable to the solvent, but not the solute) separating two solutions of different concentrations. The osmotic pressure is the external pressure that should be applied in order to stop the passing of water through the membrane. The reverse osmosis happens when a pressure greater than the osmotic pressure is applied. In this case a flow of solvent molecules of the more concentrated solution goes in the low concentrated solution. This process is used for example to purify the water or for desalinization.
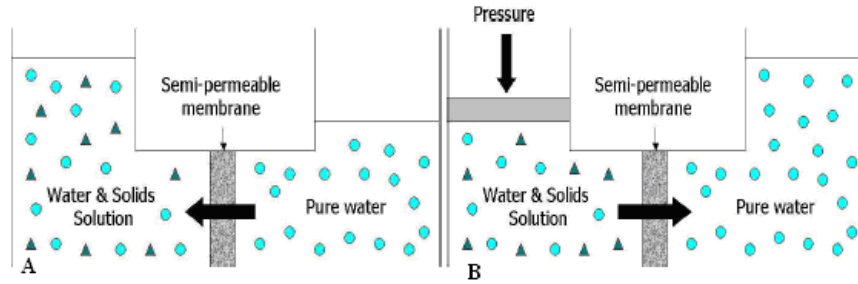
Fig. 22. The osmotic process: A) Forward Osmosis; B) Reverse Osmosis

Ideally the osmotic pressure (Π) depends only by the ions concentration and not by their nature. The formula that describes the osmotic pressure is:

$$\Pi \cdot V = n \cdot R \cdot T \cdot i \;\; \rightarrow \quad\quad \Pi = \frac{n}{V} \cdot R \cdot T = C \cdot R \cdot T \cdot i \quad\quad\quad (8)$$

Where:

R: Universal Gas Constant (0,08205784 L atm K^{-1} mol^{-1})

T: temperature (Kelvin degree)

V: volume of the solution (L)

n: moles of solute

C: molar concentration (mol/L)

i: Van't Hoff coefficient [93] that takes care of the percentage of electrolyte that is dissociated

The resulting osmotic pressure in a real set up results lower than the one expected by the formula. This difference is due to a non homogeneous distribution of the concentration in proximity of the membrane that results in a lower concentration in the more concentrated solution and a greater concentration in the less concentrated solution (Fig. 23)
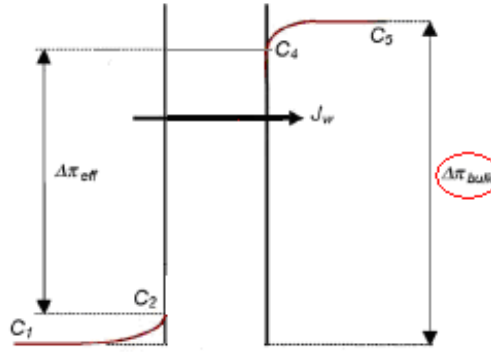
Fig. 23. Concentration gradient across the membrane

The theoretical working principle of the plant inspired electro-osmotic actuator is now described in detail. Fig. 24 shows two cells connected through a semi-permeable membrane. Each cell has a metallic electrode (M and N) immersed in a water solution of own ions (M+ and N+, respectively molal concentration C_{M+} and C_{M-}) in presence of a counter-ion (X-), required for the electro-neutrality of the solution. If the concentration of the two cells is different, the osmotic pressure π is given by the Van t'Hoff's low (8):

$$\pi = \left(c_{M^+} - c_{N^+}\right) \cdot R \cdot T \cdot i \qquad (9)$$

On the base of the (9) it is possible to evaluate the theoretical pressure achievable by using the osmotic mechanism. Considering a difference of electrolytic concentrations between the two cells of 1M (a realistic achievable concentration) and considering the molal osmotic coefficient $\Phi = 1$, we obtain a pressure of about 2.5MPa (25 Atm).

The force that can be exploited by this pressure is obviously essentially related to the geometry and dimensions of the transduction mechanism. Few examples of devices that use pure osmotic actuation mechanism are available in literature ([94]).

Fig. 25 shows a simplified ideal mechanism that should convert the difference of pressure between cells in a displacement.
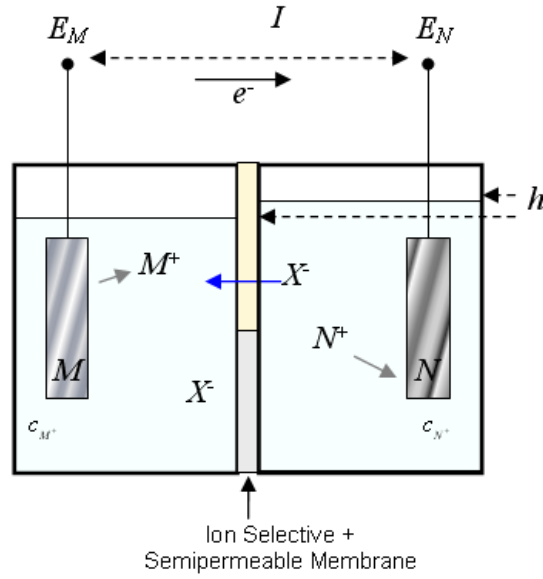
Fig. 24. Schematic diagram of osmotic cells
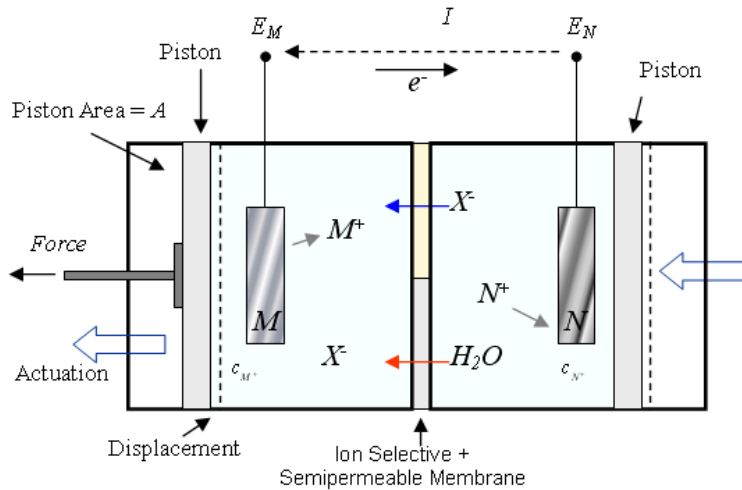
Fig. 25. Schematic of hypothetic electro-osmotic actuator

In the simple case of a cylinder with a base of surface A the calculation of force achievable by the mechanism is trivial, being the force F given by:

$$F = \pi \cdot A \qquad (10)$$

In a cylinder with a base of 1cm^2 area, 2.5 MPa of pressure can produce 25 Kg of force, in absence of friction. In this proposed study, the displacement of the "piston" happens because the water flows through the semi-permeable membrane from the cell with minor concentration to the cell with greater concentration, decreasing in this way the concentration differences between cells. This process occurs until the concentration in the two cells becomes the same or until the external forces balance the actual osmotic force.

In order to control the displacements and the forces generated by such kind of osmotic actuator it is necessary to control the ion concentrations on the cells. This goal can be achieved by using

electrochemical reaction. If the membrane that connects the two cells allows the passage of some kind of ions (not simply a semi-permeable membrane), thus the cells can work as a battery (it can generate an electrical current) or conversely work as electrolytic cells (applying a suitable external voltage). Fig. 26 shows the different steps of the electro-osmotic mechanism.
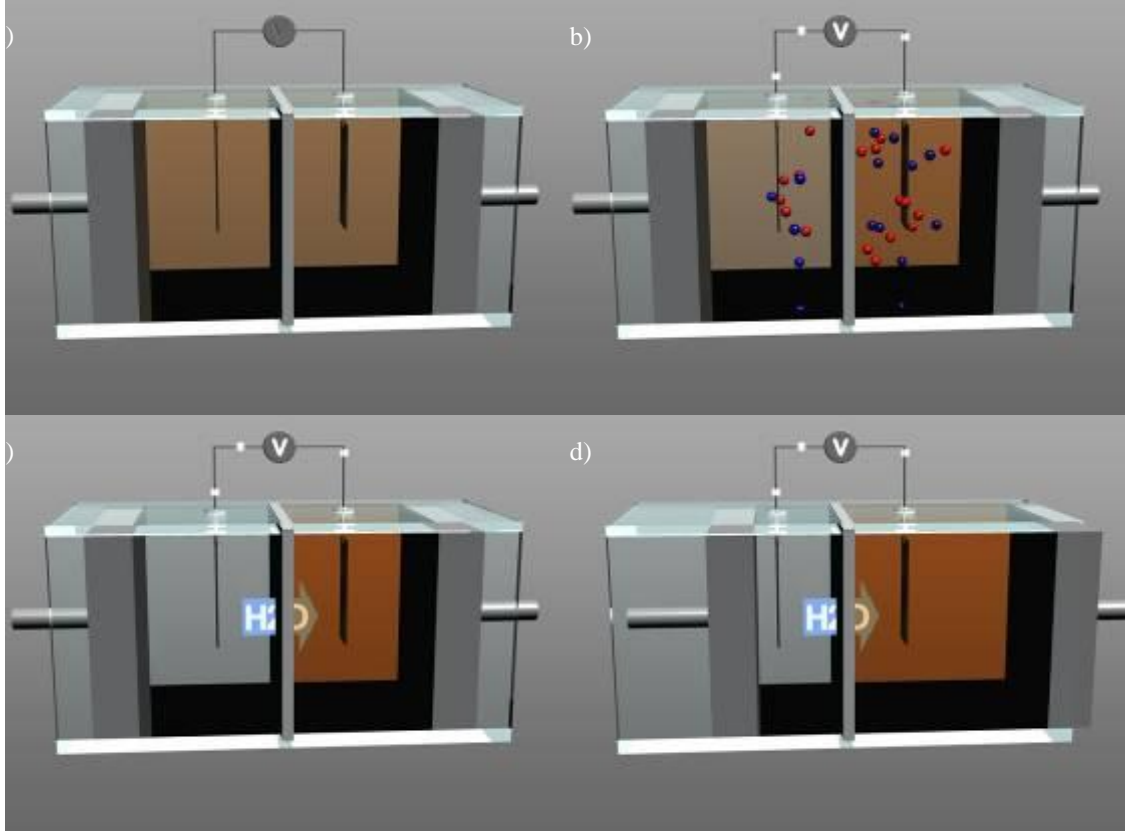
Fig. 26. a) The two cells have the same ion concentration; b) Electrolytic process induces a change in ions concentration; c) Osmotic pressure is induced across the two cells; d) The osmotic pressure drives the actuation.

The two reduction semi-reactions involved in the process are:

$$\begin{cases} M \rightarrow M^+ + e^- \\ N^+ + e^- \rightarrow N \end{cases} \quad (11)$$
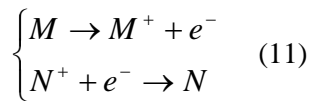
Providing a suitable current to the cells it is possible to control the concentrations of the electrolytes. The electrical potential needed to induce a current in the cells is in the order of few Volts (at the considered concentrations). The induced variation of electrolyte concentration within a cell, after application of a current I for a time t, is given by the following equations:

$$\begin{cases} C_{M+}(t) - C_{M+}(0) = \dfrac{I \cdot t}{m \cdot F \cdot V} \\ C_{N+}(t) - C_{N+}(0) = \dfrac{I \cdot t}{n \cdot F \cdot V} \end{cases} \quad (12)$$

The electric potential across the two electrodes ΔE is given by the Nerst equation:

$$\Delta E = E_M - E_N = \left(E_M^0 - E_N^0 \right) + \frac{RT}{F} \ln \left(\left[c_{M^+} \right] / \left[c_{N^+} \right] \right) \tag{13}$$

where E_M^0 and E_N^0 are the semi-reaction standard red-ox potentials, and F is the Faraday constant (F = 96,485.34 s A mol^{-1}).

It is important to underline that in front of the variation of concentration of the active electrolytic chemical species (in this case the cations M$^+$ and N$^+$) due to the red-ox process, the ionic transport of counter-ions (in this case X$^-$) must be allowed (otherwise electrode gets polarized), by means of a ion selective membrane. Clearly the active ionic species must be blocked by this membrane otherwise a net variation of concentration is not achievable.

The current flowing within the two cells depends ideally from the Ohm's Law

$$I = \left(\Delta E_{ext} - \Delta E - E_{sovr} \right) / R \tag{14}$$

where ΔE_{ext} is the external potential applied, E_{sovr} is the over potential (that depends from electrodes type, geometry and work conditions) and R the resistance of the cell. The applicable external potential on the cells is limited, because a too high voltage can create collateral unwanted reactions (e.g. water electrolysis). The resistance of the cells depends both from the ionic concentration (ionic transport mechanisms) and from the resistance across the membrane, but in the operative conditions the membrane resistance is much more important (usually it is very high). For this reason it is not possible to apply an arbitrary current. Applicable currents are in the range of mA.

In order to estimate the reaction time, we can suppose to start the reaction from a condition of equilibrium and the final concentration displacement that must be obtained is 0.5M.

The initial conditions are:

$$I(t = 0) = 0$$
$$C^+(t = 0) = C^-(t = 0) = C_0$$
$$\Delta C(t = 0) = 0 \tag{15}$$
$$V^+ = V^- = V$$

Where:

C^+, V^+ are concentration and volume of the solution contained in the anodic cell.

C^-, V^- are concentration and volume of the solution contained in the cationic cell.

Supplying to the system a charge q in a time t:

$$C^+(t) = C_0 + \frac{q}{z \cdot F \cdot V}$$

$$C^-(t) = C_0 - \frac{q}{z \cdot F \cdot V} \tag{16}$$

$$\Delta C(t) = C^+(t) - C^-(t) = \frac{q}{z \cdot F} \cdot \left(\frac{1}{V} + \frac{1}{V} \right) = \frac{2 \cdot q}{z \cdot F \cdot V}$$

Considering that $q = I \cdot t$ and assigning the following values: V=5 cm^3, z=2, I=5mA, ΔC=0,5M; it is possible to obtain a time of reaction of 13.4 hours.

The time required to exploit the actuation does not depend only on the generation of a difference of concentration between the electro-osmotic cells: in fact, once the difference of osmotic pressure is generated, the water contained into the cell at greater pressure flows through the osmotic membrane into the cell at minor pressure. In particular the water flow through the membrane J_W (m^3/s * 1/m^2) is given by the follow equation ([95]).

$$J_W = K \cdot (\sigma \cdot \Delta\Pi - \Delta P) \qquad (17)$$

Where:

K: membrane permeability constant respect to the solvent;

σ: rejection coefficient (ideally 1 for the membrane that filters completely the solute);

$\Delta\Pi$: difference of osmotic pressure between the two cells;

ΔP: applied external pressure on the most concentrated solution.

The two processes (the electrolytic change of concentration and the osmotic water flow) have a comparable timescale; in this condition the limiting process (the slower) is essentially due to the working conditions like pressure required and applicable current.

4.2.3   Selection of the components

Selection of the chemical species

The choice of the chemical species that are part of the electrolytic process is the first step for the realization of the osmotic actuator. The electrolytic solutions and the electrodes must be selected on the base of the follow requirements:

- oxide-reduction reaction must be reversible;

- no water electrolysis and consequently gas formation;

- no secondary electrochemical reactions (current efficiency 100%).

For the realization of the cell it has been decided to use the same specie in both the semi-cells (M): the same material for the electrodes immersed in the same solution (M^{n+}). Changing the current direction the role of anode and cathode can be exchanged by the two cells:

$$\begin{cases} M \rightarrow M^{n+} + ne^- & \text{Anode} & \text{(oxidation)} \\ M^{n+} + ne^- \rightarrow M & \text{Cathode} & \text{(reduction)} \end{cases} \qquad (18)$$
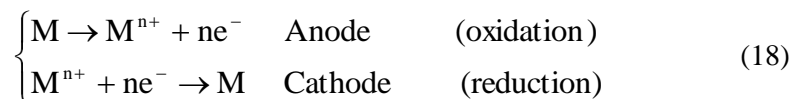
This is an example of electrochemically reversible cell, because the inversion of the current causes the inversion of the process at the two electrodes.

The oxidation at the anode of M causes an increasing of the ionic concentration C_{M+} in the semi cell. In the same time, in the second semi cell, the cathodic reduction causes ionic concentration decreasing.

The metal (M) selected for the electrodes is "lead", because it satisfies the requested characteristics and, moreover, it is used in many electrochemical applications (e.g. lead batteries). The electrodes must be immersed in lead salt solution that contains Pb^{2+} cations. The oxide-reduction reactions are:

$$\begin{cases} Pb^{2+} + 2e^- \rightarrow Pb \quad \text{Cathode (reduction)} \\ Pb \rightarrow Pb^{2+} + 2e^- \quad \text{Anode (oxidation)} \end{cases} \qquad (19)$$
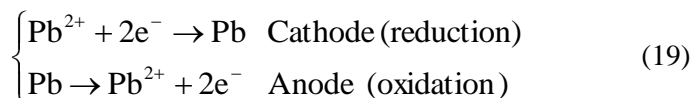
During the electrochemical process, it is important to avoid the water electrolysis that brings to the formation of gaseous hydrogen (in case of water reduction) and oxygen (in case of water oxidation).

The lead can prevent the hydrolysis because the standard potential of the lead is lower than the two involved in the water electrolysis:

$$E^0_{Pb^{2+}/Pb} = -0,13V$$

$$E^0_{H_2O/H_2} = -0,83V \qquad (20)$$

$$E^0_{O_2/H_2O} = +1,23V$$

The lead salt must satisfy the following characteristics:

- water solubility;
- electrolytic dissociation in Pb^{2+} and X^- in water solution;
- secondary unwanted reactions must be prevented;
- high conductibility of the electrolytic solution.

For the experimental phase three lead salts have been identified:

1. lead nitrate $Pb(NO_3)_2$, lead salt of the nitric acid:

$$Pb(NO_3)_2 \rightarrow Pb^{2+} + 2NO_3^-$$
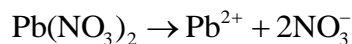
2. lead perchlorate $Pb(ClO_4)_2$, lead salt of the perchlorate acid:

$$Pb(ClO_4)_2 \rightarrow Pb^{2+} + 2ClO_4^-$$
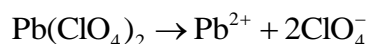
3. lead acetate $Pb(CH_3COO)_2$, lead salt of the acetate acid:

$$Pb(CH_3COO)_2 \rightarrow Pb^{2+} + 2CH_3COO^-$$
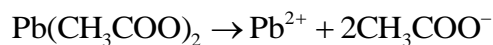
Pure mercury (99.99%) has been used (265918 Aldrich Lead foil) for the realization of the electrodes, in order to avoid contaminant materials that can cause unexpected reactions. For the same motivations also the lead salts have been chosen with a high degree of purity (99.99%) and the solutions have been prepared with deionized water.

Selection of the anionic membranes

As already presented, in order to guarantee the electro-neutrality of the solution, the unbalance of charge caused by the reaction must be compensated by the migration of the X^- ions from a semi-cell to the other one. For this reason, an ion selective membrane has been adopted to separate the two semi-

cells. In particular, a membrane that permits the negative ions passing and blocking the positive ions must be adopted (anionic membrane).

Two commercial available membranes produced by SYBRON have been selected for the experiments:

- IONAC MA-7500
- IONAC MA-3475

The chemical/physical characteristics are reported in the following table:

Typical Characteristics**		Anion MA-3475	Anion MA-7500
Width	meters	1.22	1.22
	inches	48	48
Length	meters	3.1	30
	inches	122	
Thickness	mils	16	18
Exchange Capacity	Meq/gm	0.9	1
Mullen Burst Test, min.	psi	150	150
	bar	10.3	10
Area Resistance, Ohm/cm	0.1 N NaCl	50	30
	1.0 N NaCl	25	10
Permselectivity	0.5 N NaCl/1.0 N NaCl	99	99
Water Permeability	ml/hr/ft^2 @ 5 psi	25	50
Temperature Stability, max.	°C	80	80
	°F	176	176
Chemical Stability, pH		1 to 10	1 to 10
Current Density, max.	ampere/ft^2	50	50
Ionic form, as shipped		Chloride	Chloride

From the table (and also from the experimental tests) is possible to see that the MA-7500 is characterized by a lower electric resistance. This is a preferable characteristic because a lower resistance permits a higher current in the cell (with equal electrodes voltage) and so a quicker reaction. A second important advantage of this membrane is the higher water permeability. For these two reasons the MA-7500 has been chosen for the experimental setups.

Selection of the osmotic membranes

The electro-osmosis bases its working on the forward osmotic (FO) principle. This membrane is not available on the market at the moment but the reverse osmotic (RO) membranes can be also used for this application (even if with lower performance). In this experimental phase the objective is to validate the principle, so achieving the best performances is not necessary.

In literature two membranes for reverse osmosis are most used: polyamide and cellulose acetate. For the experiments, the commercial membranes from Sterlitech Corporation have been selected:

- YMCFSP3001 CA (Cellulose Acetate) RO CF Membrane;
- YMAGSP3001 Polyamide RO AG Membrane.

The main characteristics are reported in the following table:

Designation	Polymer	Rej-Size	25C pH Range	Typical Flux/psi GFD@PSI
AD	Polyamide RO AD Membrane	99.5	4-11	15/800
AG	Polyamide RO AG Membrane	99.5	4-11	26/225
CE	CA (Cellulose Acetate) RO CE Membrane	97	2-8	23.5/420
CF	CA (Cellulose Acetate) RO CF Membrane	92	2-8	30/420

The cellulose acetate membranes are characterized from greater water permeability respect to the Polyamide membranes. That property permits an osmotic flux of high intensity.

In the same time the cellulose acetate membrane respect to the polyamide membrane presents a less capability to filter the solute (Rejection-Size 92-97% instead of 99.5%).

4.2.4 Experimental setups and tests

Setup for electrochemical experiments and tests

The experimental setup realized for the electrolysis tests is composed by two semi-cells (with the same volume) separated by the anionic membrane. The dimension of the setup does not affect the result of the experiment because the system is completely scalable. According to the Faraday's law (with the hypothesis to impose a constant current) a greater volume of solution needs a major reaction time.

$$\Delta C(t) = \frac{I \cdot t}{z \cdot F \cdot V} \qquad (21)$$

For this reason in order to obtain quick test time and to maintain the system easy to handle a compromise has been chosen. With the selected size each semi-cell can contain 5 ml of solution. The membrane is applied on a grid (Fig. 27b) that sustains the membrane and separates the two semi-cells (Fig. 27a).
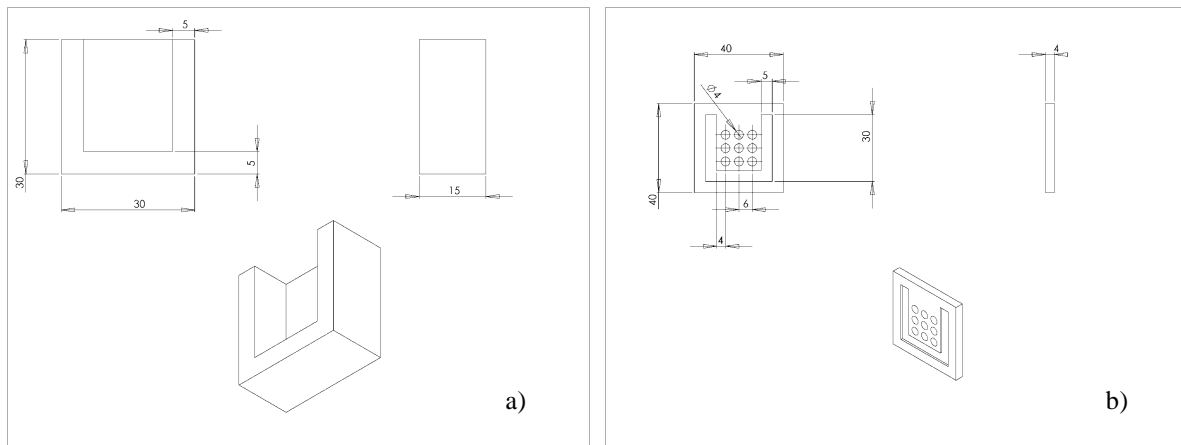
Fig. 27. a) Semi-cell and **b)** grid design and dimensioning

This system has been realized in this way in order to permit an easy disassembling between a test and another in order to change the membrane. In Fig. 28 the pictures of the developed prototype are shown.

Fig. 28. Pictures of the setup disassembled and composed

The lead electrodes are cut by planar foils. Several dimensions have been realized in order to test the change between them and in this way to characterize electrodes and solution. For the tests a potentiostat has been used (Potentiostat-galvanostat Model 7050 Amel Instrument). This instrument permits to perform experiments at fixed voltage monitoring the current or with fixed current and monitoring the voltage. Moreover this instrument is simply to manage directly by the PC through its software interface.

Connecting the instrument to the electrodes immersed in the solution in the two semi-cells, it is possible to control the electrolysis, monitoring the interesting parameters directly by PC (Fig. 29).

Fig. 29. Pictures of the experimental setup

In order to proceed with the electrolytic tests some preliminary experiments have been performed on the proposed solutions. In particular, an important parameter (as already explained) is the resistance, in this case the solution resistance. Three solutions have been prepared and tested, one for each selected lead salt: $Pb(ClO_4)_2$, $Pb(NO_3)_2$, $Pb(CH_3COO)_2$. A concentration of 0.3M has been selected because this concentration can be used as starting concentration for the solutions in the semi-cells; that assures different of concentration of at least 0.5M that guarantees good osmotic pressure.

The results are:

- $Pb(ClO_4)_2$ → 15,6 Ω
- $Pb(NO_3)_2$ → 20,9 Ω
- $Pb(CH_3COO)_2$ → 90,9 Ω

Another aspect that must be taken into account is the formation of unwanted reactions. For this analysis a visual test has been performed. In particular the lead nitrate produces secondary products around the electrodes. In conclusion, the most suitable solution resulted to be the lead perchlorate.

At this point we want to characterize better the cell resistance. The complete system is composed by two semi-cells separated by the anionic membrane. This system can be schematized as in Fig. 30.
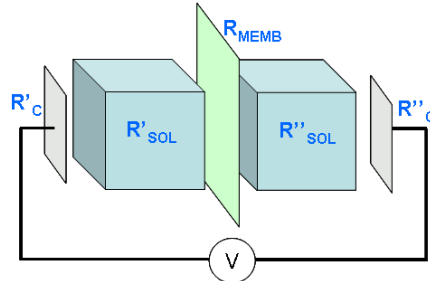
Fig. 30. Contributions to the cell resistance.

In particular there are the two contributions due to the contacts between electrodes and solution ($R_C^{'}$ and $R_C^{''}$), the contribution from the solution resistance ($R_{SOL}^{'}$ and $R_{SOL}^{''}$) and the membrane resistance (R_{MEMB}). In order to investigate the contact and solution resistances a series of tests have been performed on the cell by changing the dimensions of the electrodes (S = 6, 25, 100, 200 mm^2) and the distance between them (d = 10, 20, 30, 40, 50 mm). An alternate voltage ($\pm$ 1 V) has been applied for the measurements. This kind of voltage is necessary in order to avoid the electrolysis that changes the concentration of the solution. A solution of 0.1M of lead acetate is used for the test in order to consider the worst conditions (in terms of resistance). The results are shown in the graph in Fig. 31.
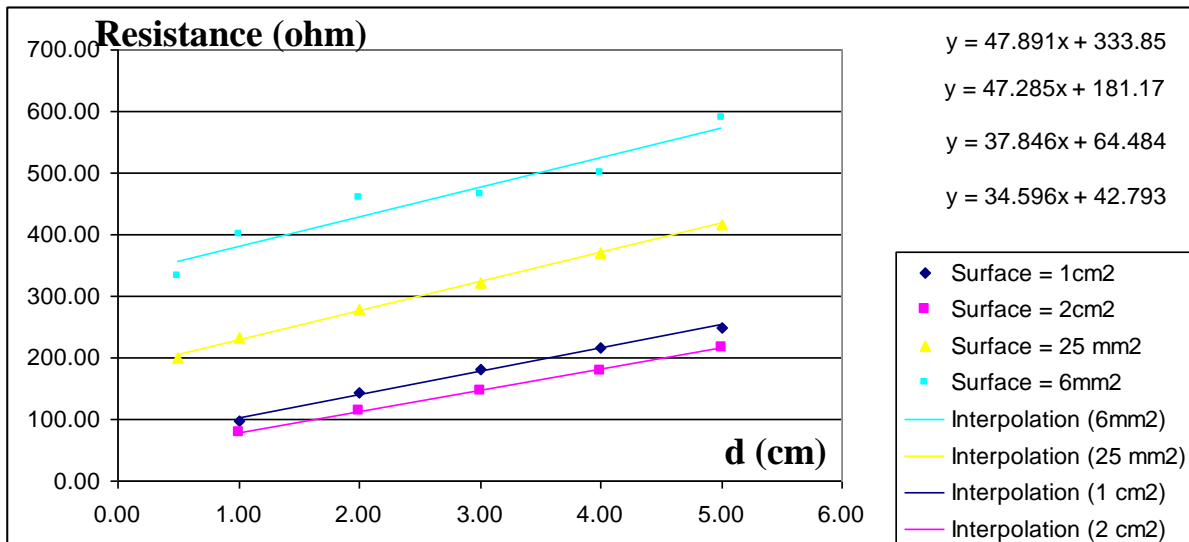
Fig. 31. Resistance vs. distance between the electrodes for different electrodes surfaces.

From the results shown in the graph it is possible to observe these main features:

- there is a constant contribution that represents the contact resistance ($R_C^{'}$ + $R_C^{''}$); this contribution is inversely proportional to the electrodes area (not considering in a first

approximation the human error in the realization of precise small electrodes and neglecting the board effects that are present for the small electrodes);

- Another contribution called R_0 must be introduced to take into consideration the overvoltage cell effect;

- the slope (that is almost constant for all the couples of electrodes) represents the resistance of the solution that grows linearly with the distance (d) between the electrodes;

At the end the equation that describes the cell resistance is:

$$R = R_C + R_S + R_0 = \rho_C \cdot \frac{1}{S} + \rho_S \cdot d + R_0 \qquad (22)$$

where ρ_S, ρ_C are the solution resistivity and the contact resistivity, respectively.

In order to quantify all the parameters the data have been analyzed by the method of the least square in Matlab (Fig. 32).
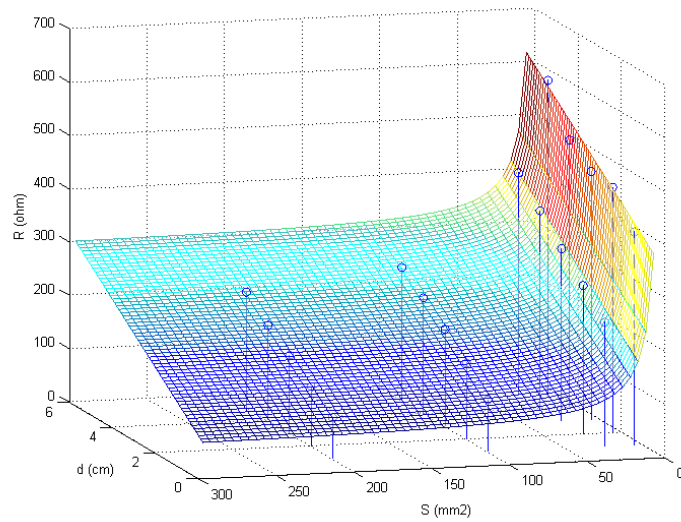
Fig. 32. Fitting curve obtained with the method of the least square by Matlab.

The obtained values are:

$$\rho_C = 1927 \ \Omega \cdot mm^2$$

$$\rho_S = 4 \ \frac{\Omega}{mm}$$

$$R_0 = 55 \ \Omega \qquad (23)$$

$$R = 1927 \cdot \frac{1}{S} + 4 \cdot d + 55$$

By repeating the test with a concentration of 0.3M of lead acetate it has been obtained:

$$\rho_C = 1800 \ \Omega \cdot \text{mm}^2$$

$$\rho_S = 2.2 \ \frac{\Omega}{\text{mm}}$$

$$R_0 = 20 \ \Omega \qquad\qquad (24)$$

$$R = 1800 \cdot \frac{1}{S} + 2.2 \cdot d + 20$$

ρ_S changes considerably with the solution concentration, while ρ_C remains almost constant.

The last contribution to be considered is the one due to the anionic membrane. To perform a valid measurements this membrane must be leave in the solution for some hours in order to reach a correct working state. The resistance of the membrane depends from the dimension (the surface) and from the solution concentration. However it can be affected by several other secondary effects, for this reason in order to find the right resistance offered by the membrane it should be tested in the setup where it will work. In our case the membrane has been tested in the setup presented in Fig. 27 and Fig. 28.

The selected solutions are 0.1M and 0.3M. The measurement has been performed for difference, i.e. the cell resistance has been measured with and without membrane.

The results are a membrane resistance R_M equal to 130Ω for the 0.3M solution and 300Ω for 0.1M solution. The R_M can be written has:

$$R_M = \frac{\rho_M}{A} \qquad\qquad (25)$$

With A that is the active surface of the membrane and in the proposed setup is 113mm^2 and ρ_M that is the resistivity of the membrane.

In this way we obtain a resistivity of about 15000 $\Omega \cdot$mm^2 for the 0.3M solution and 34000 $\Omega \cdot$mm^2 for the 0.1M solution.

At the end the equation that represents the total resistance of the cell becomes:

$$R_{TOT} = R_C + R_S + R_0 + R_M = \rho_C \cdot \frac{1}{S} + \rho_S \cdot d + R_0 + \rho_M \cdot \frac{1}{A} \qquad (26)$$

In a practical example, considering the experimental setup proposed and the real geometrical values, we can evaluate the contribution of each single term:

$$R_C = \frac{\rho_C}{S} = \frac{1800\,\Omega \cdot \text{mm}^2}{200\,\text{mm}^2} = 9\,\Omega$$

$$R_S = \rho_S \cdot d = 2{,}2\,\frac{\Omega}{\text{mm}} \cdot 20\text{mm} = 44\,\Omega$$

$$R_0 = 20\,\Omega \qquad\qquad (27)$$

$$R_M = \frac{\rho_M}{A} = \frac{15000\Omega \cdot \text{mm}}{113\,\text{mm}} = 132\,\Omega$$

$$R_{TOT} = 205\,\Omega$$

These results have been verified simply applying a 1V to the cell and obtained as expected a current of about 5mA.

As already explained the target difference of concentration between the two semi-cells that we want to reach is $\Delta C=0.5M$. To analyze the electrolysis process we use again the Faraday law. Supposing to start from an equilibrium condition (the concentrations in the two semi-cells are the same), it is possible to write:

$$
\begin{aligned}
&I(t = 0) = 0\\
&C^+(t = 0) = C^-(t = 0) = C_0\\
&\Delta C(t = 0) = 0\\
&V^+ = V^- = V
\end{aligned}
\qquad (28)
$$

Where:

- C^+, V^+ concentration and volume of the solution in the anodic semi-cell
- C^-, V^- concentration and volume of the solution in the cathodic semi-cell

Supplying to the system an amount of charge q in the time t:

$$C^+(t) = C_0 + \frac{q}{z \cdot F \cdot V}$$

$$C^-(t) = C_0 - \frac{q}{z \cdot F \cdot V} \qquad (29)$$

$$\Delta C(t) = C^+(t) - C^-(t) = \frac{q}{z \cdot F} \cdot \left(\frac{1}{V} + \frac{1}{V} \right) = \frac{2 \cdot q}{z \cdot F \cdot V}$$

In case of constant current the variation of concentration is linear and the electrochemical process can be described and characterized easily:

$$\Delta C(t) = \frac{2 \cdot I \cdot t}{z \cdot F \cdot V}$$

(30)

$$t_R = \frac{\Delta C \cdot z \cdot F \cdot V}{2 \cdot I}$$

By using as input the experimental setup previously proposed and a current of 5mA a reaction time (t_R) of about 13 hours has been obtained. The result has been also verified experimentally by the setup realized and applying a constant current of 5mA by the potentiostat.

By using instead a constant voltage (1V) as input it is experimentally verified that the current increases during the reaction. However the slow current increase (it reaches at the end a maximum of 6mA) is not sufficient to modify significantly the reaction time that remains about 13 hours.

Setup for osmotic experiments and tests

Starting from the consideration that the objective is to test the pressure performance with the different solutions, a suitable setup chamber has been realized. This chamber must permit the developing of at least of 10 atm, the separation of the two semi-cells by an osmotic membrane, an architecture that sustains the membrane avoiding breaks during the generation of high pressure.

The cell proposed is shown in Fig. 33 (semi-cell) and Fig. 34 (grid to sustaining the osmotic membrane).
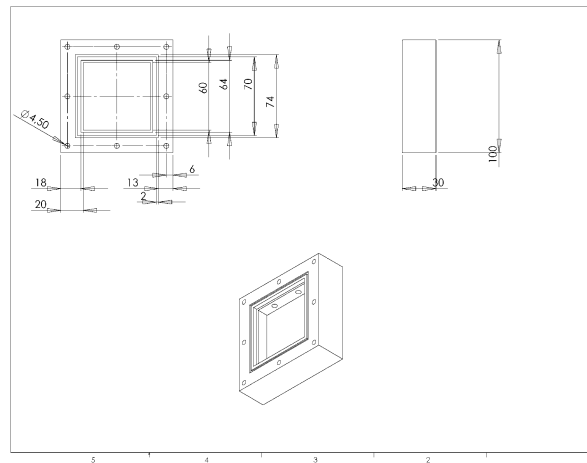
Fig. 33. Geometry and dimensions of the two semi-cells for testing the osmotic principle.
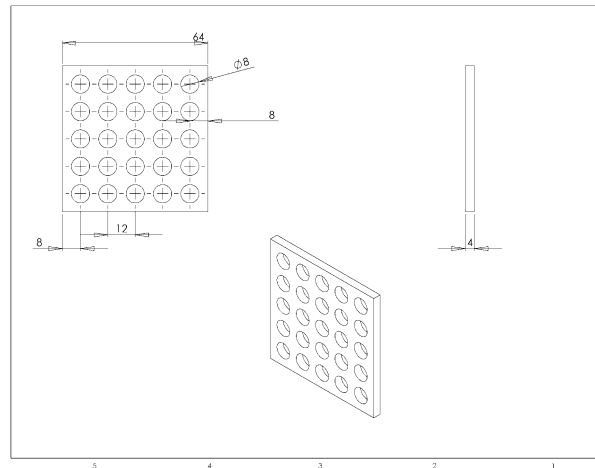
Fig. 34. Geometry and dimensions of the grid for sustaining the osmotic membrane.

The cell must be closed by 8 screws to guarantee the sealing both externally and between the two semi-cells. The overall system is shown in Fig. 35. The cell presents 4 hydraulic connections that permit a correct filling of the two semi-cells. The semi-cells must be accurately filled with the solution in order to not leave air inside, air is compressible and, it causes a delay in the pressure increase. Then two of these connectors are closed by two sorts of caps. The other two are connected by a differential pressure sensor that will monitor the pressure during the experiments. The data are collected by a data acquisition system (National Instruments NI-USB-6218).
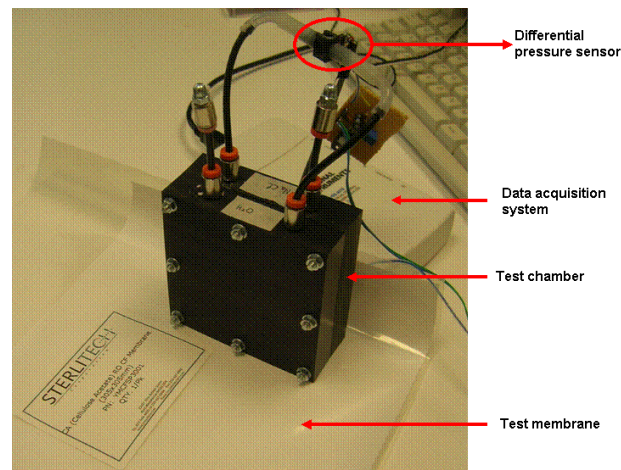
Fig. 35. The experimental setup for testing the functionalities of the membranes.

Preliminary tests have been performed with water and NaCl as salt; in particular a semi-cell has been filled with a solution at 1M of NaCl and the other one with pure water. This test is necessary to test the functionalities of the cell (to verify the sealing capabilities), the functionalities of the osmotic membranes and of the overall measuring setup. The results are shown in Fig. 36. In particular, it is possible to see that, with the cellulose acetate membrane, the maximum pressure that has been obtained with the setup is more than 10 atm. This limit is quite far by the theoretical limit ($\Delta\Pi = \Delta C \cdot R \cdot T \cdot i = 48$ atm). This is due to: the not ideal seal of the setup; the not perfect

dissociation of all the solute; a lower real difference of concentration across the membrane due to the not perfect mixing of the solutions; the cellulose acetate membrane characteristics that have a rejection size of 92-97%, that means that part of the solute can pass through the membrane and after some hours the effective difference of concentration between the two semi-cells is lower than 1M. The polyamide membrane permits flow of water more limited; in fact the maximum of pressure is reached after 25 hours (instead than after 3 hours with the cellulose acetate membrane). Also the maximum reachable pressure is lower (3 atm).
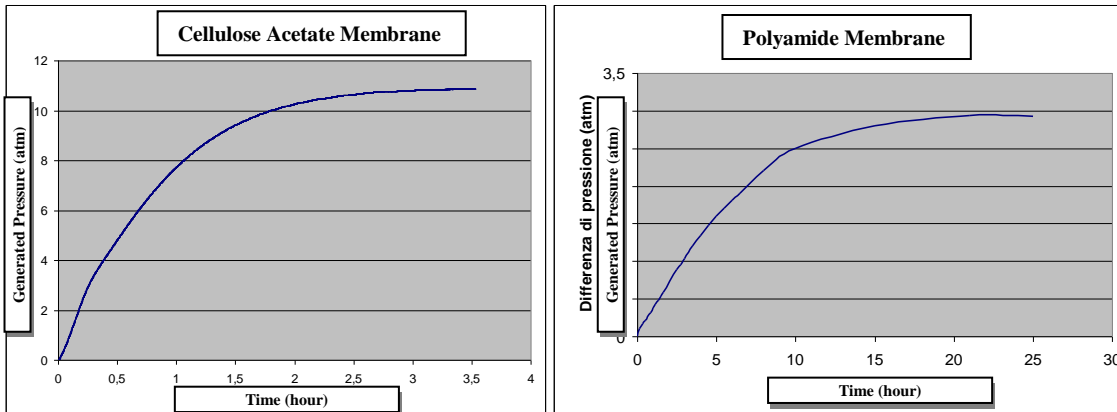
Fig. 36. Osmotic experiments with cellulose acetate membrane and with polyamide membrane

Following these results, cellulose acetate membrane has been selected for its speed and high pressure performances. At this point in order to test the compatibilities of the membrane with the lead salts (lead perchlorate $Pb(ClO_4)_2$, lead nitrate $Pb(NO_3)_2$ and lead acetate $Pb(CH_3COO)_2$), the same experiments have been performed with these salts.

The results for different initial concentrations between the two semi-cells are shown in Fig. 37. In particular, it is possible to see that for the cases 0.1M/1M and 0.1M/0.5M a break in the membrane occurs in correspondence of 2.5atm (pressure drops instantly to 0 atm). This behaviour verified in several test is not justified by the mechanical resistance of the membrane that has reached pressure up to 11atm without problems. This behaviour depends from a weakening of the membrane caused by the lead perchlorate. For this reason the lead perchlorate seems to be not suitable for the proposed actuator, even if it showed the best performances for the electrolytic process.
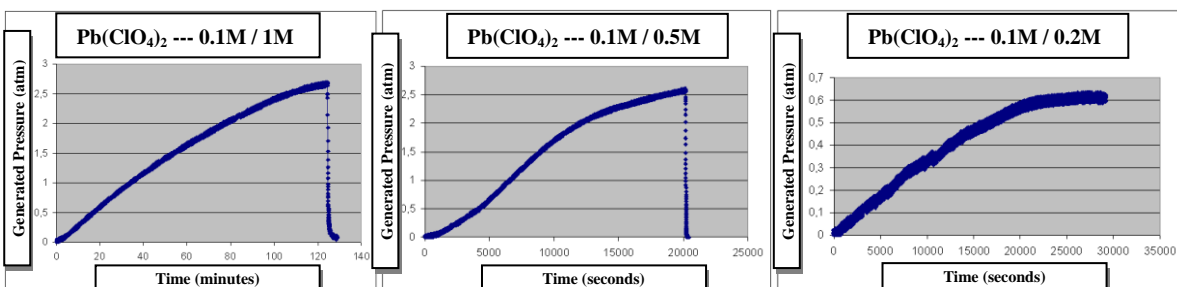
Fig. 37. Osmotic experiments with lead perchlorate at different concentrations

About the lead nitrate the results are shown in Fig. 38. Also in this case there is a break in the membrane, even if it seems to be more resistant to this salt. However this solution was already discharged because it presents some unwished reactions during the electrolysis.
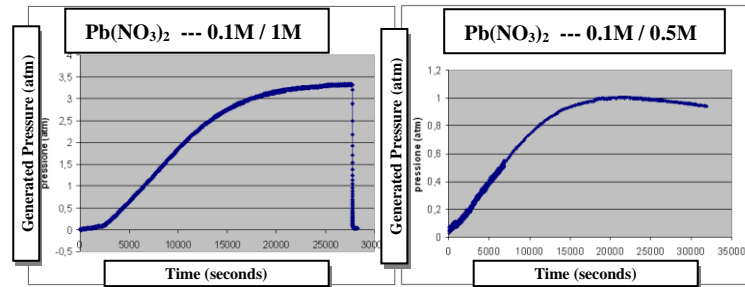
Fig. 38. Osmotic experiments with lead nitrate at different concentrations

Regarding the lead acetate, the results of the experiments performed are shown in Fig. 39. In particular a concentration of 0.1M in a semi-cell and 1M in the other results also in this case in a break of the membrane (Fig. 39a). With lower concentrations, 0.1M / 0.5M, the membrane resists (Fig. 39b) and by inverting the solutions in the two cells (i.e. inverting the pressure) as shown in Fig. 39c, the system continues to work fine (without any break). The greater pressure (3.1 atm) has been obtained with 0.1M / 0.6M (Fig. 39d).
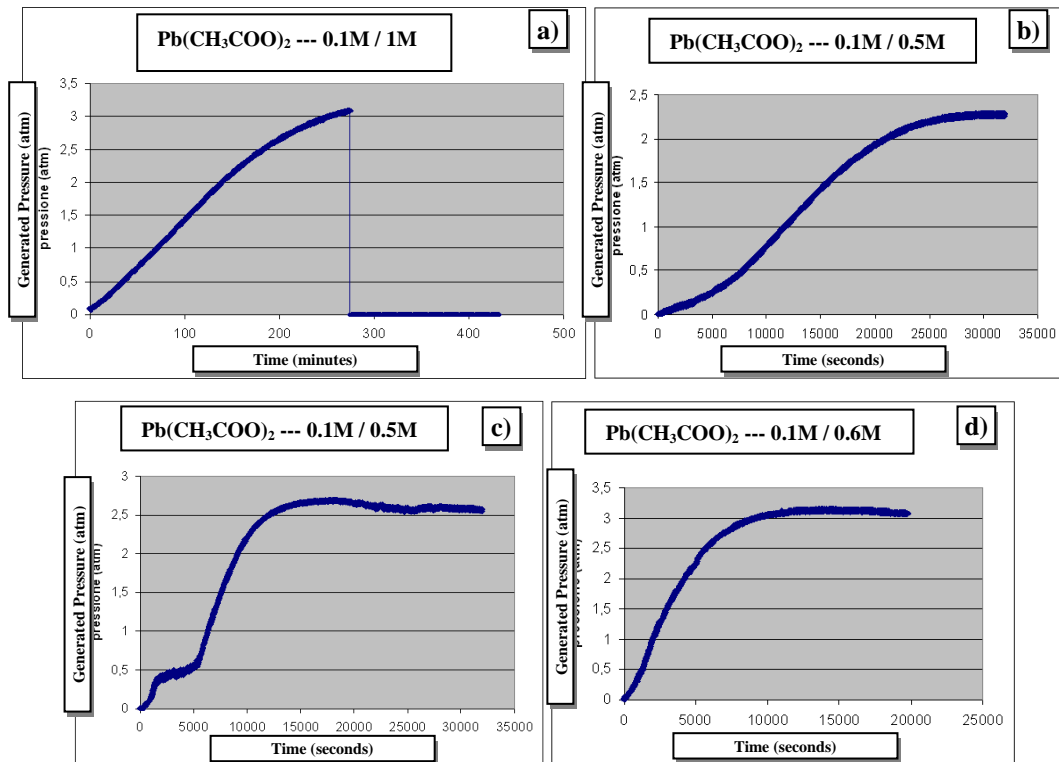
Fig. 39. Osmotic experiments with lead acetate at different concentrations

- In conclusion, the following components have been selected for the realization of the osmotic actuator: IONAC MA-7500 as anionic membrane for its low resistance;

- Sterlitech CA (Cellulose Acetate) RO CE as osmotic membrane for its good compromise between water flux and rejection size;
- Lead acetate as salt because it is compatible with the membrane adopted;
- Pure lead for the electrodes.

Setup for complete actuator experiments and tests

At this point the two functionalities (osmosis and electrolysis) must be tested together. In order to realize the new setup, the one used to test the osmotic principle has been opportunely modified. In particular the setup for the osmosis presents too large semi-cells that implies a long time for the electrolysis. So size has been decreased. Also the grid must be changed because now they need to host two membranes (osmotic and anionic). Moreover the electrodes must be fixed in the two semi-cells and the contacts moved out to allow the application of a current.

The design and realization of the grids for the membranes has required a great effort, for the difficult to reach a suitable level of sealing. The solution finally adopted is shown in Fig. 40. These grids foresee the space to lodge the two membranes with different thickness (0.2mm the osmotic membrane, 0.6mm the anionic membrane).
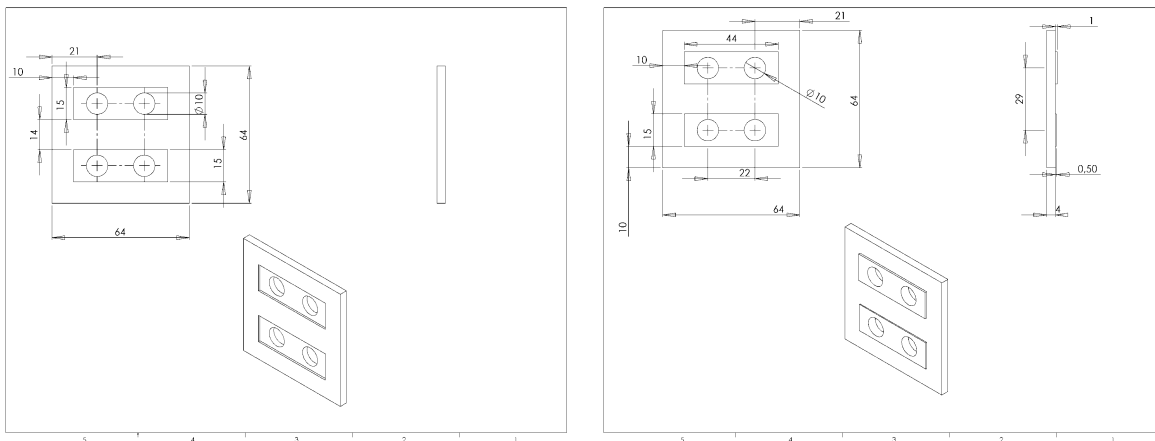
Fig. 40. Grids to support the two membranes (anionic and osmotic)

The setup has been mounted with the components previously identified. The result is shown in Fig. 41. The two red wires are the connections for the electrodes and they are connected to the potentiostat in order to monitor the supplied current. The system used to filling the chambers and for measuring the generated pressure is the same presented for the osmosis setup.

The two semi-cells have been filled with lead acetate solution at 0.3M.
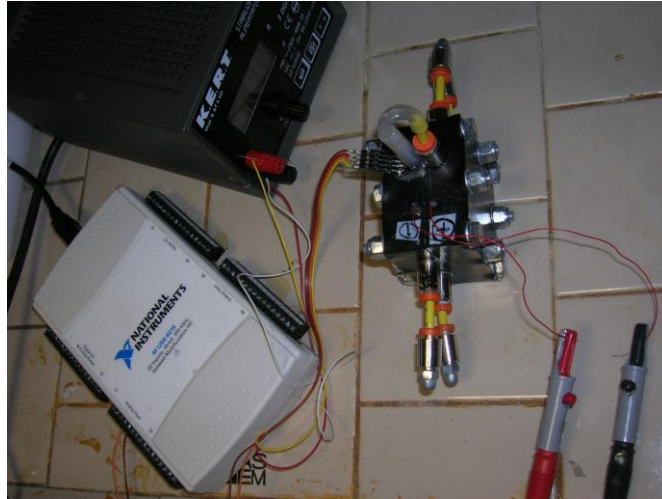
Fig. 41. Setup for the complete osmotic actuator.

The experimental tests have been carried out by following these steps:

- Starting from the equilibrium (0.3M solution in both the chambers), a constant current is supplied to the system in order to produce a difference of concentration between the two semi-cells;

- After a sufficient time to permit a significant difference of concentration, the direction of the current will be inverted;.

In this way it is possible to verify that the process is invertible and so that is possible to invert the actuation mechanism. Results of the experiments are reported in Fig. 42 where generated pressure versus time is reported graphically; in the graphs the cusps represent the inversion of current. As is possible observe, the system follows the expected behaviour, thus demonstrating the proposed principle. Nevertheless many studies must be carried out in order to obtain an actuator with good performances.
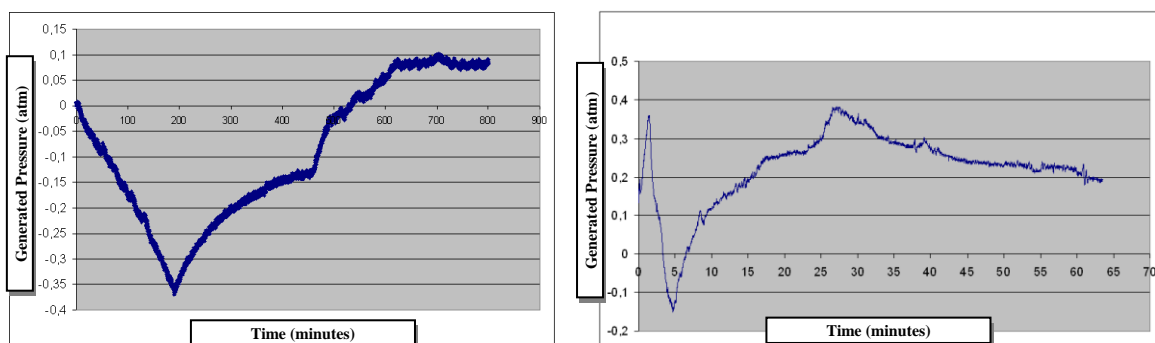
Fig. 42. Pressure generated in the electro-osmotic actuator.

4.2.5 Three cells osmotic actuator

The concept of an osmotic actuator with two cells has been extended to a 3-cells actuator. This solution maintains the osmotic process and allows the steering of the root in all the directions in a compact and easy way.

The three cells have a circular shape and are separated by three couples of membranes (semi-permeable osmotic membrane and ion selective membrane) and contain one electrode each.

This design of the actuator (Fig. 43) is more compact and scalable and it allows the control of the flux of water with 3 lines (one per electrode) instead of 6 (as in the case of three simple 2-cells actuator). It is possible to set the potential of electrodes two at time or all together, changing the concentration across the three cells and generating the expected water flow.
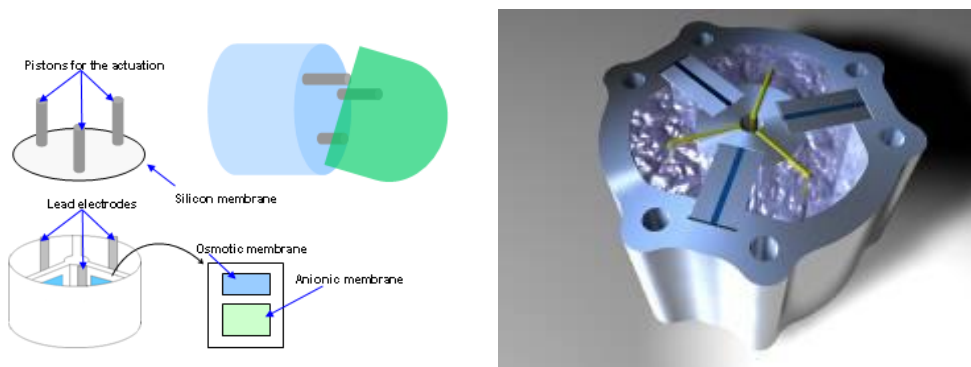
Fig. 43. Three cells osmotic actuator.

4.3 Root Apex Mechanical Design

4.3.1 The robotic tip

In the following, a design of the robotic root apex, whose steering actuation relies on the bioinspired osmotic principle previously described, will be presented.

The apex structure can be divided in two main parts:

- Osmotic module;
- Control and sensing module.

The two parts are connected by means of a spherical joint, which allows the rotational movement of the apex.
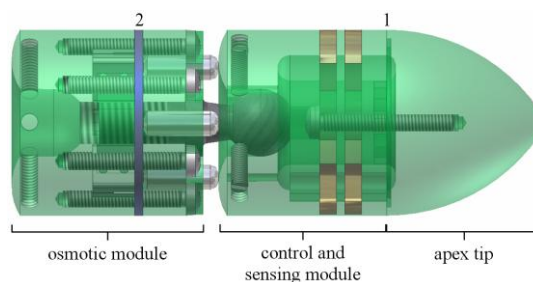
Fig. 44. Structure of the first robotic root apex: Side perspective of a three-dimensional CAD model of the first proof-of-concept structure of root apex; the frame is transparent-green in order to make visible the internal features and structural parts.

A general approach to convert pressure into an actuating force is to use a piston system. In the present application the osmotic module is devoted to generate and contain the osmotic pressure and transform that in an axial force by means of pistons. Each actuated piston applies a momentum onto the apex control and sensing module, which is forced to rotate around a spherical joint. In order to obtain the steering of the robotic apex in a three-dimensional space, at least 3 pistons positioned around the circular section of the apex at 120° between each others are necessary. The miniaturization of these actuators and the aim to fabricate a robotic apex of relatively small size require to integrate all the three actuators in a single device.

The osmotic module is a system whose frame is composed by two parts (Fig. 45):

- a sub-module hosting three consecutive osmotic cells separated by gratings, each contains the two osmotic and anionic membranes.
- a head block that compress and fasten a deformable silicon membrane over the osmotic chambers and works also as a guide for the stroke of the pistons.

By exploiting the osmotic principle, it is possible to regulate the concentration of ions in the chambers and, consequently, to drive the water in a selected chamber in order to make the membrane locally expand into the piston guide and push the corresponding piston.

The pushing force applied by the piston equals the product of the internal pressure generated in the chamber by the cross-sectional area S of the piston (which is obviously limited by the external diameter of the apex).

(a)   (b)
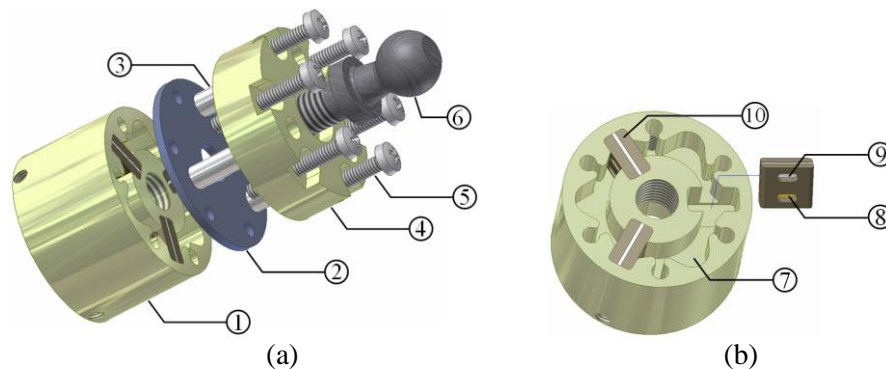
Fig. 45. CAD drawing of the osmotic actuation module: a) Exploded view, with (1) osmotic chambers, (2) silicon membrane, (3) piston, (4) head, (5) screw, (6) spherical joint; b) Closer view to the osmotic chambers, which are only 4.5 mm deep, with (7) osmotic chamber, (8) osmotic membrane, (9) anionic membrane, (10) mounted grating with membranes.
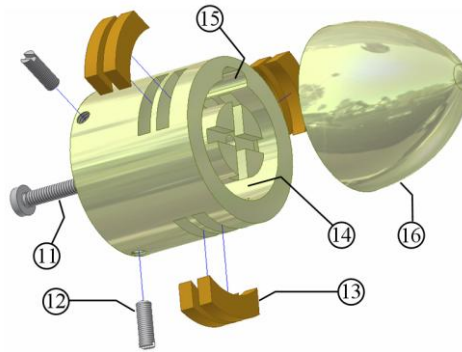
Fig. 46. CAD drawing of the control and sensing module and the tip: (11) tip screw, (12) blocking pin for the spherical joint, (13) electrode for moisture analysis, (14) annular cavity for electronics, (15) cavity for hosting accelerometer, (16) apex tip.

Fig. 46 shows the control and sensing module, together with the tip. It presents an internal annular cavity where it is possible to place a flexible circuit with the mounted electronics, suitably design to fit into the empty space. In particular, a small channel is formed along an external wall of the annular cavity to host the accelerometer and thus fixing its position relatively to the apex

Electrical wiring has not been reported in the CAD drawing for clarity. Following the approach to maintain the complexity of the system minimal, the design has been done taking into account the possibility to use some structural parts as electrical conductors. Each driving signal for the osmotic chambers (one for each chamber) is wired from the electronics integrated into the control module to at least one of the screw fastening the head of the osmotic module (see Fig. 45a), which, as visible in Fig. 45b is partially exposed to the chemical solution in the osmotic chambers, allowing direct electrical contact with the lead electrode. Even though small batteries could be integrated in the tip in order to power both electronics and chemical processes in the apex for at least several hours, the plantoid was conceived as a larger robotic system capable to operate much longer by means of an external energy source, e.g., as it happens for plants, solar power. This means that power and ground lines should be distributed all over the roots down to the apexes. The central screwing system, namely the tip screw, and the spherical joint, can work as a main central electrical conductor, which runs internally along all the apex (and the root) and can maintain the electrical contact between different rotating metallic part by brushing wires (see also Fig. 45a, where at the base of the osmotic module it appears in transparency a cavity for the insertion of another spherical joint, which will allow the docking of the first root module or eventually another osmotic module, in order to have more apex steering). This internal wiring system can be used as a common electrical line (power or ground). An external membrane should finally envelope the whole root system, except the apex, in order to protect the joint mechanisms, and to be fabricated in low-friction materials in order to facilitate penetration of the root into the terrain.

4.4 Electronic and sensors design

The transition zone of the plant root apex can be considered a sort of processor or command centre which processes sensory information from the surrounding environment (gravity, gradient of humidity in the soil, nutrients). The apex "takes decisions" about future exploration on the basis of the tropistic behaviour. Analogously, an electronic circuit has been embedded in the robotic root tip for implementing these plant behaviours.

The core of the unit is a microcontroller (a PIC18F2520 from Microchip) that, as it happens in the transition zone in plants, performs the acquisition from the sensors and it drives opportunely the actuators for the bending of the root on the base of the gradient of water and of nutrients, and following the gravity (Fig. 47).
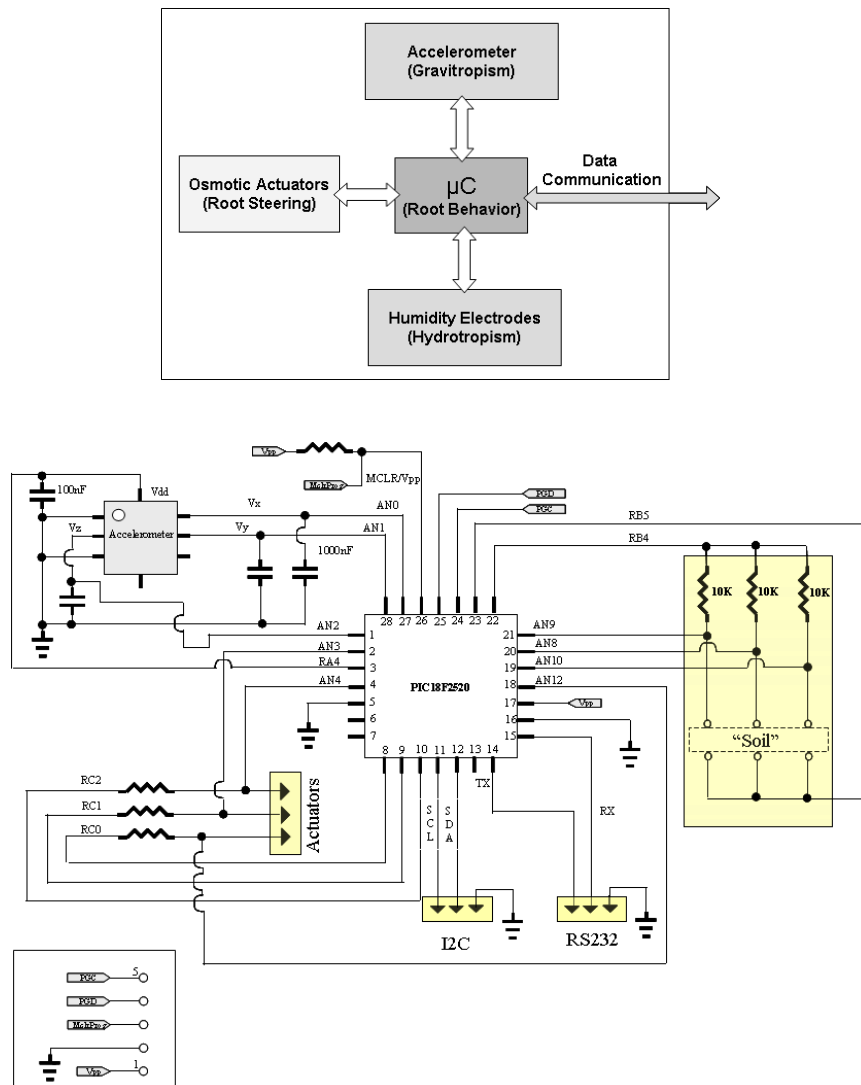
Fig. 47. Electronic apex scheme.

In these prototypes two kinds of sensors have been integrated: an accelerometer to implement the gravitropism behaviour; and a soil moisture sensor (measuring the conductivity of the soils) to implement the hydrotropism behaviour.

The accelerometer embedded in the robotic apex is the LIS3L02AL by STMicroelectronics. It is a tri-axial accelerometer, which assures the possibility to establish correctly the relative apex position. It has ±2g of full-scale, suitable to measure the gravity acceleration. The sensor has been lodged in a chamber (Fig. 48) appositely fabricated in the tip in order to obtain a precise position respect to the osmotic actuators.
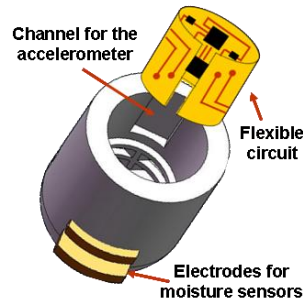
Fig. 48. Accelerometer and soil moisture electrodes position in the root apex.

The commercial available moisture sensors are normally used in the agriculture field and for this reason are relatively large. Moreover, this kind of sensors requires to be calibrated for a specific soil because different soils show different physical properties.

The electrical resistivity variation of soil is a function of several properties: particle size distribution, porosity, water content, ions concentration ([108], [110]). Consequently, the electrical resistivity shows a large range of variation, from one to several thousand ohms per meter.

In this specific application, because of the quite restricted area involved in the plant action, the composition of soil, the texture, salts content and the porosity are quite similar in this specific zone. Therefore the change in the resistivity of the soil can be attributed to a different water concentration. Fig. 49 shows the resistivity for different soil composition.
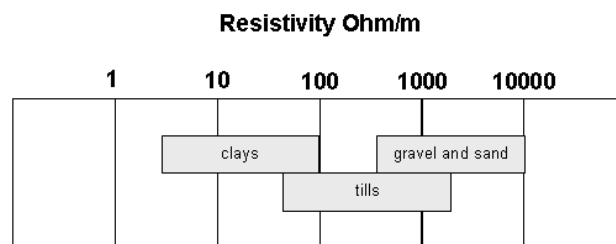
Fig. 49. Graphical representation of the resistivity of different kinds of soils.

This information helps in conditioning the soil moisture sensors and allows increasing the sensibility of the sensors for a defined soil. Exploiting this concept, a customized array of soil moisture sensors has been designed and developed. The sensor is composed by three electrodes, made in brass and with a size of 10×2 mm and a distance of 1mm each other.

Changing the electrode size and the distance among them determines the variation of the resistance measured. Three couples of electrodes have been mounted on a cylindrical support (that simulates the robotic root apex) at 120° spacing. The aim is to detect a gradient of the relative moisture distribution,

instead of a precise determination of the relative moisture percentage in a specific soil. Consequently, the apex can steer in the direction of the maximum moisture level.

Several experiments have been performed with different kinds of soil in order to verify the electrodes reply to a soil humidity variation. In particular, the device with the integrated electrodes has been put in a cylindrical container with 5cm of radius and filled with 10cm of soil (of different type). The sensor has been put in the centre at a depth of 5cm of deepness. Fig. 50a shows the top view of the experimental set up. The test has been performed with the injection of a known quantity of water (5ml), in precise points, at a fixed time intervals. Fig. 50b shows the variations of the soil resistance measured from the three couples of electrodes. The dotted lines represent the injection time of water in the container in the points indicate in Fig. 50a. From the graph, it is possible to note the rapidity of response of the sensors, the wide range of variation of measured resistance and, consequently, it can be concluded that is quite easy to identify soil with higher water content.
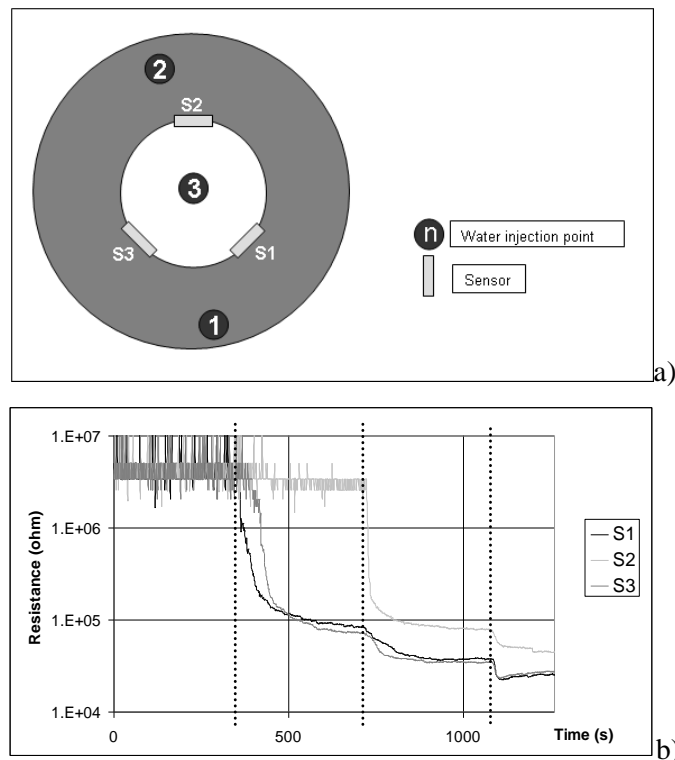
Fig. 50. Soil moisture sensor tests: a) Top view of the used set-up; S1-S3 are the 3 couples of electrodes, 1-3 are the water injection points; b) Typical electrodes output signal, the dotted lines represents the time of the three sequential injections.

The sensors implemented in the robotic root apex allow acquiring information on the root apex position and on the soil water content, in this way it is possible to mimic the root gravitropic and hydrotropic behaviours commanding the steering by means of the osmotic actuator. In this first implementation, the robotic root behaviour has been simplified separating the control of the two environmental stimuli. The steering capabilities of the robotic root apex, as result of following gravity and humidity gradient, were implemented and tested in a second prototype version, whose size has been optimized taking also into account penetration capabilities and actuation time.

4.5   Dimensioning

The second model of the robotic root apex was designed taking into account three main requirements:

- Penetration capability;
- Steering capability (i.e., apex capability to give proper direction to the penetration according to control signal);
- Actuation times (based on the osmotic and electrolytic process).

4.5.1   Penetration Considerations and Experimental Tests

In the dimensioning of the robotic root apex it is crucial to consider how the root diameter and the tip shape affect the penetration capabilities. In particular, we considered how the soil resistance changes towards different penetrating root probes. This consideration is important in the hypothesis that the robotic root system is propelled by the osmotic pressure. In fact, in this case, varying the apex size, the osmotic pressure remains constant and the optimization of the penetration is made by trying to minimize the resultant soil resistance. Differently, considering a constant generated force, the optimization is obtained by decreasing the root diameter. Several theoretical and experimental works were performed in this field in order to correlate the effective soil resistance to the resistance measured by means of a penetrometer [109]. For uniformly compacted soil, the force applied by penetrometer probes increases with the probe diameter [99]:

$$F = \frac{\pi \cdot b \cdot (d + x)^2}{4} \qquad (31)$$

where F (in [N]) is the compressive force applied to the penetrometer, b (in [MPa]) is the effective soil pressure resistance, d (in [m]) is the probe diameter and x (in [m]) represents a sort of thin soil layer, which leads to an apparent increase in the probe diameter (d). Both x and b parameters are constant for a particular soil with a known water content. In many cases x can be considered close to 0.6mm, but for some soils and conditions, can be greater or smaller than this value. For this reason, a 1-mm probe exerts a pressure typically 45-55% greater than a 2-mm probe. This aspect, graphically shown in Fig. 51, recommends maintaining the root diameter above 8-10mm in order to have lower penetration resistance in several kinds of soils. Moreover, greater probe diameters do not make worse the penetration capabilities.
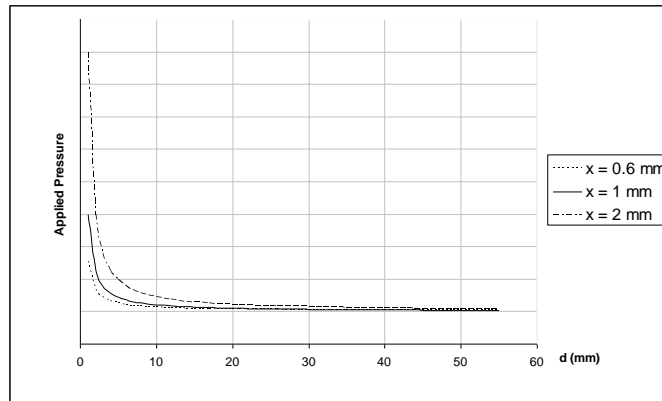
Fig. 51. Result soil pressure *vs* probe diameter for different kind of soil.

This trend, demonstrated in [99] relatively to probe diameters ranging from 0.1 to 2mm has been verified for larger diameters by performing several penetration tests. A test bench was set-up consisting of an Instron testing machine 4464 equipped with a 1kN load cell, a large container filled in with soil and a computer running a Labview program for data acquisition (see Fig. 52). Cylindrical probes ending in a 60°-aperture cone were fabricated in Delrin® with the following diameter: 50 mm, 35.7 mm (standard probe size used in the Cone Penetration Tests, CPTs, in order to have a valuable reference, e.g. see [100] and [101]), 22 mm (as a first developed apex prototype), 8 mm. The probes penetration speed was kept constant during the process, precisely at 1 mm/s. Although slower speeds were tried (e.g. 0.1 mm/s) in order to operate in quasi-static conditions, as it occurs for plant roots, results did not significantly vary, thus the above mentioned speed was used to limit the testing times required for experiments A mixed clay/sand soil, both in wet and dry conditions was tested. The resistance force experienced by the load cell during the penetration was acquired continuously with a resolution of about 0.1 mm. As it might appear intuitive, smaller the diameter of the probe, lower the force required to reach a specific depth (200 mm in the tests). It is very interesting to consider the case of an apex pushed into the terrain by a root-system actuated by osmotic pressure, as described before, see Fig. 18 and Fig. 19. In this case the force generated is proportional to the diameter of the system body, i.e., the actuation force results from the product between the internally generated pressure and the section area of the system body. Having in mind such a system, the most relevant parameter in the tests becomes the force per unit area applied to each probe, thus the applied pressure (on the cross-section area of the probe).

The results of these tests are that the smaller probe sizes were the most demanding in terms of required pressure, in particular at low depth. In addition, it was demonstrated that soil penetration in a common terrain down to a depth of 200 mm could theoretically be achieved with an osmotic actuation with suitable pressure (< 5 atm) using probes with different sizes.

Results of applied pressure plotted to the soil depth in the container are reported in Fig. 53. From the plots, it clearly appears that the penetration performed by larger probes gives a monotone trend in the plotted curve, while smaller probes show trend inversions: this is probably due to the smaller size of the probe that is affected by the local characteristics of the soil.
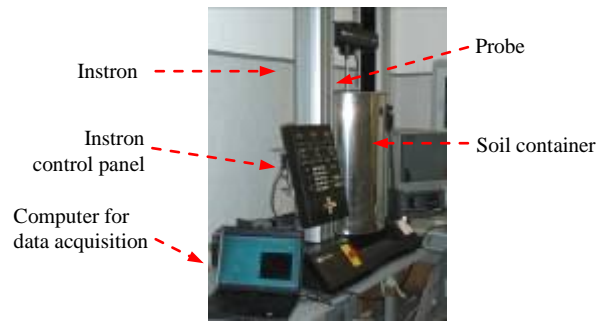
Fig. 52. Experimental set/up for measuring resistance force during penetration up to 1kN.
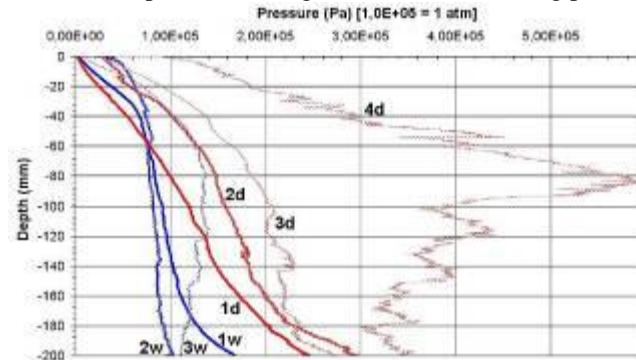
Fig. 53. Resistance pressure exerted by the mixed clay/sand soil during penetration of the probes plotted to the soil depth, for probe diameters of (1) 50 mm, (2) 35.7 mm, (3) 22 mm, (4) 8 mm, in case of wet ("w") or dry ("d") condition of the soil.

Other aspects affect the penetration capabilities of plant roots inspired probes. The resistance of a soil shown to a penetrometer can be up to three times greater than the one necessary to a root to penetrate the same soil [102]. This is partially explained by the difference in the friction between an artificial probe and the real root. In fact the root cap is characterized by the continuous production and sloughing of cells that decrease the friction at the soil-root interface [46]. A second consideration is that with a rotating penetrometer (e.g. 1 revolution every 5 mm penetration) the metallic probe resistance decreases until it remains equal to that shown by a real root [103]; the plant roots do not make a real rotation but a spiralling movement named nutation that some studies (e.g. [104], [105]) suggest may aid the root penetration. These final considerations will be useful during the robotic apex control but do not affect the mechanical design. Another important factor is the tip shape; in [106] it was experimentally shown as a flat tip can experience until two times the soil resistance experienced by a 60° cone tip.

4.5.2 Steering Performances

The size of the system, i.e., the diameter of the cylindrical body, is responsible in defining not only the penetration performances, but also the steering capabilities. As mentioned before, the force, which pistons can exert, results from the multiplication of the osmotic pressure by the piston section area. Nevertheless, an increase of the overall dimensions brings to a greater amount of soil to be moved.

It was consequently decided to develop a simple parametric model of the robotic apex, in order to parameterize the structure and obtain the variation trends of important parameters. These points have been achieved by expressing most of the geometrical features of the apex shown in Fig. 54 as a function

of the apex radius R and some fixed constants, e.g., minimum wall thickness, margins between integrated parts, maximum steering angle, and the aperture angle of the apex tip.
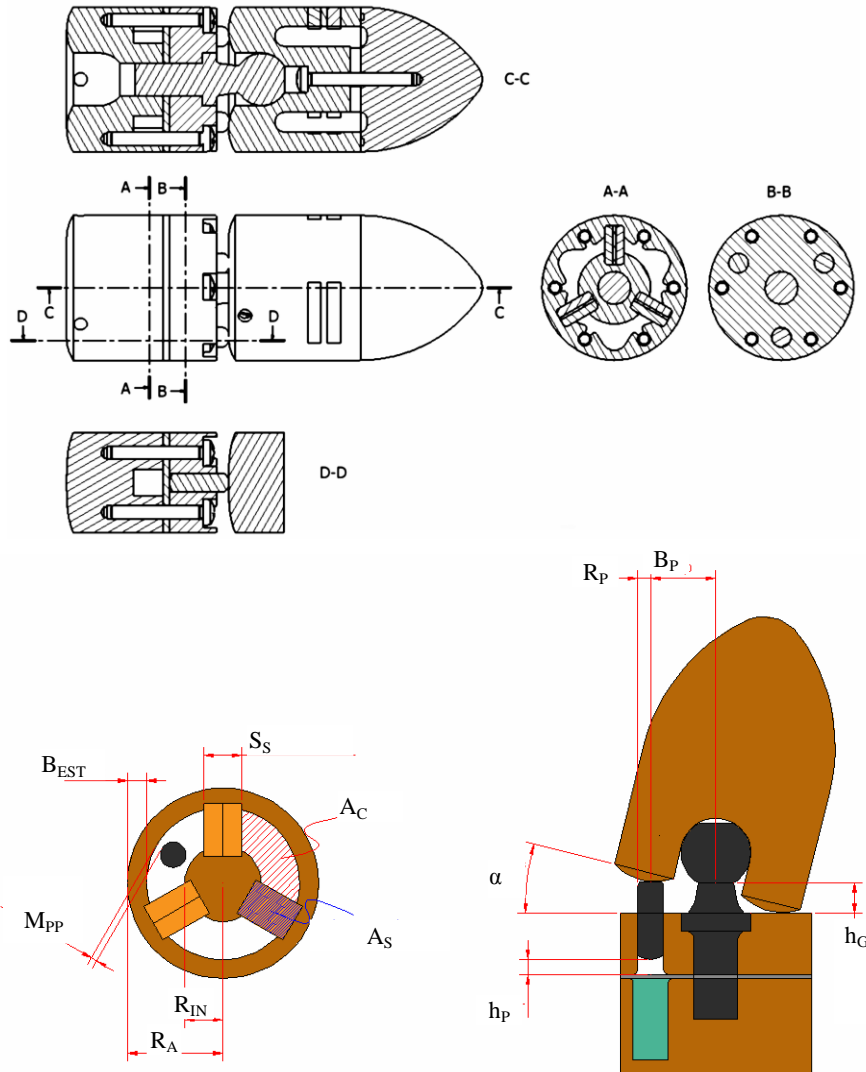
Fig. 54. Parameterization of the root apex dimension

In particular, in Fig. 54 are shown several constant parameters that can remain constant varying the apex radius (R_A). These are physical constraints limited by the materials and fabrication technologies used. Some of these parameters are listed below:

- Internal radius of the osmotic module R_{in};
- Thickness of the external walls B_{est};
- Thickness and height of the grids for the membranes S_s e h_s;
- Margin between the spaces for the membranes and the edges of the grid M_s;
- Margin between the piston and the bottom of the cell M_{pf};
- Margin between the piston and the wall of the cell M_{pp};
- Width of the well in the bottom of the cell positioned near the grids l_p;
- Height of the tip h_{tip};

- Half opening angle of the tip θ;
- Maximum steering angle α.

These parameters (together with R_A) are enough to describe the mechanical features of the system:

- Transversal area of the osmotic cell;

$$A_c = \frac{(R_A - B_{est})^2 \cdot \pi - R_{int}^2 \cdot \pi}{3} - S_s \cdot (R_A - R_{int} - B_{est})$$

- Height of the spherical joint in order to permit the maximum steering;

$$h_g = R_A \cdot sen\alpha$$

- Radius of the pistons (R_p);

$$R_p = \frac{R_A - B_{est} - R_{int} - 2 \cdot M_{pp}}{2}$$

- Lever arm of the pistons (B_p);

$$B_p = R_A - B_{est} - M_{pp} - R_p$$

- Stroke of the pistons (h_p);

$$h_p = B_p \cdot tg\alpha$$

- Height of the osmotic cells (h_c);

$$h_c = h_p + M_{pf}$$

- Osmotic cells volume (V_c);

$$V_c = h_c \cdot A_c + 2 \cdot l_p \cdot (R_A - R_{int} - B_{est}) \cdot (h_s - h_c)$$

- Total area available for the two membranes on the grids (A_m);

$$A_m = h_s \cdot (R_A - R_{int} - B_{ets}) - 3 \cdot [M_s \cdot (R_A - R_{int} - B_{est})] - 2 \cdot M_s \cdot (h_s - 3 \cdot M_s)$$

- Volume of water necessary in order to move the piston from the rest position to the maximum extension position (maximum apex steering);

$$V_{att} = R_p^2 \cdot \pi \cdot h_p$$

A first result of this parametric model is that the steering capability (into the soil) increases almost linearly with the apex radius R_A. This is given by some physical considerations and from the root apex design. The steering capabilities can be expressed as the ratio between the momentum of the force generated by the piston and the area of the apex section, which takes into account the soil amount that the tip must move during the steering. Expressing these two quantities in function of R_A it is possible to find that: the piston radius (R_P) is proportional to R_A; consequently the force generated by the piston on the tip is proportional to R_A^2. The distance between the centre of the piston and the apex centre, i.e. the arm of the force applied by the piston on the tip, is proportional to R; consequently the momentum of the force is proportional to R_A^3. The section area of the tip has a term that grows proportional to R_A and another (the tip area) that grows with R_A^2. At the end, the ratio between the momentum of the force generated by the piston and the area of the apex section is proportional to R_A. This ratio has been expressed as *q* and shown in Fig. 55.
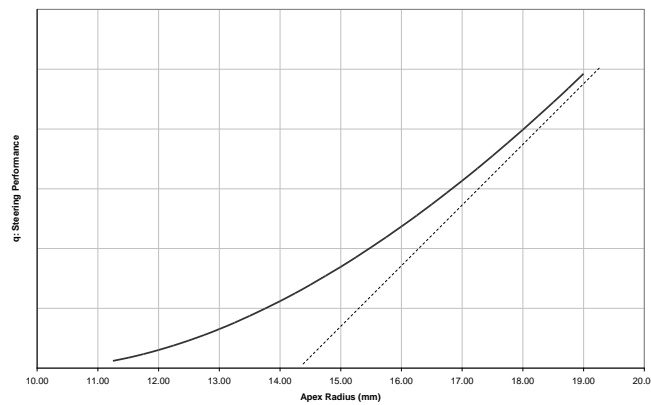
Fig. 55. Steering performance *vs* R_A.

This means that larger the probe better it is from the viewpoint of the steering capability.

4.5.3 Actuation Time

With these parameters it is possible to calculate the time necessary to complete the actuation (t_{att}). From equation (9) and (16) it is possible to write:

$$\Delta\Pi(t) = i \cdot R \cdot T \cdot \Delta C(t) = i \cdot R \cdot T \cdot \frac{2 \cdot I \cdot t}{z \cdot F \cdot V_C} \quad (32)$$

Where the variation of the volume of the two cells during the process has been neglected ($V_{C+} = V_{C-} = V_C$). Considering the equation (17) and in the hypothesis that there are not external pressures ($\Delta P = 0$) and that the osmotic membrane that separates the two semi-cells has an area A_{OSM}, it is possible to obtain the volume of water that must be moved in order to obtain the wished actuation:

$$V_{H_2O}(t) = A_{OSM} \cdot J_W(t) = A_{OSM} \cdot K \cdot \sigma \cdot \Delta\Pi(t)$$

$$V_{H_2O} = A_{OSM} \cdot \int_0^{t_R} J_W(t)dt$$

$$V_{H_2O} = A_{OSM} \cdot K \cdot \sigma \cdot \int_0^{t_R} \Delta\Pi(t)dt \tag{33}$$

$$V_{H_2O} = \frac{K \cdot A_{OSM} \cdot \sigma \cdot i \cdot R \cdot T \cdot I \cdot 2 \cdot t_R^2}{z \cdot F \cdot V_C}$$

With t_R that is the reaction time. At this point it is possible to insert in the equation the current expressed as the applied voltage (V_{MAX}) and the cell resistance as calculated in the previous sections.

$$I = \frac{V_{MAX}}{R_{TOT}} = \frac{V_{MAX}}{(R_0 + \dfrac{\rho_c}{S_c} + \rho_s \cdot d + \dfrac{\rho_M}{A_{AN}})} \tag{34}$$

Where:

- R_0, ρ_C, ρ_S are the electric parameters of the system as proposed in the previous sections;
- ρ_M resistivity of the anionic membrane;
- A_{AN} area of the anionic membrane;
- S_C electrodes surface;
- d electrodes distance;
- V_{MAX} maximum voltage that is possible to apply to the electrodes.

Assuming that $V_{H2O}=V_{att}$ and that $r_m = \dfrac{A_{AN}}{A_m}$, at the end we obtain:

$$V_{H_2O} = \frac{K \cdot A_{OSM} \cdot \sigma \cdot i \cdot R \cdot T \cdot V_{MAX} \cdot 2 \cdot t_R^2}{z \cdot F \cdot V_C \cdot (\rho_C \cdot \dfrac{1}{S} + \rho_S \cdot d + R_0 + \dfrac{\rho_M}{A_{AN}})}$$

$$t_{att} = \sqrt{\frac{V_{att} \cdot z \cdot F \cdot V_C \cdot (\rho_C \cdot \dfrac{1}{S} + \rho_S \cdot d + R_0 + \dfrac{\rho_M}{r_m \cdot A_m})}{2 \cdot K \cdot (A_m - A_m \cdot r_m) \cdot \sigma \cdot i \cdot R \cdot T \cdot V_{MAX}}} \tag{35}$$

The optimal apex dimension for the actuation time depends essentially by R_A and r_m. The actuation time is calculated by means of Matlab and the result is shown in Fig. 56.
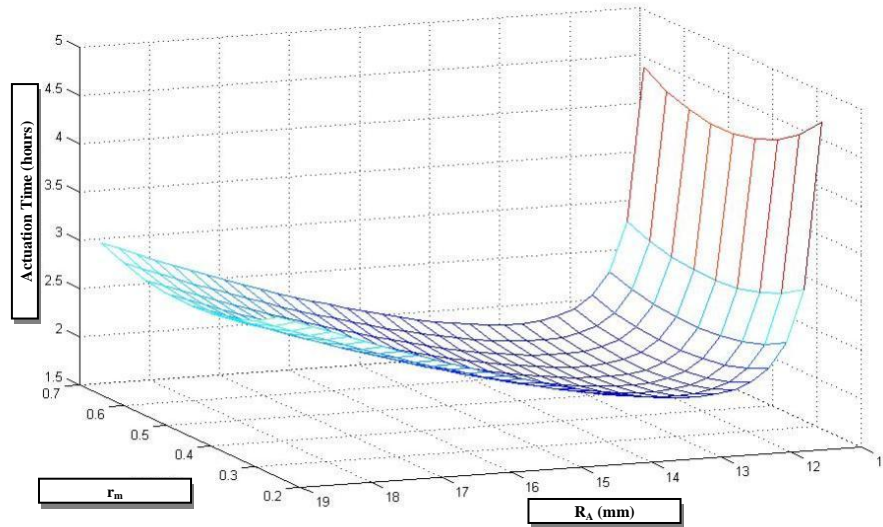
Fig. 56. Graph of the actuation time in function of R_A and r_m

The minimum of the curve and so the minimum of the actuation time is for:

- a radius of about 13 mm;
- a ratio $r_m = 0.45$;

That results in a steering time (with a maximum steering angle of about 15°) of ~ 6 hours, a comparable time scale with the plants' growth ([53]).

Fig. 57a highlights that the surfaces of the osmotic and anionic membranes should have a similar size in order to balance the time requested by the osmotic process with that requested by the electrolytic process, and thus to optimize the whole process time. Indeed, from eq. (5) it results that with $R_K = 0$, the final t_F would be maximum having $A_{AN}/A_{TOT} = 0.5$, i.e. the two membranes have the same area. In real conditions, the value of R_K slightly unbalances the area ratio of the two membranes (see Fig. 53a). Fig. 57b shows that the process time dramatically increases for low apex radius R_A, because the surface areas of the osmotic and anionic membranes tend to become extremely small (although the ratio A_A/A_{TOT} is maintained). This result is related to the geometrical constraints imposed in the parametric model. For large radius the process time slowly increases, because more time is requested for reaching a suitable ΔC in a larger volume (anionic process), more time is requested to transfer a higher volume of solution for the actuation (osmotic process). This effect is a natural consequence of the fact that chamber volumes increase with the cube of the radius R_A, while the membrane areas increase with the square of R_A.
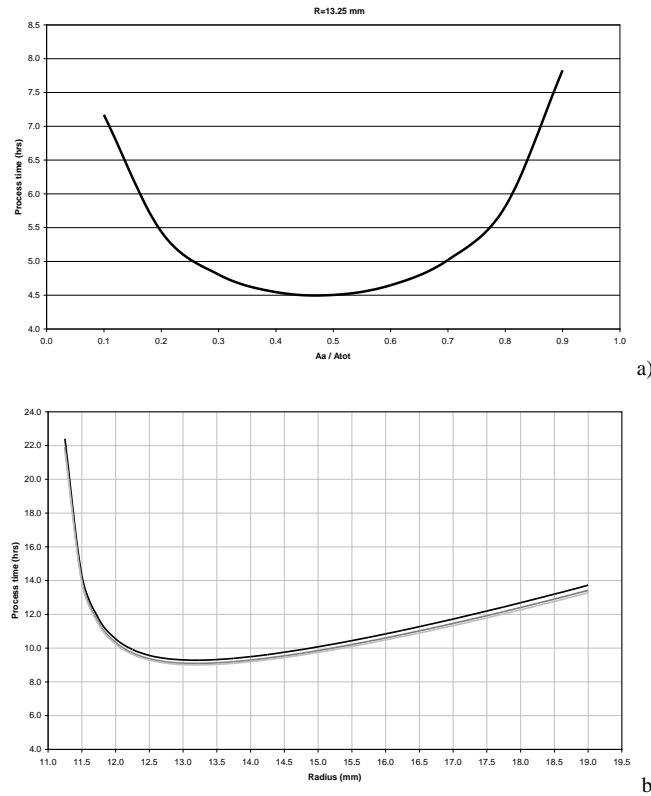
Fig. 57. The dependency of the actuation process time on a) the ratio A_A/A_{TOT} (radius R_A fixed) and b) the radius R_A of the apex body (A_A/A_{TOT} fixed).

4.5.4 Design conclusions

The analysis performed takes in consideration three main aspects in order to obtain an optimal size of the robotic root apex: penetration capability, steering performance and actuation time. The results obtained, from the experimental tests and the parametric model, show that:

- The penetration capability (with an applied constant pressure) is improved with larger apex radius; however, in a range between the 11 and 25 mm (22 and 50 mm of diameter) the improvement of penetration performance of the root is low, and, moreover, the soil resistance pressure is under 3 atm, obtained in preliminary tests with the osmotic actuator. Consequently, an apex radius range between 11 and 25 mm can be considered effective for the apex dimensioning.

- The steering capability improves almost linearly with the apex radius. The choice of an optimal apex radius depends by the soil characteristics. The steering pressure generated should be capable to generate an apex bending in the specific soil, for this reason a radius threshold must be overtaken in order to obtain the steering. This aspect will be further investigated in next works.

- The actuation time was obtained by physical and chemical considerations. This time depends strongly by the solution and membranes characteristics, but the parametric model obtained permits to change these parameters easily. However, the time obtained varying these parameters

changes in absolute value but it maintains the minimum around 13 mm of apex radius. Moreover, between 12 and 15 mm of R_A, the process time can be considered practically constant and all these ranges are suitable for the apex optimization.

Fig. 58 summarizes the obtained results. It results an optimal R_A between 13 and 15 mm in order to maximize the steering performance, maintaining the penetration capabilities and the time process almost constants.
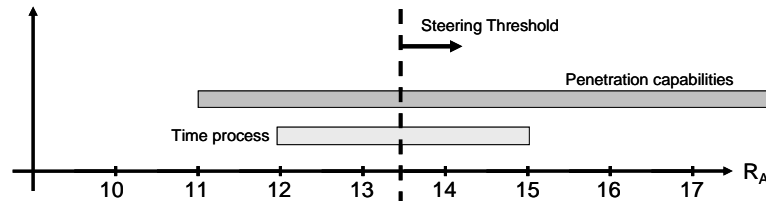
Fig. 58. Summary of the results in terms of optimal R_A for the different aspects evaluated. The position of the line of the steering is only an example. It depends from the kind of soil chosen.

A further optimization process of the apex geometrical features should eventually follow by considering the required steering capability of the system depending on the soil, where the steering should actually take place. On the other hand, the steering actuation should occur dynamically, that means progressively during the penetration of the apex itself into the soil. It follows that the resistance opposes by the terrain to the apex penetration will contribute to steer the apex into the desired direction, regardless the nature of the soil itself (starting from a straight position of the apex). However, it will be important to calibrate the static steering force of the apex to fulfil the requirements of the particular soil to be probed, in order to maintain the diameter of the apex as close as possible to the previously mentioned value, which minimize the time in the steering process.

4.6   Developed Prototypes and Tests

The first prototypes of the robotic apex were fabricated by a 3D printer InVision si2, with a plastic material, including osmotic actuators, gravity and humidity sensors, and the electronics for sensory data acquisition, aimed at testing the sensors functionalities (Fig. 59).
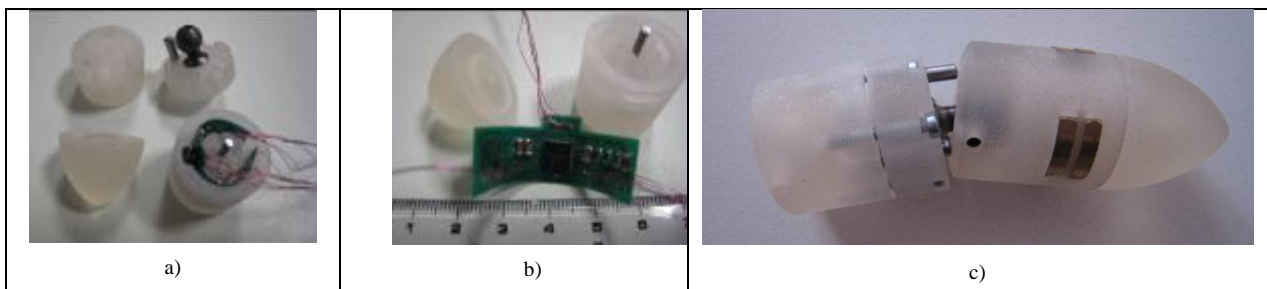
Fig. 59. Robotic apex prototype: a) basic parts fabricated in rapid prototyping: in foreground, the tip and the control and sensing module with the flexible PCB inside, integrating the accelerometer; in background, the osmotic

chambers and the head with the spherical joint and one piston; b) closer view of the flexible PCB, with the visible microprocessor; c) assembled prototype.

The material used in this phase is not the best in term of resistance, but a rapid prototyping solution has been chosen in order to test the overall functionalities of the system. More in detail, the following aspects have been verified:

- The assembling of the components;
- The assembling of electronics and sensors;
- The functionalities of the piston based mechanism.

With this prototype then a series of tests have been realized in order to test the electronic system and the silicone membrane resistance to the applied pressure.

4.6.1   Pressure seal test and silicone membrane characterization

The tests were conducted with a modified osmotic module. A physical separation between the three chambers was performed by means of the insertion of the produced gratings keeping in between a 127 µm – thick polyimide layer in order to emulate the presence of the osmotic and anionic membrane. The silicone membrane fabricated and inserted in the module has a thickness of 1mm. The polyimide layer was glued to the grating along the borders by UV curable glues. Gratings were inserted in the slots of the main case after this was heated up to about 65° C. While cooling down, the case compresses the gratings, increasing the sealing between the chambers (

Fig. 60).
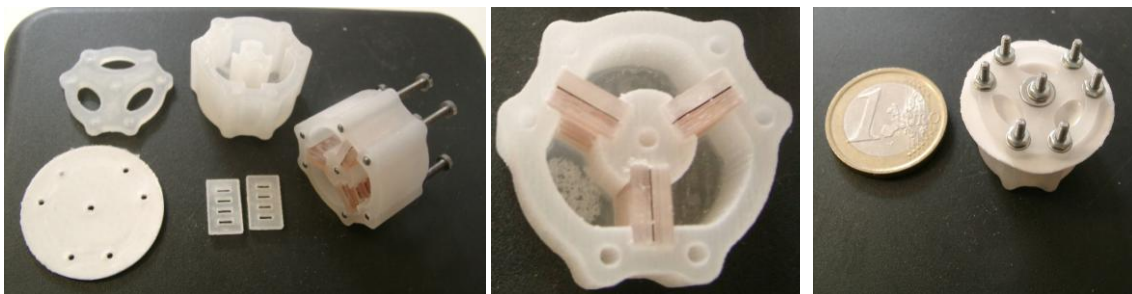
Fig. 60. Components used for the assembly of the module, a close view that shows the gratings with polyimide inserted in the case and the module fully assembled.

A 1.7 mm large hole was done through the bottom base of each chamber of the module and a plastic syringe tip (1.65 mm external diameter) was inserted in each hole and properly sealed with acrylic glue, see Fig. 61.

Fig. 61. Pictures of the assembled module with the syringe tips inserted, test setup and membrane deformation.
The membrane has been tested with about 3-4 atm of pressure, all the chambers proved total sealing (pressure maintained in the chamber after switching off pressure). The membrane fabricated guarantees the expected functionalities, even if much of the produced pressure is used by the membrane (due to its thickness) and so the resulting force on the piston in the final setup is lesser than expected. For this reason other solutions were investigate, in particular the most simple and functional was the use of a lattice glove for its small thickness and high resistance.

4.6.2   Accelerometer testing and calibration

As already explained in the previous section (4.4) an accelerometer (the LIS3L02AL model by STMicroelectronics) has been integrated in order to emulate the gravitropic behaviour. The accelerometer has 3-axes. In the realized prototype the y axis is oriented in the apex main direction (i.e. when the apex is directed in the ground direction the accelerometer gives 1 G on the y axis). So the y output gives the information about inclination between the apex and the gravity vector. The other two outputs (x and z) are necessary in order to find the rotation of the apex tip around the gravity vector.

In this phase, a firmware that reads the signals coming from the three accelerometers output and returns the value by the serial digital interface has been implemented in the pic microcontroller integrated in the root apex. These signals acquired by a software interface (developed in Visual Basic) were used to calibrate the device, in order to remove the intrinsic offset of the sensor and the positioning error during the assembly.
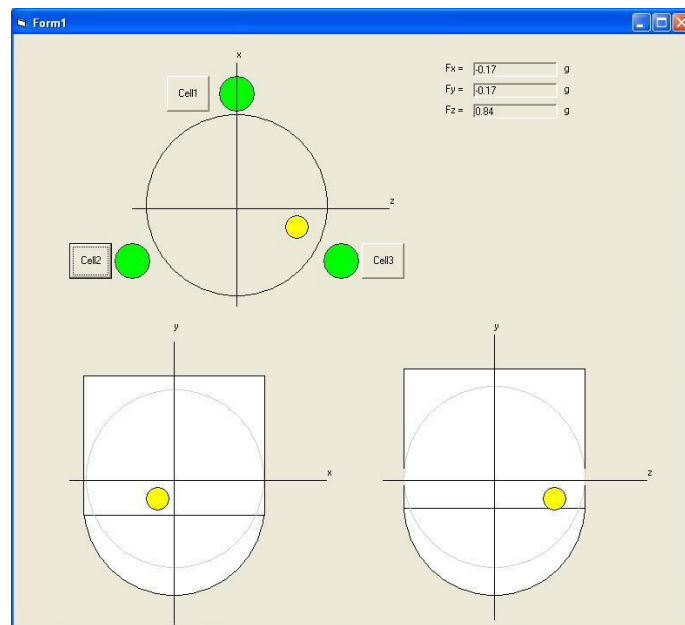
Fig. 62. Accelerometer calibration setup

The knowledge of the values of the gravity in the x and z directions is important to determinate the rotation of the robotic root apex and consequently it permits to determinate the right pistons to be actuated in order to obtain the bending in the gravity direction.

5 Design and development of a root apex with hydraulic pump for testing

5.1 Motivation

The studies on the osmotic actuator are in a preliminary phase. Although the principle has been demonstrated and some results in terms of generated pressure have been already obtained, in this phase, the osmotic process integration on the root apex is not yet possible. For this reason, in order to test the robotic root apex, the osmotic actuator has been modified (respect to the one designed and realized in the previous chapter), maintaining the overall dimension (in particular the pistons and cells sizes), but using an external pressure instead of the internal chemical process.

In order to maintain the new system similar to that realized with the osmotic actuator, the actuation will be performed with pressurized water (that differently from the air is not compressible).

5.2 Design

5.2.1 Mechanics and electronics modifications

A system with pressurized water has been applied to the piston chambers by the use of three electro-valves. In

Fig. **63** is shown the modified prototype realized for the tests.
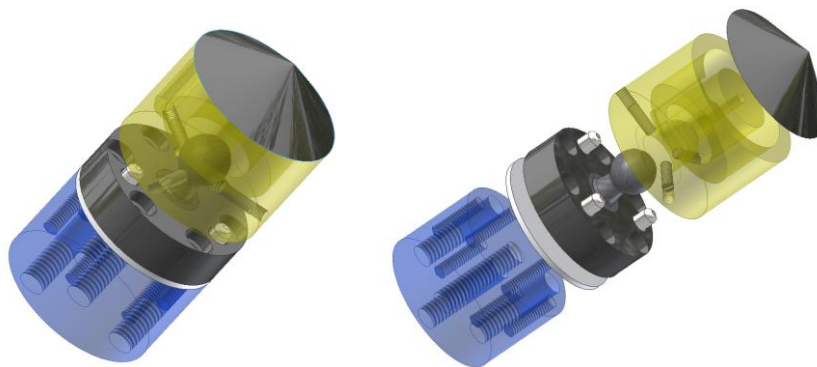
Fig. 63. Root Apex modified design

In particular, there are three pneumatic joints for a 4-mm tube that connects the chamber inside with the three electro-valves. The electro-valves used are of the type 3/2 normally-closed (series A331 from Camozzi), i.e. 3-ways and 2-positions are available. In this application one position has been used to connect the source of pressurized water to the piston. The other position is used to permit the discharge of the water from the chamber to the outside.

5.2.2 Algorithm for gravitropism and hydrotropism control in the mechatronic root apex

Although all the roots (or at least the greater amount of those) react to the gravity and humidity following these stimuli, each plant reacts to the stimuli in different ways. For example, the rate of curvature of the root tip changes depending on the kind of plant. Therefore, in order to implement an algorithm that mimics the root behaviour, a plant species must be selected. The more studied plant root in literature in this field is the *Arabidopsis*.

Several papers try to explain the kinetics of the root of this plant. In particular, regarding the gravitropic behaviour, in [111] it has been demonstrated that the rate of curvature of the root tip, maintaining a constant angle of stimulus, approximates the sine rule for angles of stimulation between 20° and 120°.

The relation can be expressed as:

$$y = a \cdot x \cdot \sin(x - \phi_C) + y_0 \qquad (36)$$

Where y (in [° h^{-1}]) is the rate of curvature, x (in [°]) is the stimulation angle, and a, ϕ_C, y_0 are experimental parameters [30] and for Arabidopsis they are equal to 15.9h^{-1}, 14.7° and 7.9° h^{-1} respectively. This study supplies two main indications in the implementation of the root gravitropic behaviour: there is a thresholds angle (ϕ_C) under which the gravity stimulus has not effect ($y = 0$ for $x < 14.7°$); for $x > 14.7°$ the rate of curvature is proportional to the sine of the stimulus angle (x) and has a maximum at $x = 90°$ of $y = 25°$ h^{-1}.

Regarding the hydrotropic behaviour the current state of knowledge is scarcer. Hydrotropism evaluation is difficult to achieve because the response of the root to gravity strongly interacts with its positive hydrotropic response [31]. However, some tests performed on *agravitropic mutant* [112], confirm this behaviour.

The last studies performed in this field demonstrate the positive response of the root to a gradient of humidity and that the sensing elements are located in the root cap [113]. With this state of knowledge the implementation solution is following the resultant of the three vectors supplied by the humidity sensors.

To move the root tip, the pistons height must be regulated in order to regulate two angles (Fig. 64)

- α, that indicates the rotation of tip around its axes;
- β, that is the bending of the tip respect to the rest of the root;
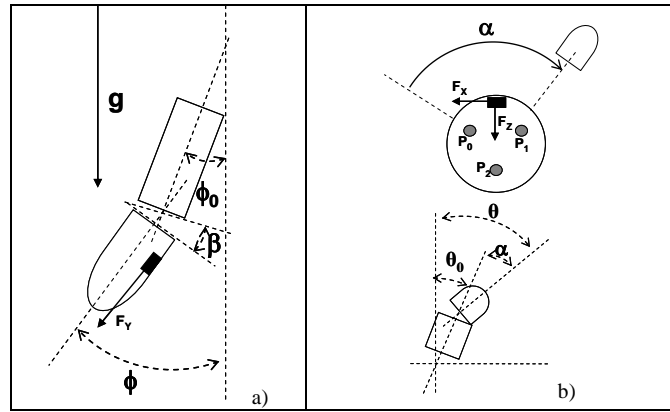
Fig. 64. Representation of the angles that define: a) the inclination of the tip respect to the actuator; b) the rotation of tip respect to the actuator.

These two angles define the height of the three pistons:

$$h_{Px} = B_P \cdot \sin(\beta) \cdot \sin(\alpha + \Delta_x) \qquad (37)$$

where B_P is the distance between the centre of the piston and the centre of the apex and depends from the mechanical design; Δ_x depend by the reference chosen for the angle α, however Δ_0, Δ_1 and Δ_2 result at 120° between them; and β has a maximum (13° for the realized prototype) fixed by the mechanical design.

From (37) it is possible to obtain the graph in Fig. 65, where the Δx phases have been set as follow: $\Delta_0 = -60°$; $\Delta_1 = + 60°$; and $\Delta_2 = + 180°$.
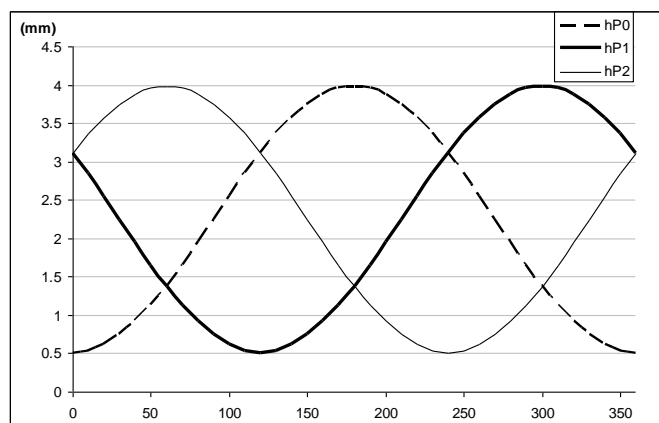
Fig. 65. Pistons height in function of α, with fixed β.

From the graph (and also from the formulas) is easy to obtain that the sum of the height of the three pistons is constant in each position (for each α and β). This brings to the consideration that control of this system can be realized moving the proper amount of water from a cell to another (the total amount of water is constant). This transfer can be made as proposed in this thesis by osmotic processes or in a preliminary test phase by hydraulic pumps.

Gravitropism Control

To imitate the gravitropic behaviour of the root, an accelerometer has been put in the robotic apex as shown in the previous section. This accelerometer has the Y axis oriented in the tip direction and the X and Z axes on the perpendicular plane. Two main parameters can be obtained by the three outputs (F_X, F_Y and F_Z):

$$\phi = \arccos\left(F_Y / g\right)$$

that is the stimulus angle as in the biological root (Fig. 64a);

$$\theta = \arctan\left(F_Z / F_X\right)$$

that is the angle of rotation of the tip respect to its axis (Fig. 64b).

In order to obtain α and β from the measurements given by the accelerometer (ϕ and θ), the same quantities for the actuator should be known (ϕ_0 and θ_0). This is possible only placing another gravity sensor on the actuator. However this solution does not represent the simple behaviour of the root tip. The control of the cell growth, for apex bending, is made by opening and closing ionic channels on the basis of the gravity sensor placed on the tip by an open loop control.

Therefore, the adopted solution has been simplified. No flow control has been implemented and the actuation is controlled by changing the flow of water between the actuator cells, on the basis of the measured angles (ϕ and θ).

In particular, ϕ is used as threshold for beginning the actuation and as speed of actuation that results from the biological consideration reported before and consequently by (36); θ instead is used to discriminate from the cells that must be filled and emptied. As already explained there is no feedback on the elongation of the pistons, therefore it is not possible to fix a right height on each of them. The only commands that can be applied are "fill" and "empty". This brings to the consideration that only 6 pistons configurations are available with this system. The result flow diagram is shown in Fig. 66.

Θ	P_0	P_1	P_2
0÷60°	0	1	0
60÷120°	1	1	0
120÷180°	1	0	0
180÷240°	1	0	1
240÷300°	0	0	1
300÷360°	0	1	1
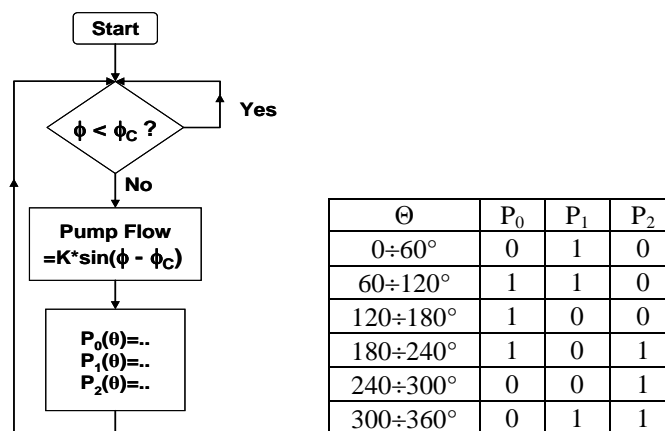
Fig. 66. Control algorithm description.

Hydrotropism Control

The signals received from the three integrated moisture sensors are processed in order to imitate the hydrotropic behaviour.

The data coming from the sensors are three values that increase following the increase of the soil moisture. As already explained, the objective is not to find a precise moisture measurement but to discover a gradient. The three quantities are simply reported in the plane and the resultant is calculated. This is characterized by a module and an angle ψ, from which the angle α can be derived. Similarly to the gravitropic behaviour, also in this case a critic value can be introduced, but not fir the angles, rather for the module of the normalized resultant. Under this critic value the apex does not react to the moisture stimuli; above it, the response is driven by the resulting angle. Also in this case, there is no feedback information about the position of the pistons; for this reason the only stimuli given to the actuators are "fill" and "empty" until the stimulus is present. The resulting actuation algorithm is reported in Fig. 67.

ψ	P_0	P_1	P_2
30÷90°	0	0	1
90÷150°	1	0	1
150÷210°	1	0	0
210÷270°	1	1	0
270÷330°	0	1	0
330÷30°	0	1	1
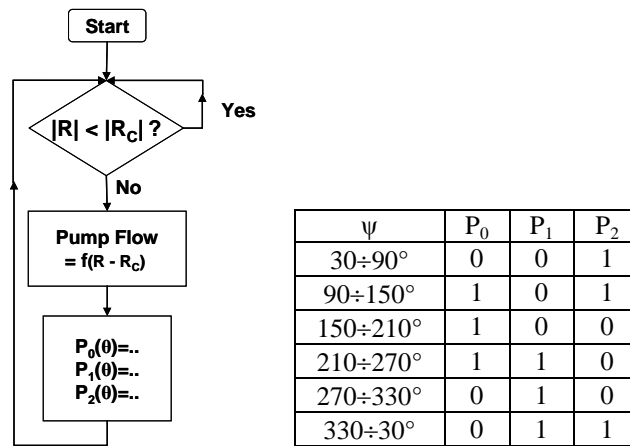
Fig. 67. Control algorithm description.

5.3 Fabrication

The modified prototype realized for the tests is shown in Fig. 68 where it is possible to see the three pneumatic joints to connect the hydraulic system to the actuator chambers.
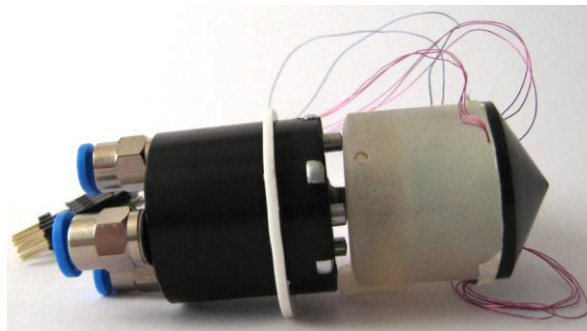
Fig. 68. Root apex prototype realized for tests with external pneumatic system.

A proper power circuit to manage opening and closure of the valve has been realized. This circuit is based on a 24V power supply and three Darlington transistors that permit the excitation of the valves solenoids. The input of the transistor is managed directly by the apex microcontroller as in the osmotic version.
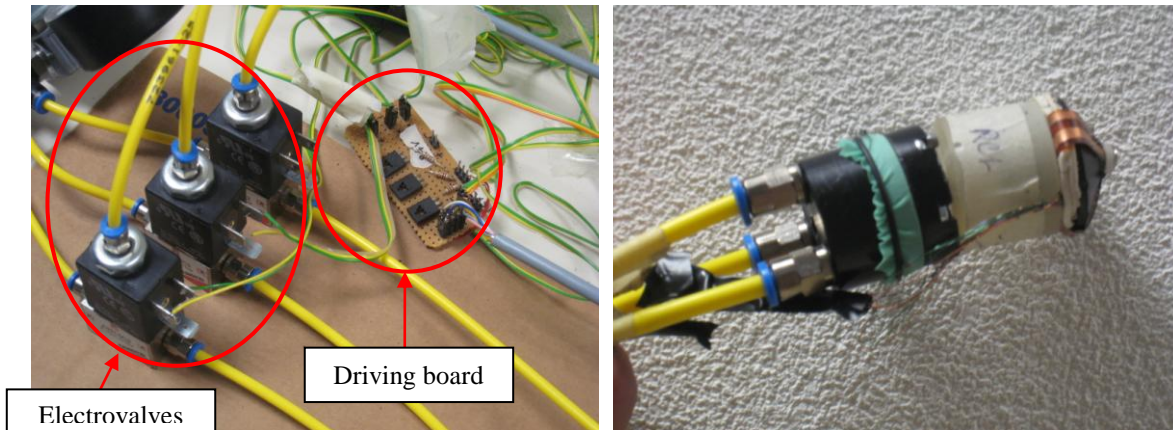
Fig. 69. Pneumatic system for hydraulic actuation of the robotic apex.

5.4 Set-Up and Testing of the Steering Capabilities

The main differences with the osmotic version are:

- The generation of a pressure in a chamber with osmotic process is a very slow action; instead with this methodology the generation of pressure is practically instantaneous;
- It is not possible to modulate the height of the pistons but it is possible only: maximum excursion, or piston free.

These differences do not permit to strictly correlate the behaviour of the apex with osmotic actuator with this, but the architecture proposed permits to test the elementary behaviour of the apex and the steering capabilities.

The tests performed have been divided in four phases:

1. The root apex has been moved in air applying pressure at one piston at time in order to test the overall mobility;

2. The algorithm that implements the gravitropic behaviour has been loaded in the integrated microcontroller and the apex has been rotated in air in order to verify the bending of the tip in the gravity direction;

3. The algorithm that implements the hydrotropic behaviour has been loaded in the integrated microcontroller and the apex has been put in contact with a soil sample (sand-clay mixture); through the successive injection of little quantities of water the bending of the tip in the water direction has been verified;

4. The overall system has been mounted on an Instron testing machine 4464 equipped with a 1kN load cell. The robotic root apex has been pushed down through a metallic shaft applied on a

joint behind the steering actuator. A rectangular plexiglas container filled of a sand-clay mixture has been used. The test has consisted in a straight penetration of 5 cm with a speed penetration of 5 mm/min, after that a piston chamber has been opened in order to permit the bending of tip in that direction. After other 15 cm of penetration the test was stopped and the bending of the tip and the displacement of the apex in the right direction has been verified.
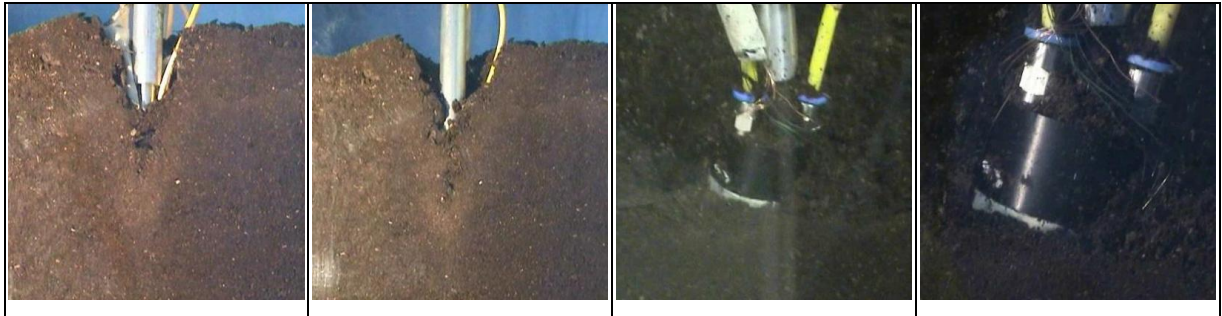
Fig. 70. Complete system testing on an Instron machine 4464.

6 Design and Realization of the Aerial Part

6.1 Concept

Within this thesis, the work on the aerial part of the plant has been mainly focused on the sensors integration. The necessity to interface a wide amount of sensors and the necessity to have different sensors for the different proposed scenarios (agriculture, pollution monitoring, space applications), have leaded to the design of a system with an open architecture. In particular, the system must be capable to interface sensors with different output signals in a plug & play way. In this way the sensors can be easily interchanged without changing any hardware and software module in the plantoid core.

The work of this thesis, has been focused on this aspect without enter in detail for the communication and energy scavenging parts.

A lot of transducers are present on the market with a multitude of different interfaces to provide the measurements. Typical front-ends are voltage output, current output, capacitive or resistive outputs, and several digital interfaces such as RS232, I2C, SPI, and bus based interfaces. The presence of a so large number of different interfaces and the requested high sensors interchange ability in the different plantoid applications are a very demanding task. To address similar issues the concept of smart sensor was introduced in the recent past. A smart sensor can be defined as a sensor with some kind of embedded intelligence (usually provided by a microcontroller) able to carry out advanced functions such as embedded signal conditioning, self-calibration, self-identification, diagnostic and networking activities ([111], [115] and [116]).

Some commercial sensors show different degrees of "smartness", anyway the standardization of the interfaces is still an open issue. An important effort in this direction was made with the introduction of the IEEE1451 standards for smart sensors (1451.0 to 1451.7). This standard proposes functionalities, data structures and communication protocols with the intent of making possible the creation of network of sensors, thus simplifying the implementation (realization) of complex monitoring systems. Unfortunately at the moment only few examples of smart sensors compliant to this standard are available on the market.

In this vision, a new low-cost system based on a single commercial chip, to convert a generic transducer into a smart sensor with standard interface has been proposed. The so called Universal Smart Sensor Interface (USSI) provides a flexible analog and/or digital front-end (including conditioning and conversion functions), able to interface different typologies of transducers, providing enhanced processing and storage capabilities and a configurable multi-standard output interface (including plug-and-play interface based on IEEE1451.3).

6.2 Development of the USSI

6.2.1 Universal Smart Sensor Interface concept and IEEE 1451 standard

The Universal Smart Sensor Interface (USSI) intends to provide a quick and reliable solution to convert a common generic transducer into a smart sensor with plug and play features [117].

To do this the USSI must provide a software configurable analog front-end circuit, some computational capabilities, a memory for data and for configuration parameters and one or more standardized output connections. The architecture of the proposed device is shown in Fig. 71.
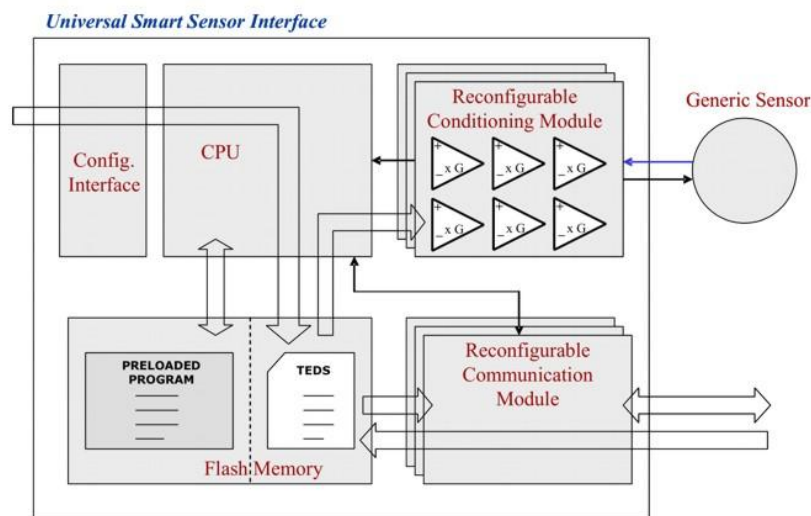
Fig. 71. Universal Smart Sensor Interface block diagram

The core of the USSI interface is a reconfigurable conditioning module, composed by several operational amplifiers (with selectable gains) and digital modules that can be connected each other via software in different ways, providing the required complete front-end for different types of sensors, including single/differential amplification, analog to digital conversion, powering and filtering. The generic sensor is connected to this conditioning module directly through a 4 lines connection (2 lines for power supply and up to 2 lines for signals). Then, in some configuration an additional resistor must be added.

The conditioning module is directly configured by the CPU block that manages also all the other functionalities of the device. The CPU configures the conditioning module at the power-up time by using the configuration data stored in a non-volatile memory; in this memory the data necessary for the plug and play functionality are also contained, stored in the form of Transducer Electronic Datasheet (TEDS) following the philosophy of the IEEE1451 standard. TEDS contains an electronic description of the board and sensors (transducer channels) connected. The board is described by the META TEDS that supplies information as the Universal Unique ID for univocal identification and the number of connected transducer channels. The Transducer channel TEDS contains information about the sensor connected

and in particular: maximum value, minimum value, physical unit, acquisition time, warm up time and more. Then a textual description for board and sensors is also supplied.

The CPU manages the signal/measurement acquisition from the sensor, through the conditioning module, executing the program stored in another area of the non-volatile memory, and using the parameters contained in the TEDS (type of data, acquisition time, update rate, calibration parameters, etc.). The acquired data are buffered in a volatile memory and then sent outside through customizable interfaces. Computational requirements to handle the whole system are sufficiently limited to be implemented by using a standard 8-bit CPU core.

The main communication interface is a bus-type interface based on the IEEE1451.3 standard, connecting the USSI device to a master external device (the Plantoid main microcontroller).

Through this interface, data and commands are exchanged between the USSI device and the Plantoid main microcontroller; providing the possibility of TEDS handling and of a plug-and-play connection. TEDS and configuration parameters for the conditioning module can be uploaded at run-time into the USSI device through this interface. Anyway the device supports other types of external connections; as the conditioning module, also the communication module can be reconfigured, by using the stored configuration parameters, to support simpler and more direct output formats, in order to make the use of the device more flexible: aiming at this, Other communications interfaces have been added: 0-5 V analog output and a RS232 digital output.

All the USSIs are loaded with the same program that allows the management of every configuration and the communication with the Plantoid main microcontroller. In a second phase when a certain USSI must be connected to a specific sensor, the TEDS are created and loaded on the USSI.

There are a total of 5 kinds of TEDS that are loaded on the USSI when it is configured:

- META TEDS: contains a parametric description of the USSI content;
- META TEXT TEDS: contains a textual description of the USSI content;
- TC TEDS: one for each transducer channel, each one contains a parametric description of the sensor or actuator connected;
- TC TEXT TEDS: one for each transducer channel, each one contains a textual description of the sensor or actuator connected;
- CONFIG TEDS: contains the parameters for the configuration of the USSI in order to manage correctly the specific sensor.

The first 4 kinds of TEDS are sent by the USSI to the Plantoid microcontroller during the plug & play service, in order to describe the new smart sensor to the system. The CONFIG TEDS is normally managed only by the configurator tools.

The whole chain that involves the USSI's programming and integration in the network is graphically schematized in Fig. 72.
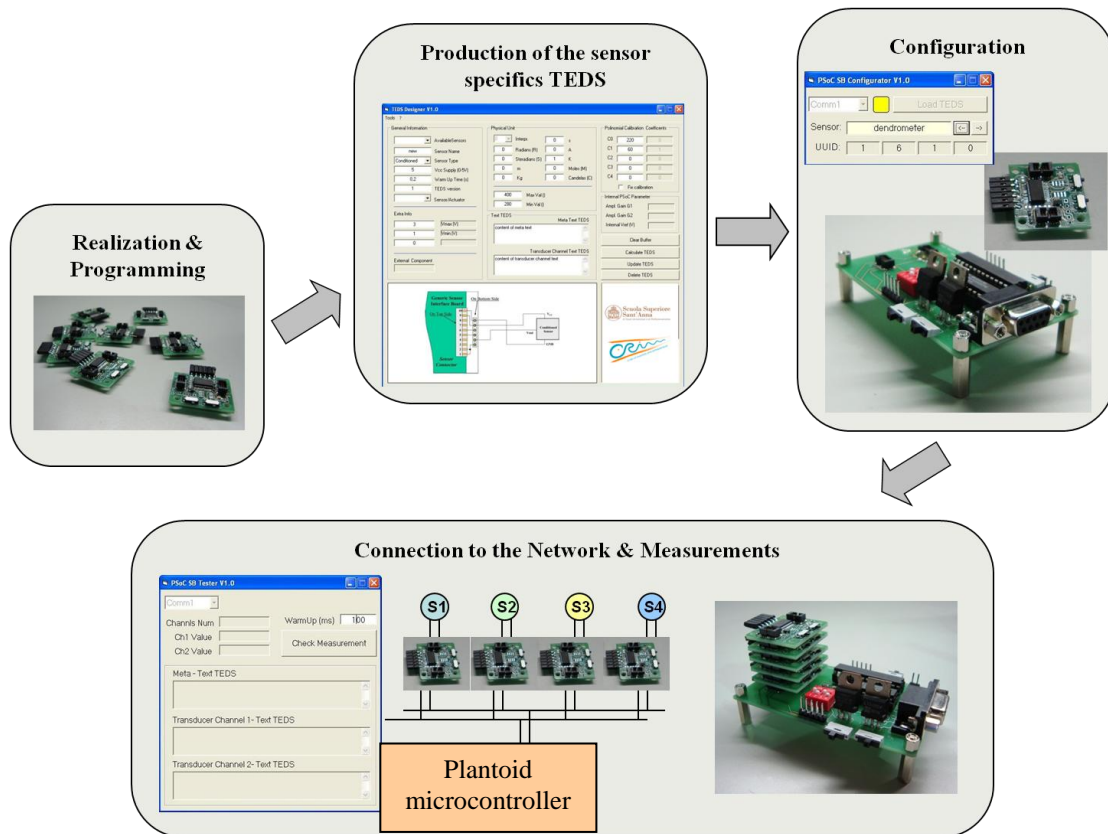
Fig. 72. USSI programming cycle: at the beginning there is the programming of all the USSIs with a common firmware that contains all the required functionalities; then on the base of the specific sensor to be integrated a TEDS is generated; the TEDS parameters are loaded on the board by configuration tools; at the end the USSI is connected to the sensor and to the NCAP and is ready for working.

In particular for the management of the USSIs along the whole chain, three software tools and a configurator device (Configuration Downloader) have been developed. The configurator device integrates a set of the Plantoid microcontroller functionalities and moreover it communicates with a PC through an RS232 connection. The three tools developed are:

- TEDS Designer software is devoted to create suitable TEDS for the specific sensors. The software allows a simple customisation of the USSI, generating automatically a TEDS that describes the sensor and storing it in a dedicated database, through the input of several parameters by the user about the specifications of the sensor.

- USSI Configurator software is devoted to download the TEDS from the database to the USSI. To perform the upload operation on the USSI, it is necessary to use the Configuration Downloader, connected to the PC by a RS232 serial connection.

- USSI Tester software visualizes the measurements sent by the USSI on the PC screen, using as an interface the Configuration Downloader.

The configuration of the USSI permits to transform a generic sensor in a smart sensor with plug & play capability (Fig. 73). All the information useful to describe correctly the sensor will be inserted in the USSI memory, structured as TEDS. This information is used for the right configuration of the

analog/digital modules of the USSI interface system and also to provide the support for Plug and Play features.
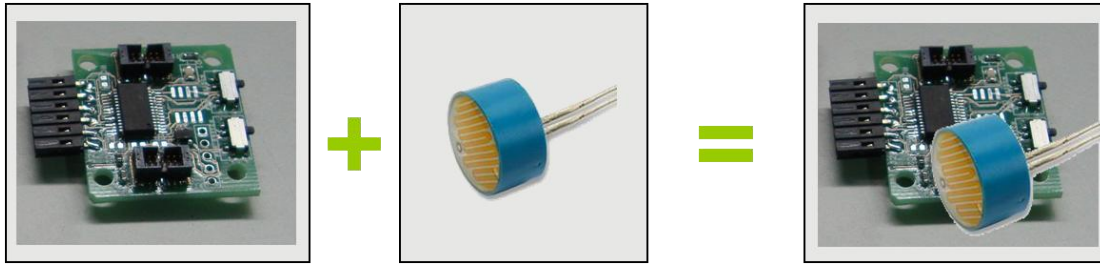
Fig. 73. USSI concept: USSI + raw sensor = smart sensor

6.2.2   Universal Smart Sensor Interface design – Hardware Board design

The specific requirements of flexibility, adaptability and functionalities that the USSI device must have can be achieved by using different technological solutions, depending on the expected performances and the costs admitted. Two possible solutions can be: the development of a digital/analog mixed ASIC with configuration capability; the development of a relatively complex electronic board including a microcontroller, operational amplifiers, programmable gain amplifiers (PGA), Analog to Digital Converters (ADC), Digital to Analog Converters (DAC) and analogical switches. However, both the solutions have several drawbacks (cost, size, etc.); for this reason a different solution, based on a commercial available multifunctional chip, has been adopted. For the USSI device implementation, a Programmable System on Chip (PSoC) produced by Cypress (http://www.cypress.com) has been used. The use of these devices makes possible the connection of analog and digital output sensors, implementing TEDS, intelligent power management and multi-standard external connections.

The PSoC™ family consists of many Mixed Signal Arrays with On-Chip Controller devices. These devices are designed to replace traditional multiple MCU-based system components with one, low cost, programmable single-chip component. A PSoC device includes configurable blocks of analog and digital logic, as well as programmable interconnections (all reconfigurable at run-time). This architecture allows creating customized peripheral configurations, to match the requirements of each individual application. Additionally, a fast 8 bit CPU, Flash program memory, SRAM data memory, and configurable IO are included.

The PSoC device chosen is the model CY8C29466. PSoC features make the implementation of USSI device possible in a single-chip: the internal analog and digital logic blocks are used to generate at run-time the front-end suitable for the generic transducer interfacing. The information for the front-end configuration is contained as TEDS in the built-in flash memory, which can be re-written at run-time.

The USSI device was built by integrating the PSoC chip in a small PCB board with two connectors. One connector is used to interface the selected transducer (sensor); the other one supplies power and connectivity to the whole device.

The transducer interface requires only 6 lines:

- two (or one) lines for the sensor signal (Gsens+, Gsens-);
- two lines for an external resistor necessary only in some configurations (R0', R0'') that can be also mounted directly on the USSI.;
- two lines for the power supply of the sensor (Vpp-sens, Gnd).

Moreover a connection for the R0 and a connection for the sensor share the same microcontroller pin, so at the end only 5 lines can be taken into account (P0-P4) to provide power and conditioning front-end to all the different types of supported sensors; the functionality of such lines depends on the sensor type (and thus on the internal configuration of the PSoC chip). In the next section all the different supported configurations will be examined into detail, including the sensor interface pin-out.

There are several connectors that guarantee the power supply and the communication. In particular, there are:

- a 2 lines connector for the power supply of the devices (3.3-5V)
- a 6 lines connector for the 1451.3 protocol implementation
- a 3 lines connector for the RS232 output of the sensor measurements
- a 2 lines connector for the analog output

In Fig. 74 is reported the schematic and a picture of the implemented USSI interface.
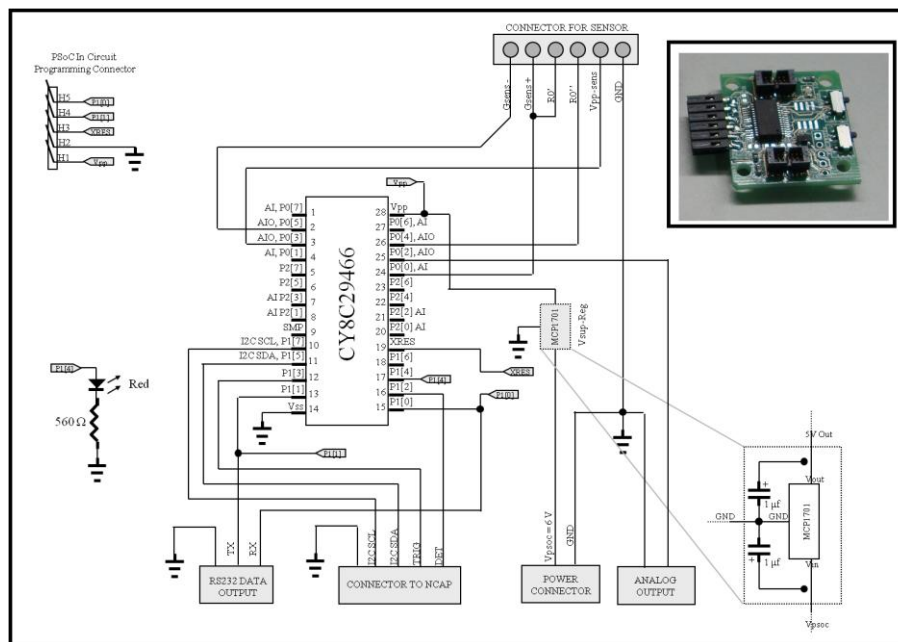
Fig. 74. Schematic and the picture of the implemented USSI interface

6.2.3 Reconfigurable Hardware design

In order to interface the selected transducer in the proper way, the PSoC device must be able to configure the analog and digital blocks obtaining the suitable front-end architecture, based on the information contained in a custom TEDS (Configuration TEDS) stored into the flash memory. All the

supported hardware configurations are implemented at design time and can be switched at run-time. The Configuration TEDS contains the parameters necessary to select and tuning the required hardware configuration.

Up to now, front-ends for 8 common sensor typologies have been implemented; in particular:

- Conditioned Sensor – Configuration 1;
- Unconditioned Sensor (Wheatstone bridge like) – Configuration 2;
- Current Output Sensor – Configuration 3;
- Resistive Sensor – Configuration 4;
- Capacitive Sensor – Configuration 5;
- Digital Sensor (Serial interface type: RS232/SPI/Microwire) – Configuration 6/7/8.

For all the supported configurations the maximum available voltage for the sensor supply is 5V, and the maximum sensor sourcing current is 30mA, being the power supplied directly by PSoC chip by using an internally buffered DAC (limitations come from the PSoC chip manufacturer specifications).

For each type of sensor a specific architecture is required. These architectures are implemented at firmware level by configuring the analog/digital reconfigurable blocks. The several implementations in the PSoC device will be discussed in details in this section; in particular, for each configuration, the general logical block scheme has explained and the implementation made by using PSoC Designer tools by Cypress has shown.

Conditioned Sensor – Configuration 1

In the case of a conditioned sensor the output is usually 0-5V (or similar); the output impedance is relative low and thus the signal does not require any amplification. Moreover the output of the sensor is referred to the ground (no differential input required).

The conditioning scheme (shown in Fig. 75) is consequently relatively simple: the acquisition module is composed by an input buffer connected to an ADC (with selectable resolution: 8-14 bit). The power for the sensor is supplied by an internal buffered 6-bit DAC.

The implementation of the analog part of this configuration, made by means of "Graphic Configurator" (included in the PSoC Designer tools), is shown in Fig. 76.
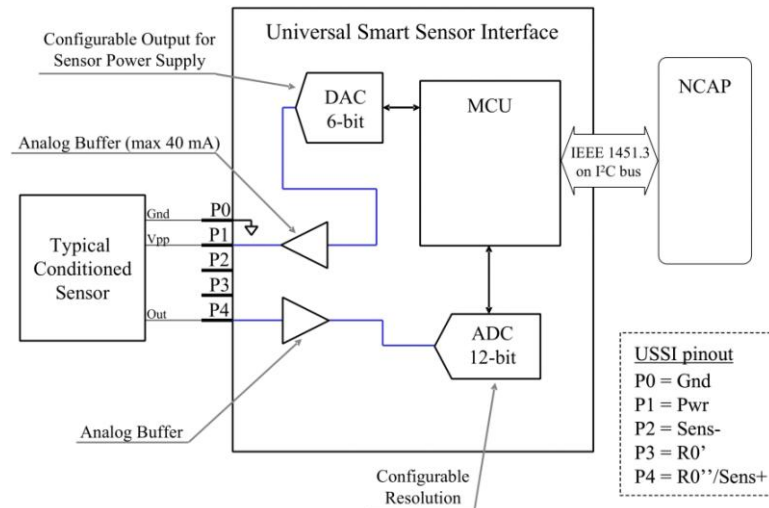
Fig. 75. Logical scheme of conditioning front-end implemented in PSoC device for conditioned sensors
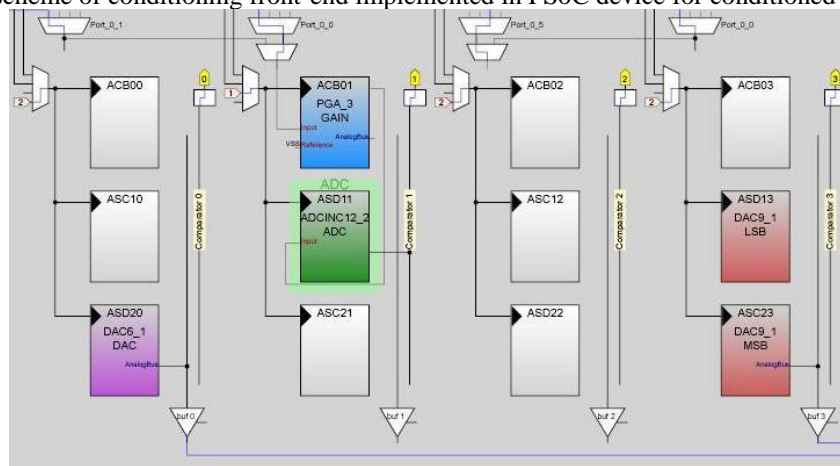
Fig. 76. Screen-shot of "Graphic Configurator" implementing the front-end for conditioned sensors.

In this configuration the first block is the DAC6_1, this is used for generating the power supply of the sensor. It is a DAC at 6 bits and guarantees a resolution of about 80 mV. The DAC6_1 output is connected with the PORT_0_3 of the PSoC that is physically connected with the output connector and in particular with the pin Vpp-sens. If 5 V is a too low voltage or the sensor needs a stable power supply (the DAC output is rather noisy), an external power supply can be used. The PGA_3 is used as an analog input buffer for the sensor signal. The output of the sensor is connected to PORT_0_0 and then with the input of the PGA_3. In this configuration (for conditioned 0-5V sensors) the gain of PGA_3 is normally set at a value of 1, but for other sensors that do not exploit the whole 0-5V dynamics a proper gain can be introduced. The ADCINC12 is an incremental ADC with 12 bit resolution. DAC9_1 is a DAC at 9 bits and it is used for the power supply of the analog output proportional to the sensor output. It is connected to PORT_0_2 and then with the analog output connector. It is present in all the configurations.

Unconditioned Sensor (Wheatstone bridge like) – Configuration 2

The differential output of an unconditioned sensor presents typically a very low voltage difference (in the range of mV). The output impedance is relatively high and thus the signal requires an amplification stage. Furthermore the signal common mode is likely different from USSI's ground, making a differential amplification necessary.

The conditioning scheme for unconditioned (Wheatstone bridge like) sensor is shown in Fig. 77. The first stage of the acquisition module is composed by a programmable gain instrumentation amplifier with gain (G1) fixed to ×10. After this pre-amplification stage, a second amplification stage with offset compensation is implemented. The offset compensation, carried out by a 9 bit DAC, is required in the case of sensors with a large initial offset (in the order of the full span of the signal). The second amplification stage is composed by a Programmable Gain Amplifier (PGA) (gain = G2, 1<G2<48). Both the offset compensation and the gain are automatically selected by software on the basis of the configuration parameters loaded in the TEDS. After the amplification stages, an ADC (with selectable resolution: 8-14 bit) is available for the acquisition. The power for the sensor is supplied by an internal buffered 6-bit DAC.

The implementation of the analog part of this configuration, made by means of "Graphic Configurator" (included in the PSoC Designer tools), is shown in Fig. 78.
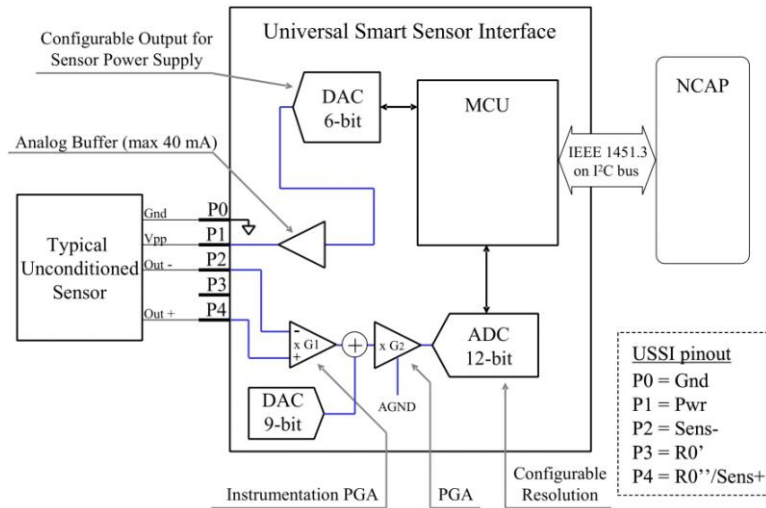
Fig. 77. Logical scheme of conditioning front-end implemented in PSoC device for unconditioned sensors
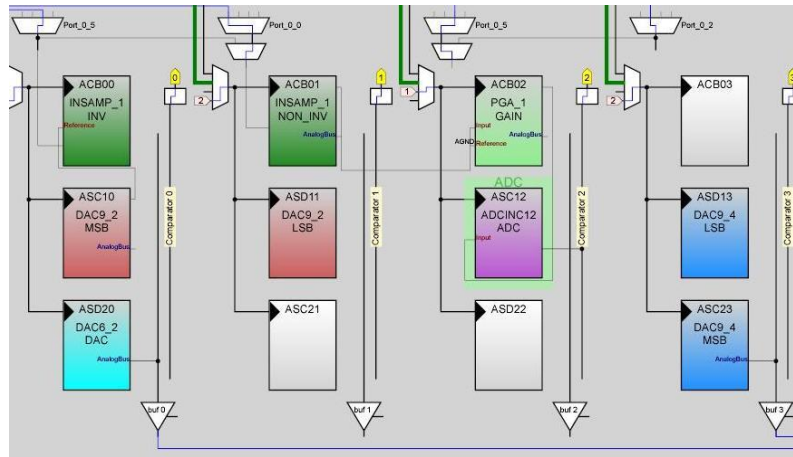
Fig. 78. Screen-shot of "Graphic Configurator" implementing the front-end for unconditioned sensors.

The first block is a DAC6 also in this configuration. It is used for generating the power supply of the sensor, with the same considerations of the Configuration1. The sensor output is connected to the PORT_0_0 (Sens+) and PORT_0_5 (Sens-) and the signal is amplified by an instrumentation amplifier (INSAMP_1) that also corrects the offset of the signal adding the voltage supplied by the DAC9_2.

$$V_{0\text{-INSAMP}} = (V_{IN+} - V_{IN-}) * G_1 + V_{DAC9}$$

At the end of this first stage of amplification, the signal has been amplified and translated at a value close to AGND that is the Analog Ground of the PSoC and corresponds to Vcc/2. The second stage of amplification is composed by the PGA_1 with a reference voltage of AGND. At the end the amplified signal is acquired by the ADCINC12. DAC9_4 is the DAC for the analog output:

$$V_{ADC} = ((V_{0\text{-INSAMP}} - V_{AGND}) * G_2) + V_{AGND}$$

Current Output Sensor– Configuration 3

In the case of a Current Output sensor an external precision resistor is required in order to perform the conditioning (the resistor is external to the PSoC but it is included in the USSI device, and cannot be changed by configuration parameters). The conditioning scheme for this configuration is shown in Fig. 79. The current output of the sensor passes through the reference resistor connected to the USSI ground; in this way, the current is converted in a voltage. The voltage drop across the resistor is amplified by a programmable gain amplifier: the gain (G) is selected by firmware based on the configuration parameters loaded in the TEDS (from G = x1 to G = x93). After the amplification stage an ADC (with selectable resolution: 8-14 bit) carries out digitalization. The power for the sensor is supplied by an internal buffered 6-bit DAC.

The implementation of the analog part of this configuration, made by means of "Graphic Configurator" (included in the PSoC Designer tools), is shown in Fig. 80.
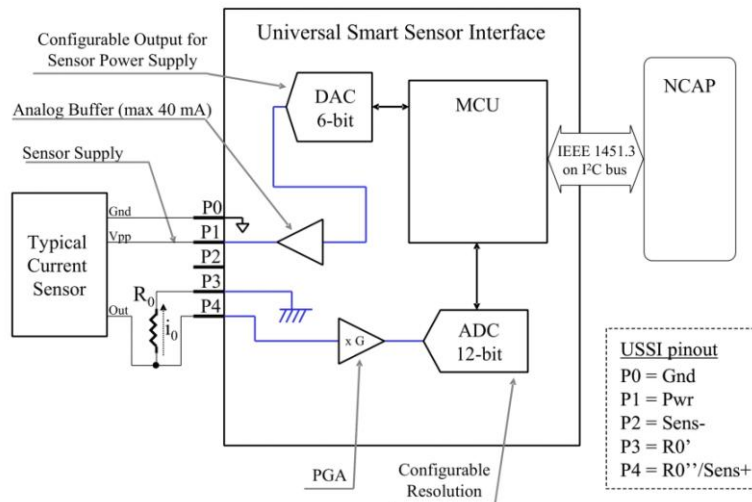
Fig. 79. Logical scheme of conditioning front-end implemented in PSoC device for current output sensors
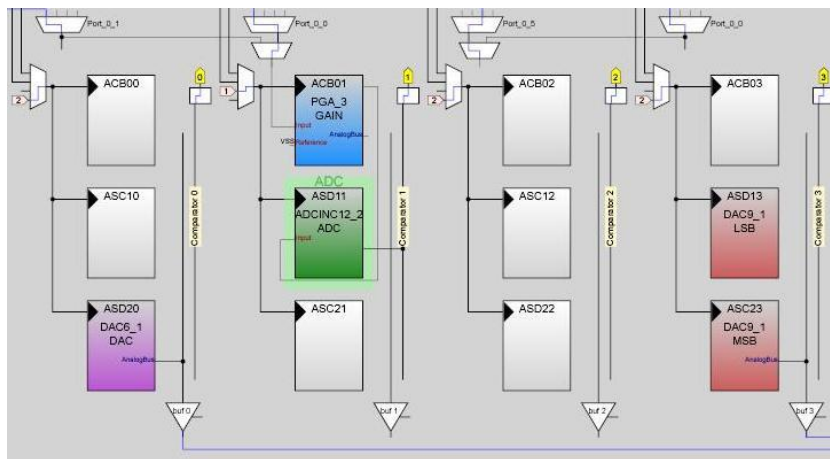
Fig. 80. Screen-shot of "Graphic Configurator" implementing the front-end for current output sensors.

This configuration is the same used for the conditioned sensor; the only difference is in the PGA that is not used only as a analog input buffer but the gain is normally not 1 and in the PORT_0_4 (R0') that is put to ground via software. DAC9_1 is the DAC for the analog output:

$$V_{ADC} = ((I_{Sensor} * R_0 + V_{SS}) - V_{SS}) * G + V_{SS} = I_{Sensor} * R_0 * G$$

Resistive Sensor – Configuration 4

The conditioning of the resistive sensor is the most complex case. Power is not directly supplied by a buffered DAC as in the other cases. In this configuration, the resistor must be supplied by a constant current generator. In order to achieve this goal, a particular configuration involving a DAC module, a differential and unitary gain amplifier, and an external precision resistor (R0) is applied (Fig. 81). The resistor (R0) is external to the PSoC but it is included in the complete USSI, and cannot be changed by configuration parameters). The reference current obtained with this configuration (the value of reference current is I0 = -V0 / R0, where V0 is fixed by DAC) passes across the resistive sensor. In this way, the

resistance is converted at the resistive sensor's terminals into a voltage. This voltage is amplified by a differential amplification stage: the gain is automatically selected on the basis of the configuration parameters loaded in the TEDS. The last module is the ADC (with 12 bit resolution).

The implementation of the analog part of this configuration, made by means of "Graphic Configurator" (included in the PSoC Designer tools), is shown in Fig. 82.


**Fig. 81.** Logical scheme of conditioning front-end implemented in PSoC device for resistive sensors

Fig. 82. Screen-shot of "Graphic Configurator" implementing the front-end for resistive sensors.

In this configuration a supply voltage directly connected to the sensor is not present. The DAC9_3 supplies the reference voltage to the circuit in order to fix (together with the R0) the current I0 that flows in the resistive sensor. The reference voltage is applied to the negative input of the INSAMP_2, set with a gain of 1. The non-inverted input is connected with the R0 and the Sensor by the PORT_0_0 and moreover it is connected with the PGA_5 that amplifies the signal that is finally acquired by the ADCINC12_1. The PORT_0_4 (R0') is connected to the ground via software. DAC9_7 is the DAC for the analog output.

$$V_{ADC} = -I_0 * R_s * G = V_0 * R_s * G / R_0$$

Capacitive Sensor– Configuration 5

The conditioning of the capacitive sensor has been obtained by the use, also in this case, of an external precision resistor. The resistor is external to the PSoC but it is included in the USSI device, and cannot be changed by configuration parameters. The conditioning scheme for this configuration is shown in Fig. 83. The internal circuit together with the external resistor and the capacitive sensor realize an oscillating circuit with time constant $\tau = 1 / R0 * CS$.

The thresholds for the commutation of the oscillator are fixed by the amplifier with amplification G, with G less than 1. In particular, with a Gain of 0.5 the thresholds of the comparator have been set to: ¼ VDD and ¾ VDD.

In this condition the period of oscillation of the circuit is:

$$T = 2 * R_0 * C_S * \ln 3$$

The output of the oscillator is sent to a counter that counts the number of pulses in a period and computes the frequency of the signal.

For a correct functioning of the circuit, the frequency of oscillation must be kept under 40 KHz. Moreover, a correcting factor has been introduced to take into account the time due to commutation from high to low and from low to high at the output of the comparator. This delay has been measured and it is equal to 5μs for each commutation for a total of 10μs in a period. So, in the calculation of the frequency a correction factor must be added:

$$f_C = 1 / (1 / f_M - 0.00001)$$

with f_M frequency measured by the circuit and f_C frequency calculated with the correction factor. The implementation of the analog part of this configuration, made by means of "Graphic Configurator" (included in the PSoC Designer tools), is shown in Fig. 84.
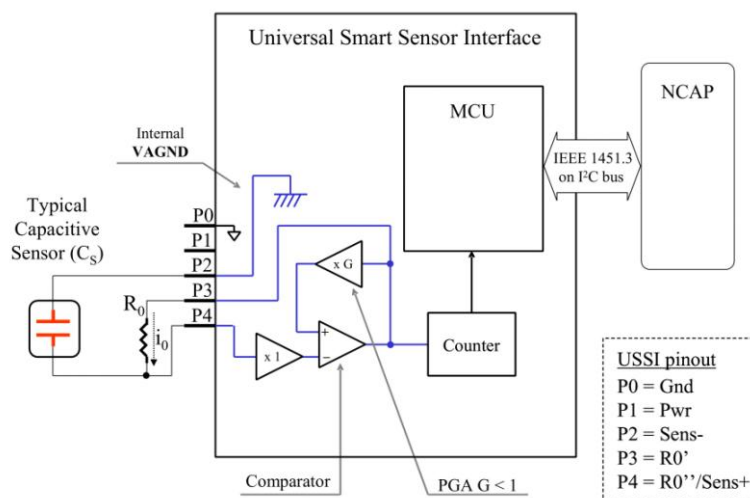

Fig. 83. Logical scheme of conditioning front-end implemented in PSoC device for capacitive sensors
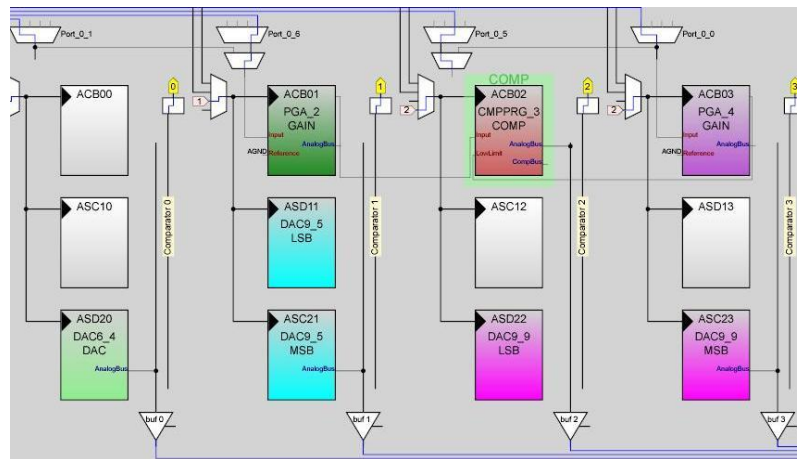
Fig. 84. Screen-shot of "Graphic Configurator" implementing the front-end for capacitive sensors.

As in the configuration 1 the first block is a DAC6 that is used for generating the power supply of the sensor. The sensor output is connected to the PORT_0_0 (Sens+) and to the PORT_0_5 (Sens-) that is internally connected to AGND by the DAC9_5. The core of the configuration is the CMPPRG_3 that has the input connected with the PGA_2. The PGA_2 has a fixed gain <1 set during the configuration and it receives the comparator output signal and carries that in input to the comparator itself. The second amplifier, the PGA_4, is used simply as an analog input buffer, which takes the signal on the capacitive sensor and puts it in input to the comparator. The Output of the comparator is sent also to a counter that measures the frequency of the signal. DAC9_9 is the DAC for the analog output.

Digital Sensor– Configuration 6, 7 and 8

A big part of commercial sensors is represented by digital sensors. The USSI device is potentially able to interface most of them. Anyway the huge numbers of different protocols and communication interfaces make not realistic the proposal of one generic configuration able to cover the entire class of sensors. In this case an ad-hoc solution is necessary for each device. For this reason configurations for digital sensors have been foreseen but not fully implemented. Three main hardware communication interfaces have been selected as representative of the digital sensors, and implemented at hardware level: RS232 serial communication (corresponding to configuration 6), SPI (corresponding to configuration 7) and Microwire (corresponding to configuration 8). All these protocols are supported by PSoC device at hardware level with working parameters completely configurable at run-time, but the software protocol must be developed ad hoc for each sensor. Obviously digital sensors do not require the configuration of analog blocks (except, optionally, for the sensor power supply). The scheme related to the implementation of digital sensor configurations is reported in Fig. 85.
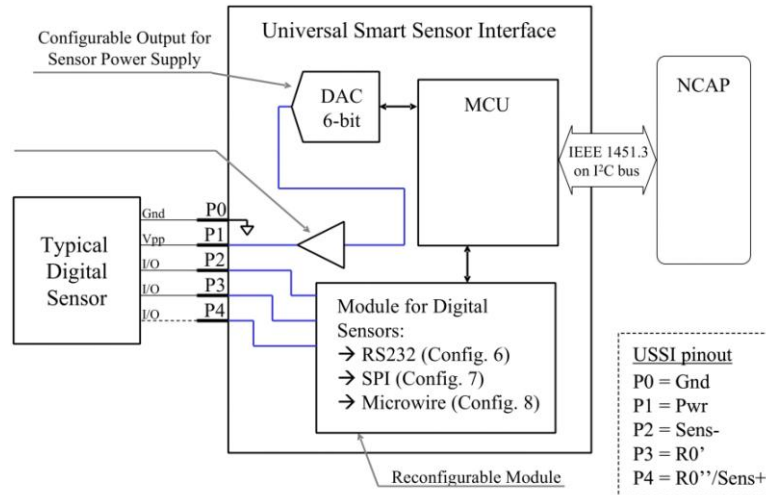
Fig. 85. Logical scheme of conditioning front-end implemented in PSoC device for digital sensors

6.2.4 Software Implementation

IEEE1451.3 over I2C implementation

The 1451.3 standard contemplates a connection between the NCAP (Network Capable Application Processor – defined in the IEEE 1451 standard, in this case the Plantoid main microcontroller) and the smart sensors (USSIs) through a bus. The physical layer adopted in this application is based on the I^2C bus. Added to the standard I^2C lines (Data and Clock) there are two other lines:

- Detection line, used for begins the plug & play service when a new USSI is connected to the NCAP;

- Trigger line, used to wake up the USSIs before the sending of a command on the I^2C bus.

Software block diagram

The USSI device has to guarantee some operational functionality to the sensor. The most important is the "Plug and Play" connectivity. When a USSI is connected (or reconnected) to the I^2C modified bus interface (or in general at the Power On Reset - POR) a procedure for the I2C_ID assignment and TEDS transmission (required operation for "Plug and Play" connectivity) is activated.

The assigned I2C_ID has to be stored in a volatile memory (to be reset at power on) and compared at each following I^2C communication with the ID sent by NCAP (Plantoid main microcontroller). After the initialization phase, the USSI runs in Low Power Mode (CPU Sleep), with all Power line of the Transducer channels switched off. The USSI must remain in sleep state until the arrive of a communication frame on the I^2C bus: the USSI wakes-up from the Sleep, decodes the I2C_ID and if it is the own I^2C address executes the command received. After command execution the USSI goes back in Sleep mode. If the I2C_ID is different from the own I2C address, USSI goes back in Sleep mode immediately, without attends the end of I^2C frame transmission.

The software for the management of the USSI is divided in two higher blocks:

- software for the management of the hardware configuration;

- software for plug&play and data communication;

About the software for the PSoC hardware configuration, it consists on a series of actions in order to set the front-end for the sensor that will be connected. In particular:

- Read from the TEDS the kind of sensor that is connected to the USSI (capacitive, resistive, unconditioned…)

- Load the proper analogical configuration for the conditioning of the sensor

- Turn on of the necessary block and selection of correct parameter (gain, supply voltage, etc.) on the base of the TEDS

- Warm up of the sensor (from 100 ms to 25.6 s) selected on the base of TEDS

- Acquisition of sensor output

- Turn off of all modules

- Return in sleep mode

Concerning the data communication several commands have been defined (taking inspiration by 1451 standard) in order to develop a data communication exchange between the NCAP and the USSI.

Basically the NCAP communicates with the USSI through the modified I^2C bus hardware; it is the master and the USSIs are the slaves. The NCAP sends a frame (a Command that could contain some Data) to the USSIs that answer with another frame (that could contain some Data). The selection of the USSI has made using the I^2C address. For this reason at the first connection with the NCAP at each USSI has assigned a unique I^2C address.

When a new USSI is connected to the NCAP, a procedure for the plug & play of the new smart sensor began. This procedure is called Discovery Service and it has the follow results:

- the assignment of the I^2C address;

- the presentation of the sensor to the Network through the transfer of the related TEDS

In order to activate the Discovery Service the new USSI connected must activate the detection line (if it is not already activated). The software implementation has been described in Fig. 86.
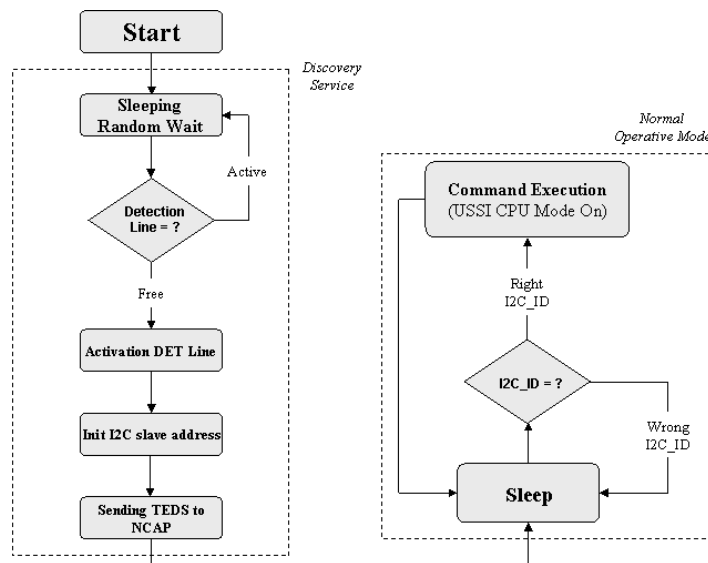
Fig. 86. Software block diagram

Protocol Description

Basically the NCAP communicates with the USSIs through the modified I^2C bus hardware; the NCAP is the master and the USSIs are the slaves. NCAP sends a Command (that could contain some Data) to the USSIs that answer with another frame (that could contain some Data).

Communication Protocol – Low Level Layer

Two different protocols with different frame length are available for the communication. Both protocols are used for single packet operation. The use of protocols is specified ahead. The two protocols are:

- Command Service Protocol: used by NCAP to send a Command to USSI;

- Reply Protocol: used by USSI to reply to a command sent by NCAP, or to send an acknowledge.

All frames are sent with the I^2C protocol; they start with I^2C Start sequence and end with I^2C Stop Sequence. The communication frame is composed of 2 bytes for the MAC header and a group of "Protocol Specific Bytes" that depend on the protocol type. The first byte, always sent by the NCAP, contains the alias ID (I2C_ID) of the USSI involved in the communication. The second byte contains the Transducer Channel Address (Ch) (of the USSI selected by I2C_ID), to which the communication has to be addressed.

A scheme of the general frame structure is reported in Fig. 87
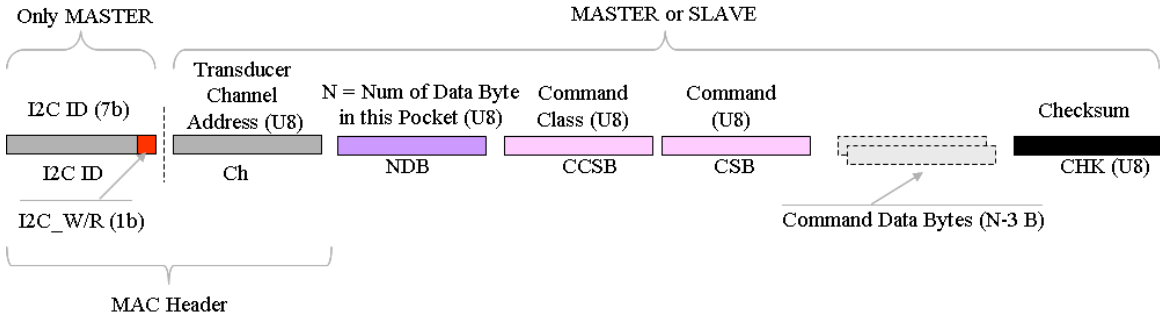
Fig. 87. Order of transmitted byte and Communication Frame structure

"Command Service" and "Reply" protocols have a payload of "Protocol Specific Bytes" to add to the MAC header. NDB is the number of byte of the payload and contains the number of byte in the "Protocol Specific Bytes", including checksum byte, excluding the NDB byte itself.

Commands are divided in different classes; it is possible to implement up 256 classes and each class can contain up to 256 commands. The CCSB byte defines the "Command Class" and the CSB defines the specific Command. The Reply to a Command must contain the same CCSB and CSB of the command itself. Reply Protocol must in addition contain always the Status Byte relative to the USSI/TC addressed by the command.

Checksum (CHK) is the 8-bit one's complement sum of all Protocol Specific Bytes, excluding the checksum byte itself.

Data field ("Reply Data Bytes" or "Command Data Bytes") must have Max 64 bytes of length. For this reason, the Maximum length of whole packet can be 71 bytes: 2 (MAC header) + 4 (Max Protocol Specific Header, Reply) + 64 (Max Data) + 1 (Checksum). Minimum length of whole packet is 6 byte for "Command Protocol" without "Command Data Bytes".

Implemented commands

A set of commands have been implemented in order to guarantee an exchange of data between the NCAP and the USSIs. These commands have been synthesized in the following table:

Plug and Play Class	
SendBroadcastQueryMessage	This command is sent when a new USSIs has been connected in the I^{2}C bus. It asks for the UUID of the new USSI.
SendAssignment	This command initializes the I^{2}C address of the new USSI.
Initialisation Class	
ReadStruct	It is a command that the NCAP sends to receive the structure of the specific USSI (number and kind of transducer channels).
Operational Class	
Trigger	Command sends by the NCAP to start a new measurement in the specific USSI.
EnableTCTrig	Enable the selected Transducer Channel.
DisableTCTrig	Disable the selected Transducer Channel.
ReadStatus	It returns the byte of flags status.
ReadTCData	Read the last acquired data from the selected sensor.
WriteTCData	Write a new value in the selected actuator.

Reset	Reset the USSI.
Query TEDS Class	
QueryMeta	These commands are used to get information about selected TEDS
QueryMetaText	in terms of TEDS_Size, that is the size in byte of TEDS, and
QueryTransducerCh	Max_Block_Size, that is the maximum size allowed by USSI for
QueryTransducerChText	read write operation on TEDS.
Read TEDS Class	
ReadMeta	This class of commands is used to read the specific TEDS of a
ReadMetaText	USSI.
ReadTransducerCh	
ReadTransducerChText	
Write TEDS Class	
WriteMeta	This class of commands is used to write the specific TEDS of a
WriteMetaText	USSI.
WriteTransducerCh	
WriteTransducerChText	

Considerations on low power consumption

One of the main issues, in the design of the USSI and development of the firmware, is the power consumption. Power safe is important because the plantoid system must be capable to have a continuous working and low power consumption has the advantage to permit the reduction of the solar panel and battery dimensions.

There are three main state of working, divided by different power consumption:

- Sleep Mode: the PSoC CPU is in sleep and all the analog and digital blocks are turned off, the USSI is waiting for a new command;

- Elaboration Mode: the PSoC CPU runs at 3MHz and all the analog and digital blocks are turned off, the USSI is elaborating a command and/or preparing an output data for the NCAP;

- Measuring Mode: the PSoC CPU runs at 3MHz and the configuration selected is turned on, the USSI is performing a new measurement;

The selection of 3MHz for the CPU clock is a compromise between different aspects. A very high clock speed is not necessary in this application because the most of time is spent in the transmission of data through the I^2C bus. From the other hand a clock too low does not permit a correct functioning of the I2C module and wake up time too high. With the solution adopted the following performances have been obtained (@ 5V):

- Sleep Mode consumption → 3.9µA

- Elaboration Mode consumption → 5.1mA

- Measuring Mode analog and digital blocks consumption $\rightarrow$ 5mA (considering the worst configuration in terms of consumption: 2 DAC9, 1 DAC6, 2 PGA, 1 ADC, 1 Timer and 1 Counter)

- Time to USSI ready $\rightarrow$ 200µs

All the USSI are waked up at the same time from trigger coming from the NCAP. In this way all the USSI present on the bus are waked up every time that whichever board is called. To avoid that the not interested USSI remain turned on when they are not involved in the communication, a control on the I2C address has been inserted, in this way the USSI return immediately in sleep after the complete receiving of the address. In this way the USSI is not in sleep for wake up time + I^2C address receiving time + return to sleep time < 500µs.

6.2.5 Experimental setup

In order to test the USSI functionalities, a Master Node that makes the function of the NCAP has been implemented. This node communicates with a PC by an UART interface and with the USSIs by the I^2C modified bus. In particular the NCAP manages automatically the plug & play of the USSIs and it assigns the I^2C addresses to them. Then, through the use of a visual basic interface, it is possible to send all the implemented commands to the specific USSI (Fig. 88).
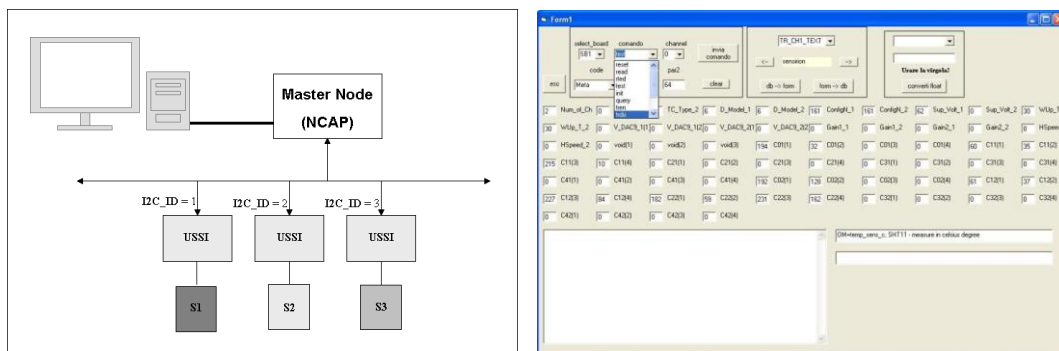
Fig. 88. a) Experimental setup scheme; b) Visual basic interface

With the developed software, it is possible to manage until 16 USSI simultaneously. To guarantee the plug&play capabilities when a stack of USSI is connected to the bus at the same time (or at the power up), a random delay time based on the univocal UUID of each USSI has been introduced at the USSI power up. In this way the risk that two or more USSIs enable the detection line at the same time is considerably decrease and with the 16 USSIs managed by the software is assured that no USSI is lost during the P&P procedure.

About the testing of all the configurations with different conditioning systems, different experimental set up have been employed. To make precise measurements on the external components connected with the USSI, two precision instruments have been employed:

- Fluke 187 Multimeter for the measurements of voltage and current;

- Agilent 4263B LCR meter for the measurements of resistance and capacity.

Fig. 89 shows the configuration set ups.
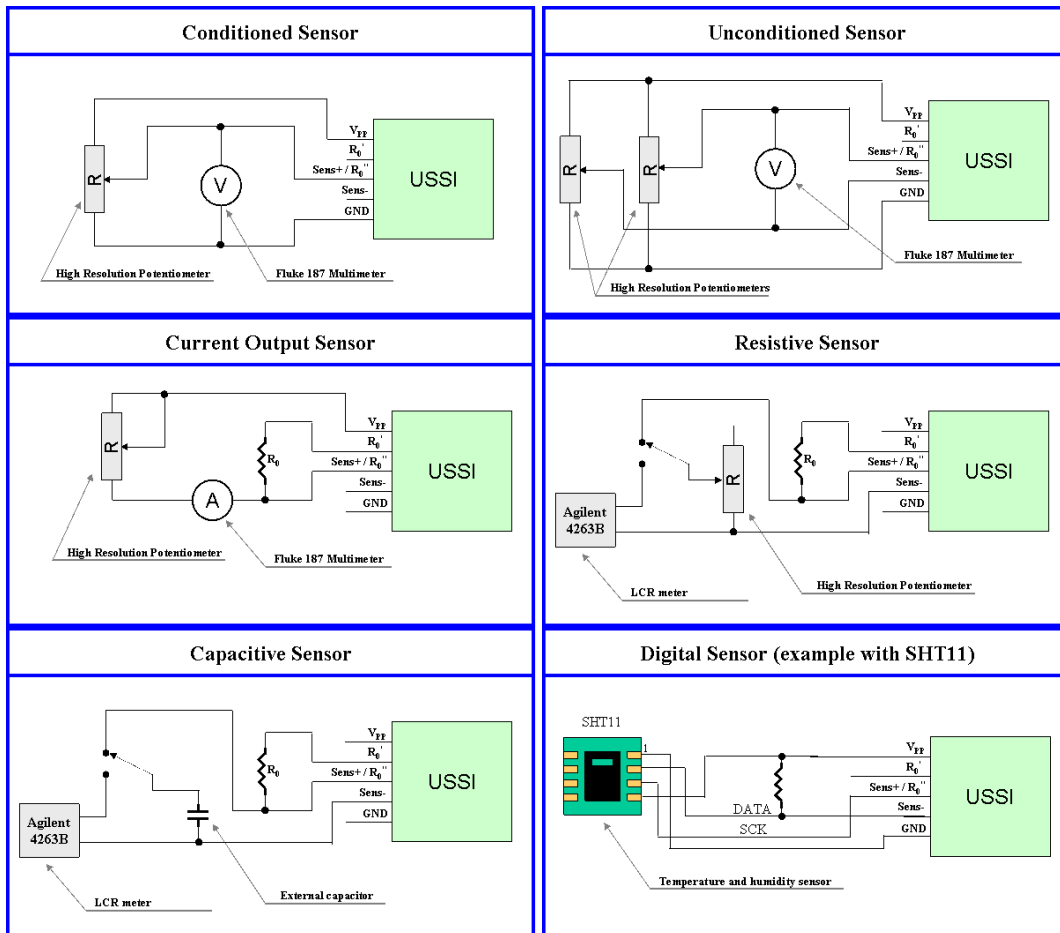
Fig. 89. Configuration setups for the proposed sensor configuration front end

6.2.6   Test Results

The USSI has been tested both for the protocol and for the electrical performance of the configurations. About the protocol, several tests have been performed with the NCAP simulator connected to the PC. All the commands developed have been successfully tested and the communication is assured for up to 16 USSIs simultaneously.

Conditioned Sensor tests

The simplest one is the "Conditioned Sensor" configuration. Only a potentiometer and a Multimeter are used in the characterization of this configuration (Fig. 89). The results are shown in Fig. 90:

- "Vin" is the voltage applied to the USSI input measured by the multimeter;
- "Data Out Value" is the output of the ADC (mean value on 16 measurements);
- "Calculated Value" is the expected output with the voltage applied;
- "Δ" is the difference between "Data Out Value" and "Calculated Value";
- "Δ mV" is Δ expressed in mV;

- "Δ % FS" is Δ (the measurement error) in percentage respect to the full scale;

The configuration shows a high precision except for input signal lower than 50mV and greater than 4.95 V where a saturation behaviour is shown.

| Vin	Data Out Value	Calculated Value	Δ	Δ (mV)	Δ % FS
0.01	39	8.19	30.81	37.61	0.08
0.02	39	16.38	22.62	27.61	0.06
0.05	38	40.96	-2.96	-3.61	-0.01
0.10	69	81.92	-12.92	-15.77	-0.03
0.20	148	163.84	-15.84	-19.34	-0.04
0.30	229	245.76	-16.76	-20.46	-0.04
0.40	313	327.68	-14.68	-17.92	-0.04
0.50	396	409.60	-13.60	-16.60	-0.03
0.75	603	614.40	-11.40	-13.92	-0.03
1.00	813	819.20	-6.20	-7.57	-0.02
1.50	1231	1228.80	2.20	2.69	0.01
2.00	1642	1638.40	3.60	4.39	0.01
2.50	2044	2048.00	-4.00	-4.88	-0.01
3.00	2465	2457.60	7.40	9.03	0.02
3.50	2877	2867.20	9.80	11.96	0.02
4.00	3266	3276.80	-10.80	-13.18	-0.03
4.25	3499	3481.60	17.40	21.24	0.04
4.50	3706	3686.40	19.60	23.93	0.05
4.60	3788	3768.32	19.68	24.02	0.05
4.70	3871	3850.24	20.76	25.34	0.05
4.80	3956	3932.16	23.84	29.10	0.06
4.90	4026	4014.08	11.92	14.55	0.03
4.95	4065	4055.04	9.96	12.16	0.02
4.98	4070	4079.62	-9.62	-11.74	-0.02
4.99	4070	4087.81	-17.81	-21.74	-0.04
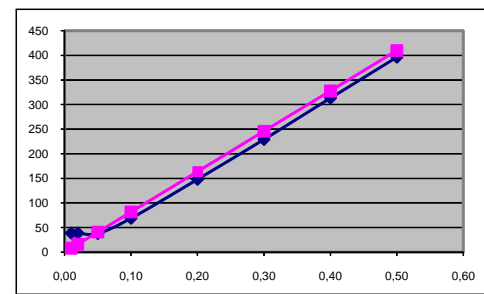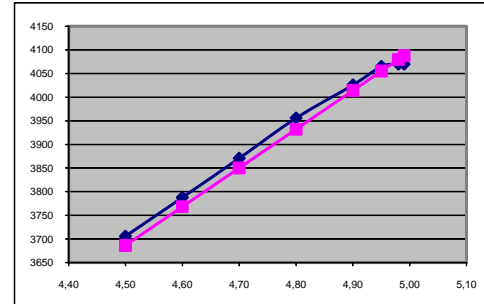
Fig. 90. Mean results of the conditioned configuration on 10 USSI board; graphics of data measured and calculated in proximity of 0 and 5V.

Current Output Sensor tests

Also in this configuration, only a potentiometer and a Multimeter are used for the characterization (Fig. 89). An external high precision resistor is necessary. The configuration has been tested for a typical current output of 4-20 mA as the output of many commercial sensors. For this current range the external resistor as been chosen to be 250 ohm. The results are shown in the following table:

I (mA)	Data Out Value	Calculated Value	Δ	Δ (mA)	Δ % FS	I (mA)	Data Out Value	Calculated Value	Δ	Δ (mA)	Δ % FS
4.00	806	819.20	-13.20	-0.06	-0.32	12.50	2566	2560.00	6.00	0.03	0.15
4.50	909	921.60	-12.60	-0.06	-0.31	13.00	2672	2662.40	9.60	0.05	0.23
5.00	1012	1024.00	-12.00	-0.06	-0.29	13.50	2776	2764.80	11.20	0.05	0.27
5.50	1115	1126.40	-11.40	-0.06	-0.28	14.00	2882	2867.20	14.80	0.07	0.36
6.00	1218	1228.80	-10.80	-0.05	-0.26	14.50	2986	2969.60	16.40	0.08	0.40
6.50	1322	1331.20	-9.20	-0.04	-0.22	15.00	3089	3072.00	17.00	0.08	0.42
7.00	1427	1433.60	-6.60	-0.03	-0.16	15.50	3196	3174.40	21.60	0.11	0.53
7.50	1531	1536.00	-5.00	-0.02	-0.12	16.00	3302	3276.80	25.20	0.12	0.62
8.00	1634	1638.40	-4.40	-0.02	-0.11	16.50	3401	3379.20	21.80	0.11	0.53
8.50	1740	1740.80	-0.80	0.00	-0.02	17.00	3506	3481.60	24.40	0.12	0.60
9.00	1843	1843.20	-0.20	0.00	0.00	17.50	3604	3584.00	20.00	0.10	0.49
9.50	1946	1945.60	0.40	0.00	0.01	18.00	3712	3686.40	25.60	0.13	0.62
10.00	2049	2048.00	1.00	0.00	0.02	18.50	3816	3788.80	27.20	0.13	0.66
10.50	2151	2150.40	0.60	0.00	0.01	19.00	3918	3891.20	26.80	0.13	0.65
11.00	2254	2252.80	1.20	0.01	0.03	19.50	4020	3993.60	26.40	0.13	0.64
11.50	2361	2355.20	5.80	0.03	0.14	19.70	4062	4034.56	27.44	0.13	0.67
12.00	2464	2457.60	6.40	0.03	0.16	20.00	4063	4096.00	-33.00	-0.16	-0.81

Similar results can be obtained with lower current value and higher external resistor.

Resistive Sensor tests

In this configuration an external precision resistor is necessary. The value of the resistor select, together with the internal USSI configuration, selects the range of the resistor that can be correctly read. To test this configuration an input resistance that vary between 1K and 100K ohm has been selected. To condition that the following parameters have been fixed:

- Gain = 1.6
- Vref = 1V
- $R_0 = 50000$

The results are shown in the following table.

Rs	Data Out Value	Calculated Value	Δ	Δ (ohm)	Δ % FS
1000	58	39.322	18.678	475.016	0.475
3000	96	117.965	-21.965	-558.594	-0.559
5000	175	196.608	-21.608	-549.520	-0.550
10000	380	393.216	-13.216	-336.100	-0.336
20000	775	786.432	-11.432	-290.731	-0.291
30000	1170	1179.648	-9.648	-245.361	-0.245
40000	1570	1572.864	-2.864	-72.835	-0.073
50000	1966	1966.080	-0.080	-2.035	-0.002
60000	2363	2359.296	3.704	94.198	0.094
70000	2763	2752.512	10.488	266.724	0.267
80000	3159	3145.728	13.272	337.524	0.338
90000	3555	3538.944	16.056	408.325	0.408
95000	3753	3735.552	17.448	443.726	0.444
98000	3871	3853.517	17.483	444.621	0.445
100000	3947	3932.160	14.840	377.401	0.377

This table shows a quite good accuracy in the measurements for values of the input between 54 and 78 mV; beyond these extremes there is a notably increasing in the error due to the saturation of the internal components. To avoid that the same test has been performed for a second stage gain equal to 4 (instead than 8). The results show a increasing of the accuracy. With a lower gain (e.g. 2) the accuracy returns to decrease. This is due to a decreasing of resolution due to too small range of the adc input signal.

Unconditioned Sensor tests

This is the most critical configuration. A very accurate set up of the internal hardware must be performed before the utilization. To test that several condition has been simulated; in detail here has been shown the results for an input signal of 0.05 to 0.08 V.

This signal presents a high offset (respect to the magnitude of the signal). To condition that the following parameters have been fixed:

- First stage gain = 16
- Vref = 1.46V
- Second stage gain = 8

The results are shown in the following table.

Vin (mV)	Data Out Value	Calculated Value	Δ	Δ(mV)	Δ % FS
50	504	475.136	28.864	0.275	0.918
52	771	684.851	86.149	0.822	2.739
54	913	894.566	18.434	0.176	0.586
56	1123	1104.282	18.718	0.179	0.595
58	1324	1313.997	10.003	0.095	0.318
60	1537	1523.712	13.288	0.127	0.422
62	1742	1733.427	8.573	0.082	0.273
64	1958	1943.142	14.858	0.142	0.472
66	2161	2152.858	8.142	0.078	0.259
68	2364	2362.573	1.427	0.014	0.045
70	2575	2572.288	2.712	0.026	0.086
72	2801	2782.003	18.997	0.181	0.604
74	3009	2991.718	17.282	0.165	0.549
76	3211	3201.434	9.566	0.091	0.304
78	3421	3411.149	9.851	0.094	0.313
80	3588	3620.864	-32.864	-0.313	-1.045

Capacitive Sensor tests

In order to calculate the capacitance value in a determinate range, the correct R_0 must be set. To test this configuration a range of capacity between 0.1 to 100 nF has been chosen. To condition that the following parameters have been fixed:

- $R_0 = 100000$
- Sampling Time = 0.5 second

The results are shown in the following table.

C (nF)	Data Out Value	Calculated Value	Δ	Δ (nF)	Δ % FS
0.102	42857.1	44637.4	1780.28	0.004	0.004
0.221	20131.7	20601.9	470.22	0.005	0.005
0.647	6979.3	7037.1	57.79	0.005	0.005
0.94	4817.4	4843.6	26.23	0.005	0.005
1.15	3969.6	3959.1	-10.41	-0.003	-0.003
1.787	2541.0	2547.9	6.89	0.005	0.005
4.04	1145.0	1127.0	-17.98	-0.063	-0.063
8.043	569.2	566.1	-3.14	-0.044	-0.044
11.25	407.7	404.7	-2.94	-0.081	-0.081
20.63	222.5	220.7	-1.80	-0.166	-0.166
31.16	144.2	146.1	1.91	0.413	0.413
42.6	106.1	106.9	0.77	0.307	0.307
62.75	72.1	72.6	0.51	0.441	0.441
98.1	46.0	46.4	0.39	0.833	0.833

6.3   Sensors integration

6.3.1   Commercial sensor integration by mean of the USSI

During this thesis the USSIs have been tested and optimized by applications in different fields.

USSI for WSN

The first application of this USSI was made to monitoring the physical parameters in the agriculture field (www.goodfood-project.org) by integrating different sensors in a wireless sensor network in a vineyard. The USSI has permitted to create an open infrastructure with the possibility to add new sensors in each moment, to exchange the old uncalibrated sensors and to permit the exchanging of the sensors between the wireless nodes. In Fig. 91 there are reported some example of sensors integrated by the USSI in the vineyard.

TMP121: digital temperature sensor for absolute temperature monitoring and differential leaf temperature (digital configuration).

Soil moisture sensor: capacitive like sensor for soil moisture (capacitive configuration).

Dendrometer: potentiometer like sensor for limbs diametric growth monitoring (conditioned configuration).

SHT11: digital temperature and air humidity sensor (digital configuration).

Fig. 91. Examples of sensors integrated in a vineyard

USSI for Pollution Monitoring

The USSI was applied also in a mobile robot application to mapping the pollution distribution in the urban environment [118]. In this case the sensors are mainly for gas pollution monitoring (Fig. 92). In this application the USSI is important both for the possibility to exchange frequently the gas sensors for the calibration inserting the new one with the own calibration curve, than for the possibility to integrate in each moment new sensors without changing anything in the acquisition module.

| Aeroqual sensors: preconditioned gas sensors for Carbon Monoxide (CO), Nitrogen Dioxide (NO$_2$) and Ozone (O$_3$) (conditioned configuration).	MOX sensors: From Applied Sensor and Figaro. The heat resistance is powered by a regulated voltage, the resistance is read by the resistive configuration.
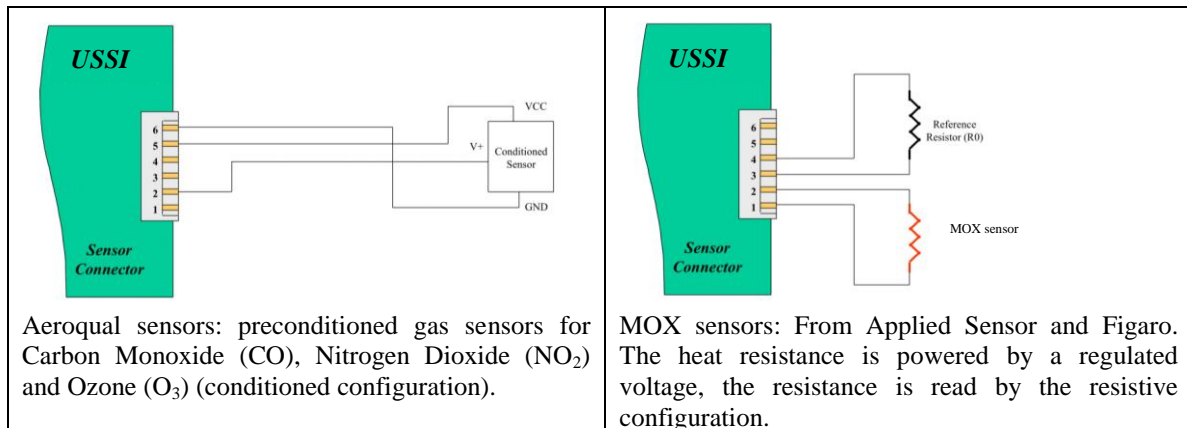
Fig. 92. Examples of sensors integrated in the mobile robots.

The same concept is used also in several other applications (e.g. in the automotive field for integrating hydrogen sensors, in geotechnical application to integrate sensors for landslip monitoring and others).

7 Conclusions

Plants are amazing organisms that show interesting features both for the aerial and underground parts. The aerial part is capable to respond to a large number of stimuli, it collects energy for the whole plant, and it is capable to manage and optimize the energy distribution. The roots are able to explore the soil searching for water and nutrients following the external stimuli by complex behaviours named tropisms and, moreover, it is able to anchor the whole plant to the soil.

In this thesis, these mechanisms have been studied and imitated in order to realize a robot inspired by plants (a *plantoid*) extending for the first time the concept of biorobotics to the plant world. The plantoid robot has been designed to explore and monitor the environment both in the air and in the soil. These plant-inspired robots will be used for specific applications, such as in situ monitoring analysis and chemical detections, water searching in agriculture, anchoring capabilities and for scientific understanding of the plants' capabilities/behaviours themselves by building a physical model.

This thesis has addressed different aspects for the development of this innovative robotic platform. A great effort has been spent in the design, modelling, and development of a mechatronic root apex able to imitate the powerful performances of the plant root system. In particular, a novel actuator has been proposed and tested. The proposed actuator is based on the osmotic principle (osmotic actuator) and permits to realize the elongation and the typical steering capabilities of the root apex, generating high forces with low power consumption (in the time scale of the plant). An embedded microcontroller implements the basic root behaviour on the basis of the information coming from the sensors.

For the aerial part an innovative board has been proposed that is capable to conditioning a wide amount of sensors with plug and play capabilities assuring a wide range of possible applications.

Several aspects of the plantoid system have not been faced yet and they will be part of the future work (i.e. the growing mechanism of the roots and the integration of chemical sensors in the root apex).

References

[1]   G. A. Bakey, "*Autonomous Robots From Biological Inspiration to Implementation and Control*", Preface. The MIT Press, Massachusetts Institute of Technology, Cambridge, 2005.

[2]   P. Dario, *Robotica Biomedica*, "*Storia della Bioingegneria*" E. Biondi, C. Cobelli, pp. 389 – 425, Patron Editore, 2001.

[3]   P. Dario, and M.C. Carrozza, "The Trends towards Miniaturisation," in Proc. of the International Workshop on Innovations for Competitiveness, ESA-ESTEC, Noordwijk, The Netherlands, March 19-21, pp. 301-306, 1997.

[4]   Y. Ogura, H. Aikawa, K. Shimomura, H. Kondo, A. Morishima, H. Lim, and A. Takanishi, "*Development of a Humanoid Robot Capable of Leaning on a Walk-assist Machine*", Proceedings of the first IEEE/RAS-EMBS 2006 International Conference on Biomedical Robotics and Biomechatronics, Paper No. 299, 2006.

[5]   J. E. Clark, J. G. Cham, S. A. Bailey, E. M. Froehlich, P. K. Nahata, R. J. Full, M. R. Cutkosky, "*Biomimetic Design and Fabrication of a Hexapedal Running Robot*", IEEE International Conference on Robotics and Automation, 2001.

[6]   L. Cangiano, S. Grillner, "*Mechanisms of Rhythm Generation in a Spinal Locomotor Network Deprived of Crossed Connections: The Lamprey Hemicord*", The Journal of Neuroscience, January 26, 2005, 25(4):923–935 923.

[7]   M. Zecca, S. Micera, M.C. Carrozza, P. Dario, "*On the control of multi-functional hand prostheses by using the EMG signal*", Crit. Rev. Biomed. Eng., vol. 30, no. 6, pp. 419–416, 2002.

[8]   P. Dario, P. Ciarletta, A. Menciassi, "*Modeling and experimental validation of the locomotion of endoscopic robots in the colon*" Int. J. Robot. Res. 23(4-5):549-556, 2004.

[9]   N. Yazdi, F. Ayazi, K. Najafi, "*Micromachined inertial sensors*", Proceedings of the IEEE, 86(1998): 1640-1659

[10] P.C.H. Chan, G. Yana, L. Sheng, R.K. Sharma, Z. Tang, J.K.O. Sina, I. Hsinge and Y. Wang, "An integrated gas sensor technology using surface micromachining", Sensors and Actuators B 82 (2002): 277-283

[11] C. Tsamis, A.G. Nassiopoulou and A. Tserepi "Thermal properties of suspended porous silicon micro-hotplates for sensor applications", Sensors and Actuators B 95 (2003): 78–82

[12] I. Elmi, S. Zampolli, E. Cozzani, F. Mancarella, G.C. Cardinali, "*Development of ultra-low-power consumption MOX sensors with ppb-level VOC detection capabilities for emerging applications*", Sensors and Actuators B: Chemical, 135(2008): 342-351

[13] E. Abad, B. Mazzolai, A. Juarros, D. Gómez, A. Mondini, I. Sayhan, A. Krenkow, T. Becker , "Investigation of fabrication and encapsulation processes for a flexible tag microlab" Microsystem Technologies - 14(2008): 527 - 534.

[14] E. Abad, S. Zampolli, S. Marco, A. Scorzoni, B. Mazzolai, A. Juarros, D. Gómez, I. Elmi, G.C. Cardinali, J. M. Gómez, F. Palacio, M. Cicioni, A. Mondini, T. Becker and I. Sayhan "Flexible tag microlab development: Gas sensors integration in RFID flexible tags for food logistic" Sensors and Actuators B: Chemical 127(2007): 2-7.

[15] B. Mazzolai, V. Mattoli, A. Mondini, P. Dario, I. Elmi, S. Zampolli, A. Zani "Sistema per il monitoraggio della qualità e della sicurezza di prodotti alimentari" Italian Patent (2007)

[16] B. Mazzolai, V. Mattoli, V. Raffa, G. Tripoli, D. Accoto, A. Menciassi, P. Dario "*A microfabricated physical sensor for atmospheric mercury monitoring*" Sensors and Actuators A - Physical - 113(2004): 282-287

[17] V. Raffa, B. Mazzolai, V. Mattoli, A. Mondini, P. Dario, "*Model validation of a mercury sensor, based on the resistivity variation of a thin gold film*" Sensors and Actuators B: Chemical - 144(2006): 513-521

[18] V. Raffa, B. Mazzolai, V. Mattoli, A. Mondini, A. Menciassi, P. Dario "*Investigation on a sensitive Au thin film deposited on different substrates: physical analysis via FIB and chemical analysis via evaluation of Au sensitivity to Hg°*" Sensors and Actuators B: Chemical - 122(2007): 475-483

[19] V. Mattoli, B. Mazzolai, V. Raffa, A. Mondini, P. Dario, "Design of a New Real-Time Dosimeter to Monitor Personal Exposure to Elemental Gaseous Mercury" Sensors and Actuators B: Chemical - 123(2007): 158 – 167.

[20] G. Ferri, E. Caselli, V. Mattoli, A. Mondini, B. Mazzolai, P. Dario, "A Biologically-Inspired Algorithm Implemented on a new Highly Flexible Multi-Agent Platform for Gas Source Localization" BioRob 2006, IEEE/RAS-EMBS International Conference, Pisa, Italy, February 20-22, (2006): 573–578.

[21] G. Ferri, E. Caselli, V. Mattoli, A. Mondini, B. Mazzolai and P. Dario, "SPIRAL: A novel biologically-inspired algorithm for gas/odor source localization in an indoor environment with no strong airflow" Robotics and Autonomous Systems, 57(2009): 393-402.

[22] J.W. Judy, "*Microelectromechanical systems (MEMS): fabrication, design and applications*", Smart Mater. Struct. 10 (2001): 1115–1134

[23] J. M. Hollerbach, I. W. Hunter, J. Ballantyne, "*A Comparative Analysis of Actuator Technologies for Robotics*", in The Robotics Review, O. Khatib, J. Craig, T. Lozano-Perez, Eds, Cambridge, MA: MIT Press, Vol. 2, pp. 299-342, 1992.

[24] J. L. Pons, "*Emerging Actuator Technologies: A Micromechatronic Approach*", John Wiley & Sons, Ltd, England, 2005.

[25]   I. W. Hunter, S. Lafontaine, *A comparison of muscle with artificial actuators*, IEEE Solid-State Sensor and Actuator Workshop, pp. 178-165, 1992.

[26]   J. D. W. Madden, N. A. Vandesteeg, P. A. Anquetil, P. G. A. Madden, A. Takashi, R. Z. Pytel, S. R. Lafontaine, P. A. Wieringa, I. W. Hunter, *Artificial Muscle Technology: Physical Principles and Naval Prospects*, IEEE Journal of oceanic engineering, Vol. 29, No. 3, Luglio 2004.

[27]   Y. Bar-Cohen, Electroactive Polymer (EAP) Actuators as Artificial Muscles, Second edition, SPIE Press, Bellingham, Washington USA (2004).

[28]   R. Kratz, M. Stelzer, M. Friedmann, O. Stryk "Control approach for a novel high power-to-weight ratio SMA muscle scalable in force and length." In: IEEE/ASME Intl. Conf. on Advanced Intelligent Mechatronics (AIM), 2007.

[29]   Funakubo H Shape memory alloys. Gordon and Breach Science Publishers (1987).

[30]   C.A. Esmon, U.V. Pedmale, E. Liscum, "Plant tropisms: providing the power of movement to a sessile organism", Int. J. Dev. Biol. 49 (2005): 665-674.

[31]   D. Eapen, M.L. Barroso, G. Ponce, M.E. Campos, G.I. Cassab, "Hydrotropism: root growth responses to water", Trends Plant Sci. (2005): 44-50.

[32]   F. Baluška, S. Mancuso, D. Volkmann, P. Barlow, "Root apices as plant command centres: the unique 'brain-like' status of the root apex transition zone", Biologia (2004), 59 (Suppl. 13), pp. 1–13.

[33]   J.W. Hart, "*Plant tropisms: and other growth movements.*" (1990) (UnwinHyman: London)

[34]   K.A. Franklin, G.C. Whitelam "*Phytochromes and shade-avoidance responses in plants.*" Annals of Botany 96(2005): 169–175. doi: 10.1093/aob/mci165

[35]   S. Gilroy and D.L. Jones "*Through form to function: root hair development and nutrient uptake*", Trends in Plant Science(2000), 5: 56-60.

[36]   F. Baluska, and K. H. Hasenstein, "*Root cytoskeleton: its role in perception of and response to gravity*", Planta 203(1997): S69–S78.

[37]   F. Baluška, , D. Volkmann, and P.W. Barlow "*A Polarity Crossroad in the Transition Growth Zone of Maize Root Apices: Cytoskeletal and Developmental Implications*" J. Plant Growth Regul. 20(2001): 170–181.

[38]   E. Goulas, F. L. Dily, J. Ozouf and A. Ourry, "*Effects of a cold treatment of the root system on white clover (Trifolium repens L.) morphogenesis and nitrogen reserve accumulation*" J. Plant Physiol. 160(2003): 893–902.

[39]   J. Blake and W. K. Ferrell, "The Association between Soil and Xylem Water Potential, Leaf Resistance, and Abscisic Acid Content in Droughted Seedlings of Douglas-fir" Pseudotsuga menziesiiPhysiol. Plant. 39(1977): 106–109.

[40]   K. Chamberlain, E. Guerrieri, J. Pennacchio, J. Pettersson, P. A. Pickett, G. M. Poppy, W. Powell, L. J. Wadhams and C. M. Woodcock, Biochem. Syst. Ecol. 29(2001): 1063–1074.

[41] M. Dicke and H. Dijkman, *"Within-plant circulation of systemic elicitor of induced defence and release from roots of elicitor that affects neighbouring plants"* Biochem. Syst. Ecol. 29(2001): 1075–1087.

[42] S. Mancuso, A. M. Marras, V. Magnus and F. Baluška "*Noninvasive and continuous recordings of auxin fluxes in intact root apex with a carbon nanotube-modified and self-referencing microelectrode*" Analytical Biochemistry 341(2005): 344-351.

[43] R. Misra, A. Dexter, A. Alston, "Maximum axial and radial growth pressures of plant roots," Plant and Soil, Vol. 95, 1986, pp. 315–318.

[44] J. Vermeer, ME. McCully "*The rhizosphere in Zea: new insight into its structure and development*" Planta 156(1982), 45-61.

[45] A.G. Bengough, M.F. Bransby, J. Hans, S.J. McKenna, T.J. Roberts and T.A. Valentine, "*Root responses to soil physical conditions; growth dynamics from field to cell*" Journal of Experimental Botany 57 (2) (2006), 437–447.

[46] A. G. Bengough, and B. M. McKenzie, "Sloughing of root cap cells decreases the frictional resistance to maize (Zea mays L) root growth," Journal of Experimental Botany 48, 1997, pp. 885–893.

[47] E.L. Greacen, D.A. Farrell, B. Cockroft Soil resistance to metal probes and plant roots. Transactions of the 9th Congress of the International Society of Soil Science 1(1968), 769–779.

[48] M. Iijima, T. Higuchi, P.W. Barlow, A.G. Bengough, "*Root cap removal increases root penetration resistance in maize (Zea mays L.)*" Journal of Experimental Botany 54(2003), 2105–2109.

[49] M. Iijima, T. Higuchi, P.W. Barlow, *"Contribution of root cap mucilage and presence of an intact root cap in maize (Zea mays) to the reduction of soil mechanical impedance"* Annals of Botany 94(2004), 473–477.

[50] L.J. Clark, W.R. Whalley and P.B. Barraclough, "How do roots penetrate strong soil? Plant and Soil", 255, 93–104, 2003.

[51] Z. Hejnowicz, K. Hejnowicz, "*Modelling the formationof root apices*", Planta 184(1991): 1-7

[52] Z. Hejnowicz and J. Karczewski "*Modeling of Meristematic Growth of Root Apices in a Natural Coordinate System*" American Journal of Botany 80(1993): 309-315

[53] G. T. S. Beemster and T. I. Baskin, "Analysis of Cell Division and Elongation Underlying the Developmental Acceleration of Root Growth in Arabidopsis thaliana," Plant Physiol. 116(1998): 1515–1526.

[54] R.O. Erickson and K.B. Sax "*Rates of Cell Division and Cell Elongation in the Growth of the Primary Root of Zea mays*" Proc. of the American Phil. Society, 100(1956): 499-514

[55] A. Chavarría-Krausera and U. Schurr, "*A cellular growth model for root tips*" Journal of Theoretical Biology 230(2004): 21-32

[56] W.K. Silk, "*Steady form from changing cells*", Int. J. Plant Sci. 153 (1992): 49–58.

[57] P. Schopfer, "*Biomechanics of plant growth*" Am. J. Bot. 93(2006): 1415-1425.

[58] A. Chavarría-Krauser, W. Jager, U. Schurr "*Primary root growth: a biophysical model of auxin-related control.*" Functional Plant Biology, 32(2005): 849-862.

[59] W. Teale, I.A. Paponov, F. Ditengou, K. Palme "*Auxin and the developing root of Arabidopsis thaliana.*" Physiologia Plantarum 123 (2005), 130–138.

[60] J.A. Lockhart "*An analysis of irreversible plant cell elongation.*" J Theor Biol., 8(1965):264-75.

[61] G. Muday, P.W. Murphy, A. "*Vesicular cycling mechanism that control auxin transport polarity*", Trends Plant Science, 8(2003): 301-304.

[62] J. Friml, "*Auxin transport – shaping the plant.*" Curr. Opin. Plant Biol., 6(2003): 7-12.

[63] G. Muday Auxins and tropisms. J Plant Growth Regul 20(2001): 226–243.

[64] C. Darwin, F. Darwin, "*The Power of Movement in Plants*". John Murray, London. (1880)

[65] E.B. Blancaflor, and P.H. Masson, "*Plant gravitropism: unraveling the ups and downs of a complex process*" Plant Physiol. 133(2003): 1677-1690.

[66] E. Liscum, "*Phototropism: Mechanisms and outcomes.*" In The Arabidopsis Book, Somerville, C.R. and Meyerowitz, E.M. (Eds.), American Society of Plant Biologists, Rockville, Maryland, doi/10.1199/tab.0042, (2002).

[67] S. Mugnai, E. Azzarello, E. Masi, C. Pandolfi, S. Mancuso "*Nutation in plants.*" In: Mancuso and Shabala (eds) 'Rhythms in Plants,'Sprinter-Verlag, Berlin. (2007).

[68] F.D. Sack, "*Plastids and gravitropic sensing*", Planta 203(1997): S63–S68.

[69] J. Z. Kiss, R. Hertel, and Sack, F. D. 1989. Amyloplasts are necessary for full gravitropic sensitivity in roots of Arabidopsis thaliana. Planta 177: 198-206.

[70] E.B. Blancaflor, J.M. Fasano and S. Gilroy, "*Mapping the functional roles of cap cells in the response of Arabidopsis primary roots to gravity*", Plant Physiol. 116(1998): 213-222.

[71] Z. Hejnowicz "*Biomechanics of the appendix: mechanical importance of aerenchyma.*" In W. Barthlott and W. Lobin [eds.], Amorphophallus titanum, (1998)68–80.

[72] A.M. McGillavray, Gownar "*Applied electrical fields polarize the growth of mycelial fungi.*" J Gen Microbiol 132(1986): 2515-2525.

[73] D.L. Brower, T.H. Giddings "*The effects of applied electric fields on Micrasterias. II. The distributions of cytoplasmic and plasma membrane components.*" J Cell Sci 42(1980): 279-290.

[74] W.M. Fondren, R. Moore "*Collection of gravitropic effectors from mucilage of electrotropically-stimulated roots of Zea mays*" L. Ann Bot 59(1987): 657-659.

[75] A.R. Schrank "*Electronasty and electrotropism.*" In E Bunning, ed, Physiology of Movements, Encyclopedia of Plant Physiology, New Series, 17(1959): 148-163.

[76] H. Takahashi "*Hydrotropism: the current state of our knowledge.*" J Plant Res. 110(1997):163–169.

[77] H. Takahashi, H. Suge "*Root hydrotropism of an agravitropic pea mutant, ageotropum.*" Physiol Plant.; 82(1991): 24–31.

[78] H. Takahashi, M. Takano, N. Fujii, M. Yamashita, H. Suge "*Hydrotropism in abscisic acid, wavy, and gravitropic mutants of Arabidopsis thaliana.*" J Plant Res. 109(1996): 335–337.

[79] P. Dario, C. Laschi, B. Mazzolai, P. Corradi, V Mattoli, A. Mondini, S. Mancuso, S. Mugnai, E. Masi, E. Azzarello, A. Hlavacka, C. Pandolfi, T. Seidl "Bio-inspiration from Plants' Roots" Final Report, Ariadna ID: 06/6301

[80] T. Seidl, S. Mugnai, P. Corradi, A. Mondini, V. Mattoli, E. Azzarello, E. Masi, C. Pandolfi, B. Mazzolai, C. Laschi, P. Dario, S. Mancuso, "*Biomimetic Transfer Of Plant Roots For Planetary Anchoring*", Proc 59th Int Astronautics Conf, 2008.

[81] M. Anttila, "Concept evaluation of Mars drilling and sampling instrument", Helsinki University of Technology, Laboratory of Space Technology, March 2005.

[82] Exomars rover/Pasteur System Requirements Document, EMR-SRD, Aurora/Mw/KC/006.3, July 4, 2003.

[83] Statement of Work for the Phase A Study of the Pasteur Exobiology Payload and Rover for the EXOMARS Mission, MSM-GMS-2003-001-AV. 2003.

[84] I. Sayhan, A. Helwig, T. Becker, G. Müller, I. Elmi, S. Zampolli, M. Padilla, S. Marco, "Discontinuously Operated Metal Oxide Gas Sensors for Flexible Tag Microlab Applications", IEEE Sensors Journal (2008)

[85] www.goodfood-project.org

[86] G.D. Massa and S. Gilroy, "*Touch modulates gravity sensing to regulate the growth of primary roots of Arabidopsis thaliana.*" Plant J. 33(2003): 435-445.

[87] B. Mazzolai, P. Corradi, A. Mondini, V. Mattoli, C. Laschi, S. Mancuso, S. Mugnai, and P. Dario, "Inspiration from plant roots: a robotic root apex for soil exploration," In the Proc. Of Biological Approaches for Engineering, 17-19th March, 2008, pp. 50-53.

[88] A. Mondini, B. Mazzolai, P. Corradi, V. Mattoli, S. Taccola, C. Laschi, P. Dario, "A Preliminary Study of a Robotic Probe For Soil Exploration Inspired By Plant Root Apexes" in the Proc. Biorob2008 (2008): 115-120.

[89] G. Bengough, C. Croser and J. Pritchard, "A biophysical analysis of root growth under mechanical stress, Plant and Soil", 189, 155–164, 1997.

[90] J. Pritchard, "The control of cell expansion in roots." New Phytol. 127: 3-26, 1994.

[91] M.C. Probine and R.D. Preston, "Cell growth and the structure and mechanical properties of the wall in internodal cells of Nitella opaca. II. Mechanical properties of the walls", J. Exp. Bot., 13 111–127, 1962.

[92] E.L. Greacen and J.S. Oh, "Physics of root growth," Nature New Biol., 235, 24–25, 1972.

[93] P.W. Atkins, Physical Chemistry, 1997, Oxford University Press.

[94] Y. Su and L. Lin, "Water-Powered Micro Drug Delivery System", Journal of Microelettromechanical Systems, 13, 75–82, 2004.

[95] W. Ludwig, A. Seppälä, M.J. Lampinen, "Experimental study of the osmotic behaviour of reverse osmosis membranes for different NaCl solutions and hydrostatic pressure differences", Experimental Thermal and Fluid Science, 26, 963–969, 2002.

[96] V.Mattoli, S.Taccola, B.Mazzolai, A.Mondini, C.Laschi, P.Dario, "Development of new plant-inspired electro-osmotic actuator" to be submitted to Sensors & Actuators B

[97] Atkins P.W., Physical Chemistry, 1997, Oxford University Press.

[98] W.Ludwig, A.Seppälä, M.J.Lampinen, "Experimental study of the osmotic behavior of reverse osmosis membranes for different NaCl solutions and hydrostatic pressure differences", Experimental Thermal and Fluid Science, 26 (2002) 963–969

[99] G.M. Whiteley, and A.R. Dexter, "The dependence of soil penetrometer pressure on penetrometer size" J. Agric. Eng. Res., Vol.26, No.6, 1981. pp. 467-476

[100] H.-H. Hsu and A.-B. Huang, "Calibration of Cone Penetration Test in Sand," in Proc. Natl. Sci. Counc. ROC(A), Vol. 23, No. 5, 1999. pp. 579-590.

[101] A. Puech and P. Foray, "Refined Model for Interpreting Shallow Penetration CPTs in Sands", in Proc. of the Offshore Technology Conference, Houston, Texas U.S.A., 6–9 May 2002.

[102] A.G. Bengough, C.E. Mullins, "Mechanical impedance to root growth: a review of experimental techniques and root growth responses" J. Soil Sci. 1990, 41, 341–358.

[103] W.R. Whalley, P.B. Leeds-Harrison, L.J. Clark, D.J.G. Gowing, "The use of effective stress to predict the penetrometer resistance of unsaturated soils" Soil Tillage Res. 2005, 84, 18–27.

[104] J.E. Fisher, "Evidence of circumnutational growth movements in rhizomes of Poa pratensis L. that aid in soil penetration." Can J Bot 1964, 42:293–299.

[105] N. Inoue, T. Arase, M. Hagiwara, T. Amnao, T. Hyashi, R. Ikeda, "Ecological significance of root tip rotation for seedling establishment of Oryza sativa L." Ecol Res 1999, 14:31–38.

[106] B. Zhang, R. Horn, and T. Baumgart, "Changes in penetration resistance of Ultisols from southern China as affected by shearing," Soil & Tillage Research, Vol. 57 (4), 2001, pp. 193-202.

[107] R. O. Erickson and K. B. Sax, "Rates of Cell Division and Cell Elongation in the Growth of the Primary Root of Zea mays," Proc. of the American Philosophical Society, Vol. 100, No. 5, 1956 pp. 499-514.

[108] A. Samouëlian, I. Cousin, A. Tabbagh, A. Bruand, G. Richard, "Electrical resistivity survey in soil science: a review" Soil & Tillage Research Volume: 83, Issue: 2, pp. 173-193, September, 2005

[109] P.K. Robertson, "Soil classification using the cone penetration test." Canadian Geotechnical J. 27 (1990): 151-158.

[110] A. Tabbagh, M. Dabas, A. Hesse, C. Panissod, "Soil resistivity: a non-invasive tool to map soil structure horizonation" Geoderma Volume: 97, Issue: 3-4, pp. 393-404, September, 2000

[111] A. L. Mullen, C. Wolverton, H. Ishikawa, M. L. Evans, "Kinetics of Constant Gravitropic Stimulus Responses in Arabidopsis Roots Using a Feedback System" Plant Physiology Volume: 123, pp. 665-670, June, 2000

[112] T. Takahashi and H. Suge, "Root hydrotropism of an agravitropic pea mutant, ageotropum." Physiol. Plant. 82, pp. 24–31, 1991

[113] H. Takahashi and T. K. Scott, "Intensity of hydrostimulation for the induction of root hydrotropism and its sensing by the root cap" Plant, Cell & Environment; Volume 16 Issue 1, Pages 99 - 103, 1993

[114] G. Smith and M. Bowen, "Considerations for the utilization of smart sensors." Sensors and Actuators a-Physical, 47(1995): 521-524.

[115] J.M. Riviere, "Design of smart sensors: Towards an integration of design tools." Sensors and Actuators A: Physical, 47(1995): 509-515.

[116] M. Bowen and G. Smith, "Considerations for the design of smart sensors." Sensors and Actuators A: Physical, 47(1995): 516-520.

[117] V. Mattoli, A. Mondini, K. M. Razeeb, B. O. Flynn, F. Murphy, S. Bellis, G. Collodi, A. Manes, P. Pennacchia, B. Mazzolai, P. Dario, "Development of a Programmable Sensor Interface for Wireless Network Nodes for Intelligent Agricultural Applications", Proceedings of the IEE International Workshop on Intelligent Environments, Colchester, UK, 28-29 June, 2005.

[118] www.dustbot.org